Stability of dual porosity soil slope against rainfall-induced slope failure

By

Shafi Mohammad Ashrafullah-202177432, MSc Eng.

Submitted Fulfillment of the Requirements for the Degree of
Master of Science in Civil and Environmental Engineering

School of Engineering and Digital Sciences
Department of Civil & Environmental Engineering
Nazarbayev University

53 Kabanbay Batyr, Avenue,
Astana, Kazakhstan, 010000

Supervisor: Dr. Alfrendo satyanaga

Co-Supervisor: Dr. Sung-woo moon

March 2023

ORIGINALITY STATEMENT

I, Shafi Mohammad Ashrafullah, hereby confirm that this submission is entirely original work of mine, and to the best of my knowledge, it does not contain any works that have been accepted for publication or written by others before, nor does it contain a significant portion of works that have been approved for the award of any other degree or diploma at Nazarbayev University or any other academic establishment, with the exception of those that are properly acknowledged in the Dissertation.

The thesis explicitly acknowledges any contributions made to the study by individuals I have collaborated with at NU or elsewhere.

Aside from acknowledging any help with the project's conceptualization, layout, or manner, display, or linguistic expression that I received from others, I also state that the scientific material within this dissertation is entirely my own creation.

Signed on 16th March 2023

_____

ABSTRACT

Slope stability and landslides are caused by a combination of factors, including prolonged rainfall, groundwater level, slope geometry, and the geological structure of the soil have significant influences on the stability of the slope. However, a few studies have been conducted on rainfall's influence on slope stability with bimodal soil-water characteristic curves or dual-porosity soil. Therefore, the aim of this research is to analyze the stability of dual-porosity soil with various geometries under extreme rainfall in Kazakhstan. In this study, comprehensive laboratory tests were carried out to obtain index properties, saturated permeability, saturated shear strength, the bimodal soil-water characteristic curve (SWCC), and unsaturated permeability of silty sand and sandy silt. The first and second air-entry values and inflection points of silty sand are Ψa1 = 1 kpa and ψa2=10 kpa Which are lower than those of sandy silt: Ψa1=3kpa and ψa2=25kp. The slope of sub-curve 1 of silty sand is σ1=0.5 higher than those of sandy silt σ1=0.36-. The unsaturated permeability of sandy silt is 7.00E-5 which is higher than that of silty sand at 9E-7 m/s. Comprehensive numerical analyses were performed on dual-porosity soil slopes with different geometries under extreme rainfall intensity in Kazakhstan to generate variations of the factor of safety (FoS) and a decrease in pore-water pressure with time. The results indicate that the factor of safety for the shortest slope and the gentlest slope is higher than the tallest slopes with the steepest angles. It was observed that the slope with dual-porosity soil can only be constructed up to 10m and 20m slope heights and 27–35 ° slope angles since the minimum FoS for this slope geometry is FoS=1.27>1.25 (higher than the minimum FoS considered as stable slope).

Keywords: Slope stability; Dual porosity soil; Rainfall; Unsaturated soil; SWCC and Permeability function.

ACKNOWLEDGMENT

I would like to convey my heartfelt thanks and respect to Prof. Alfrendo Satyanaga, who helped as my master’s thesis advisor, for his continuous support, direction, and inspiration all throughout my master's degree. My study has been greatly influenced and improved by your superior expertise and insightful observations. Secondly, I want to express my gratitude to the civil and environmental engineering faculty’s professors for providing me with an educational environment and research facilities. Basically, Prof. Kim and my co-supervisor, Prof. Moon, helped me have access to all geotechnical engineering equipment and gave me comments and recommendations during my master's thesis work. Finally, I would like to extend my most sincere thanks to my parents for their never-ending support and inspiration. My motivation for the entire road has been your everlasting faith in me.

TABLE OF CONTENTS

ABSTRACT ..... **III**
ACKNOWLEDGMENT ..... **IV**
TABLE OF CONTENTS ..... **V**
LIST OF FIGURES ..... **VII**
LIST OF TABLES ..... **IX**
LIST OF PUBLICATIONS ..... **X**
CHAPTER 1 - INTRODUCTION 1
1.1 Background 1
1.2 Problem statement 2
1.3 Hypotheses 3
1.4 Objectives 3
CHAPTER 2 - LITERATURE REVIEW **4**
2.1 Rainfall-induced landslide 4
2.2 Unsaturated soil mechanics 4
2.3 Dual-porosity soil 5
2.4 Seepage and stability analyses 6
CHAPTER 3 - APPLICABLE THEORIES **8**
3.1 Bimodal Soil-water characteristic curve 8
3.2 Bimodal unsaturated permeability 9
3.3 Bimodal Unsaturated shear strength 10
CHAPTER 4 - RESEARCH METHODOLOGY **12**
4.1. Laboratory testing 12
4.1.1 Proctor method 12
4.1.2 Specific gravity 13
4.1.3. Index properties by Atterberg limit 14
4.1.4 Gran size distribution (GSD) 15
4.1.5 Saturated permeability Using Constant head 16
4.1.6 Shear strength Using Triaxial test. 17
4.1.7 SWCC of fine grained (MH) and coarse grained (SM) soil. 18

4.2 Numerical Analyses 19
4.2.1 Position of the ground-water table 19
4.2.2 Seepage analyses using Seep/W 19
CHAPTER 5 - RESULTS **24**
5.1 Result from laboratory 24
5.1.1 Index properties of unsaturated soil 24
5.1.2 Result from Proctor method 24
5.1.3 Particle size distribution (PSD) 25
5.1.4 Soil water characteristic curve SWCC 27
5.1.5 Unsaturated permeability function 29
5.1.6 Result from Unsaturated soil shear strength 30
5.2 Result from seepage and slope stability 31
5.2.1 Factor of safety and pore water pressure for fine grained soil (MH). 31
5.2.2 Factor of safety and pore water pressure for coarse grained soil (SM) 36
CHAPTER 6 - DISCUSSION 40
CHAPTER 7 - CONCLUSION 42
LIST OF REFERENCES **44**
APPENDIX A **52**
CHAPTER 8 52
8.1 Seepage and slope stability analyses for silty sand soil with different slope geometries. 52
8.2 Results from Seepage and slope stability analyses for Sandy silt soil with different slope geometries 79

LIST OF FIGURES

Figure 1-1 Almatinskaya landslide risk in Almaty Kazakhstan (ThinkHazard, 2020) 2
Figure 4-1 The process of proctor test for determination of maximum dry density. 13
Figure 4-2 The process of Atterberg limit for determination of LL, PL and PI 14
Figure 4-3 Sieve and hydrometer analyses 15
Figure 4-4 Constant Head Permeability Test 16
Figure 4-5The process consolidated undrained triaxial test 17
Figure 4-6 The process of Hyprop test for SWCC and unsaturated permeability 18
Figure 4-7Numerical model for seepage analyses or seep/w with a slope height of 20 m and slope degree of 27-degree. 21
Figure 4-8Numerical model for slope stability analyses or slope/w with a slope height of 20 m and slope degree of 27-degree 22
Figure 5-1 Compaction curve of fine and coarse grained soil 25
Figure 5-2 Particle size distribution curve of the soils 26
Figure 5-3Bimodal soil water characteristic curve (SWCC) fitted using Satyanaga (2021) mathematical function 29
Figure 5-4Bimodal soil permeability function based on Statistical method 30
Figure 5-5 Factor of safety (FoS) for fine grained soil, (10m with 27º,35º,45º,60º and 80º degrees) 33
Figure 5-6 Factor of safety (FoS) for fine grained soil, (20m with 27º,35º,45º,60º and 80º degrees) 33
Figure 5-7 Factor of safety (FoS) for fine grained soil, (30m with 27º,35º,45º,60º and 80º degrees) 34
Figure 5-8 Changes in Factor of safety (FoS) during 20mm/day rainfall for 10m 20m and 30m height with 27º,35º 45º,60º and 80º degrees) t=0 34
Figure 5-9 Changes in Factor of safety (FoS) after20mm/day rainfall for 10m 20m and 30m height with 27º,35º 45º,60º and 80º degrees) t=12 35
Figure 5-10 Change in pore water pressure vs vs slope with different height and angles after 20mm/day rainfall at t=12 days 35
Figure 5-11 Change in factor of safety vs slope with different height and angles after 20mm/day rainfall at t=12 days 36
Figure 5-12 Factor of safety (FoS) for coarse grained soil, (10m with 27º,35º and 45º degrees) 37

Figure 5-13 Factor of safety (FoS) for coarse grained soil, (10m with 27º,35º and 45º degrees) 37
Figure 5-14 Changes in Factor of safety (FoS) during 20mm/day rainfall for 10m and 20m height with 27º,35º and 45ºdegrees at t=0 38
Figure 5-15 Changes on factor of safety (FoS) after 20mm/day rainfall for 10m and 20m height with 27,35 and 45 degrees at t=12 days 38
Figure 5-16 Change in pore water pressure vs slope with different height and angles after 20mm/day rainfall at t=12 days.....39
Figure 5-17 Changes in Factor of safety (FoS) during 20mm/day rainfall for 10m and 20, height with 27º,35º and 45ºdegrees 39

LIST OF TABLES

Table Table 4-1 Laboratory tests based on ASTM standards 12
Table 5-1 Summary of index properties of fine grained (MH) and coarse grained SM soil.... 24
Table 5-2 particle size of Sandy silt soil 25
Table 5-3 Particle size of silty sand soil 26
Table 5-4Best fitting parameters for silty sand bimodal soil SWCC. 28
Table 5-5 Best fitting parameters for sandy silt bimodal soil SWCC. 28
Table 5-6Coarse grained soil (SM) shear strength data for slope stability. 30
Table 5-7 Fine grained soil (MH) shear strength data for slope stability. 31

List of PUBLICATIONS

A. Satyanaga, A. S. Mohammad, A. B. Ibrahimi, M. Wijaya, S.-W. Moon and J. Kim (2023). "Direct and indirect methods in determination of water retention curve of residual soils. 17ARC conference Astana Kazakhstan.

A. Satyanaga, A.S. Mohammad, R. Abishev, S.W. Moon and J.R. Kim (2023). "Stability of fine-grained soil slope with bimodal soil-water characteristic curve" Engineering Geology.

A. Satyanaga, A. S. Mohammad, A. B. Ibrahimi, A.H. Hamdany, M. Wijaya ,S.-W. Moon and J. Kim (2022). "Water Characteristic Curve for Soils in Kazakhstan. Geotechnical Engineering Journal of the SEAGS & AGSSEA.

Chapter 1 - INTRODUCTION

1.1 Background

This study represents the master's dissertation research work. It contains the key points of the research's problem statement, hypotheses, literature review, applicable theories, research methodology, the thesis's result, and discussion. Overall, it includes an introduction to the factors affecting stability of dual porosity soil slopes in order to evaluate the variations of factor of safety and pore water pressure for Silty sand and Sandy silt soils with bimodal SWCC and bimodal permeability functions under heavy rainfall. In previous studies, rainfall has been identified as the primary cause of landslides. (Kristo, Rahardjo and Satyanaga, 2017) and (Rahardjo et.al 2007). It is predicted that landslide events have caused more than 62,000 deaths and a cost of approximately $9.7 billion US dollars globally since the early 20th century (Lai et.al 2018). Therefore, it's necessary to know the features, functions, and processes of the dual porosity slope's stability under heavy rainfall and also the relationships between the factors of safety and pore water pressure in Almaty, Kazakhstan. The dissertation work focuses on laboratory testing and numerical analyses based on the finite element method (FEM) and limit equilibrium method.

Many factors influence slope stability or cause land sliding around the world, especially in residual soil regions due to the changes in unsaturated soil stiffness produced by frequent heavy rain. The stability of these slopes is heavily influenced by matric suction, or by mean negative pore-water pressure (Fredlund and Rahardjo 1993). That can cause landslides or other environmental hazards. Previous studies show that the presence of mountainous regions in the southeastern areas of Kazakhstan is especially vulnerable to landslides (Baimakhan et.al 2020). Heavy rains, snowing, glacier melting, floods, tremors, landslide-prone forest cover, and soil structure are all common landslide causes in the country. Figure.1-1 represents Kazakhstan's landslide risk (ThinkHazard, 2020). Therefore, extensive temporary seepage analyses are required in the development of slope preventive measures for determining the impact of rainwater pressure on slope stability while partially saturated. Many researchers working on residual soils have found that some residual soils have gap-graded properties with dual-mode soil water characteristic curve (SWCC) and dual-mode unsaturated permeability (k_w) (Zhai et., al 2017, 2020; Satyanaga et al., 2013; Rahardjo, Kim and Satyanaga, 2019). Until now, nearly no numerical evaluations of slope stability have considered the dual mode soil water characteristic curve of a dual-porosity soil slope.

The main aim of this research work is to study the stability of dual-porosity fine and coarse grained soil slopes associated with dual mode (SWCC) and dual-mode unsaturated permeability (k_w) functions using laboratory testing and numerical analyses. Additionally, to investigate factors influencing the factor of safety and pore water pressure of dual-porosity soil.

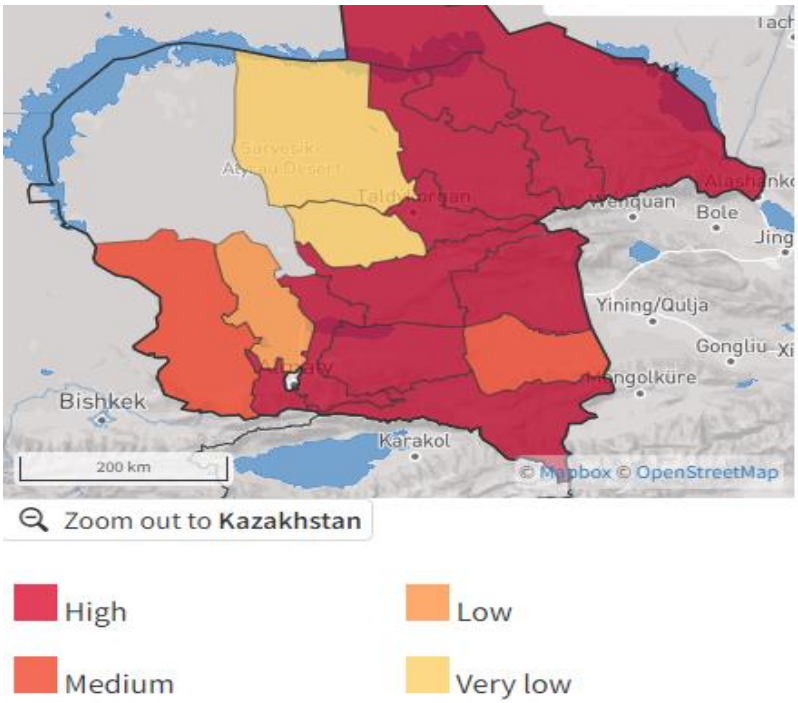

Figure 1-1 Almatinskaya landslide risk in Almaty Kazakhstan (ThinkHazard, 2020)

1.2 Problem statement

Many variables impact slope stability across the world, particularly in residual soil regions, due to the changes in unsaturated soil stiffness generated by regular high rainfall, snowfall, and underground water table. As a result, it can cause land-sliding and other environmental issues shown in figure 1-2. Besides that, only limited research has been done on this particular correlation to classify the factors that affect the dual porosity soil slope.

Figure 1-2 Stability of dual porosity soil slope

1.3 Hypotheses

The expected target of this research was to study the features, functions, and processes of slope stability under heavy rainfall with different slope geometries and how to simulate the stability of slopes during prolonged precipitation, groundwater tables, and slope geometries.

1.4 Objectives

- After consideration of the research hypotheses, the following main objectives were created.
- To investigate the effects of slope geometry (i.e. slope height and slope angle) on dual porosity soil slope.
- Characteristics of dual porosity soil slope associated with soil water characteristic curve (SWCC) and dual-mode unsaturated permeability (k_w).
- Experimental works in laboratory on fine grained and coarse-grained dual porosity soil.
- Obtaining the result of SWCC and k_w for dual porosity soil using Hyprop test.
- Seepage and stability analyses of soil slope with fine grained and coarse-grained dual porosity soil.
- Analyses of the factor of safety with respect to different slope geometry.
- Relationship between the factor of safety and pore water pressure for slope with fine grained and coarse-grained dual porosity soil.

Chapter 2 - Literature review

2.1 Rainfall-induced landslide

Numerous kinds of research have been carried out worldwide to look into the complicated relationship between slope stability and rainfall variability. They discovered that the type of rainfall, intensity, and recovery time significantly affected variations in pore-water pressures in an unsaturated sliced slope (Leong, Rahardjo and Satyanaga, 2011). For example, in Umbria, Italy, it was discovered that the probability of landslides remained stable throughout the warm-dry season; however, during the cold months, landslide incidents rose significantly when annual rainfall and quantity increased (Brocca et al., 2016). The instability of the slope happens when the slope's shear stress is higher than its shear strength. Precipitation patterns may influence initial water conditions, such as absorption and evapotranspiration, affecting groundwater pressure. The southeastern part of Almaty, Kazakhstan, is especially vulnerable to landslides such as the Ak Kain avalanche that happened in April 2004, shifting nearly a million tons of rock mass from the steep hill. It destroyed some multi-story residential buildings and killed 28 people. (Baimakhan et al., 2020). Another landslide called Kol Sai happened 300 km away from Almaty in April of 2018 when an avalanche mass of about 50 million tons, 900 m long and 177 m wide, moved rapidly for around five days (Baimakhan et al., 2020). In the early spring of 2017, 64 occurrences of uncontrolled avalanches happened in Almaty's eastern area, while in May, 35 landslides were reported as a result of rapid climate change, melting snow, and strong rainfall (Baimakhan et al., 2020). The Ak Kain and Kol Sai landslides were also caused by the high intensity of rainfall that had been falling for several days in a row (Baimakhan et al., 2020). However, advanced numerical simulation methods, computational equations, computer animation, and digging super-apparatus boreholes toward the foundation rock have not yet been used to analyze the current avalanche status of these mountains (Baimakhan et al., 2020).

2.2 Unsaturated soil mechanics

Unsaturated soil is a type of soil that includes four components: solid, water, air, and a contractile layer. Besides that, unsaturated soil has three main zones: dry soil, a two-phase zone, and a capillary zone. Hence, the pore-water pressure is negative and associated with air permeability (Zhai and Rahardjo, 2012; and Rahardjo et.al 2012). Therefore, to analyze the performance of unsaturated soils in geotechnical engineering design, it is necessary to consider

two stress controller parameters, which are net normal stress (σ-u_a) and matric suction (u_a-u_w), where σ shows the total stress of soil, ua is the total pore-air pressure, and uw is the total pore-water pressure in slope geometry (Rahardjo et.al 2012). Numerous researchers have looked into the role of pore water pressure in the load-carrying capacity of unsaturated soil (sand-bentonite mixtures). (Rahardjo et.al 2012 and Rahardjo et.al 2019). They found that the carrying capacities of coarse- and fine-grained unsaturated soils are dramatically different, necessitating distinct methods (Vanapalli and Oh, 2010). Therefore, estimating applied stress in the substantial structure is required as a first step in the mechanical parametric research of multi-phase porous materials (Huyghe, Nikooee and Hassanizadeh, 2017).

Many dual porosity soil slope observe within unsaturated conditions. Therefore, the unsaturated soil mechanic principles are necessary for design and analyses of dual porosity soil slope. In addition, the amount of rainfall in slope surface infiltrated within dual porosity soil. Hence, unsaturated soil changes volume and loses shear strength. Thus there should be a proper characterization of dual porosity soil to insure a high a curacy of unsteady state saturated, unsaturated flow situations, flux boundary conditions, and slope stability result from seepage and slope stability analyses.

2.3 Dual-porosity soil

Only limited researches attempts have been performed to develop hypothetically relevant formulation for the SWCC of dual porosity soil. The concept of dual porosity was derived from the oil and gas sectors in civil and environmental engineering. Then they discovered that sediments with dual-mode porosity had a considerable impact on water migration, particularly in the case of two-phase immiscible fluxes (Ng et al., 2003). A soil with dual porosity is modelled as a combination of aggregated particles, where each aggregation is composed of micro and macro particles that have been linked to each other, the linked spaces among particles within aggregates are accepted to be very excessively smaller in comparison to the overall surface area of the particles (Russell, 2010). Due to the aggregated character of the soil or the existence of cracks, stem paths, or insect pores, many innate and constructed soils display two separate pore sets (Russell, 2010). Therefore, for the characterization of dual porosity, fractals have been used in previous studies to describe particle and pore size distributions (Russell, 2010). The hypotheses are applied when the particle combination of soil is sand, silt, and clay-sized particles, on this case the portion of the silt and sand particles may develop coatings made of clay particles (Russell, 2010).

In previous research, scientists experimented on residual soils and found that some residual soils have gap-graded properties with dual-mode soil water characteristic curves and dual-mode unsaturated permeability (Zhai et al., 2020). The pattern of SWCC is comparable to the pattern of unsaturated permeability (k_w), according to (Chapuis et al., 2006). As a result, using the porous structure distribution principle, the unsaturated permeability may be estimated from the water retention curve (Chapuis et al., 2006). Because the finite element analysis in transient seepage investigations typically requires statistical information on unsaturated permeability. According to (WOOD et al,.2010) the regular mechanical and chemical processes that produce soil result in a cyclic pattern of crystallite size, with tiny particles tightly compacted around bulk materials. Realizing that the same particle shape might result in a range of high porosity patterns, obviously, it depends on how the soil was developed and its loading chronology. Therefore, any hypothetical statement for a soil-water characteristic curve (SWCC) should include high porosity features. Previous research by (Zhai et al., 2020), Russell 2010; (Chapuis et al., 2006) and many others characterized that some residual soils are associated with gap-graded grain-size distribution. Whereas this particular soil has dual-porosity characteristics. Additionally, soils with gap-graded grain-size distribution can be associated with unimodal or bimodal soil-water characteristic curves, and the stability of slopes with dual-porosity soil is different from that of a mono-modal soil slope.

2.4 Seepage and stability analyses

The concept of slope stability can be defined by shear strength, pore water pressure, and soil structure: how much load (stress) can a slope manage before collapse. Therefore, a mathematical formulation is required for the correct soil water characteristic curve because it allows researchers to make seepage assessment and calculation of many other water saturation qualities easier for geotechnical design (Fredlund et al. 2012). (Wijaya and Leong, 2016) divided the dual-model mathematical formulas for the soil water characteristic curves (SWCCs) into three categories. The combining point of mainly two curves was randomly selected in the very first group of equations, and the matching values of two or more sub-curves of the SWCCs were separately derived (Wijaya and Leong, 2016). The moisture content of complex and multi-pore under fluid conditions was detached in the second category of equations, and the appropriate variables of mainly two curves of the soil water characteristic curve were acquired instantaneously (Wijaya and Leong, 2016). It should be noted that the empirical equation proposed by (Fredlund and Xing 1994) is applicable only for well-graded and poorly-graded

soils. For gap-graded soil, (Satyanaga et al,.2013) proposed an equation that is subsequently used to match a curve called bimodal SWCC (Satyanaga et al, 2022)

Chapter 3 - Applicable theories

3.1 Bimodal Soil-water characteristic curve

The soil water characteristic curve (SWCC) can be determined directly using various in-situ and/or scientific experiments, but they are expensive and time-consuming. For the fine-grained soil in the unsaturated zone, matric suction (u_a-u_w) and shear strength exist, which create stability and strength in the soil. However, due to the rainfall intensity and infiltration, the matric suction changes its sign from negative to positive, and the soil loses its shear strength as the results generate a landslide or slope failure (Qian and Rahardjo, 2016). Hence, to study the degree of saturation (S%), the factor of safety, and pore water pressure and their relationship, we need to produce an SWCC of soil at different heights. Therefore, the SWCC of dual porosity soil, Satyanaga's best-fitting equation (1), is utilized to determine the bimodal properties of the soil. (Satyanaga et al., 2013).

$$\theta_w = \left[1 - \frac{ln\left(1+\frac{\psi}{C_r}\right)}{ln\left(1+\frac{10^6}{C_r}\right)}\right]\left[\theta_r + \left\{(\theta_{s1} - \theta_{s2})\left(1 - (\beta_1)erfc\left(\frac{ln\left(\frac{\psi_{a1}-\psi}{\psi_{a1}-\psi_{m1}}\right)}{s_1}\right)\right)\right\} + \left\{(\theta_{s2} - \theta_r)\left(1 - (\beta_2)erfc\left(\frac{ln\left(\frac{\psi_{a2}-\psi}{\psi_{a2}-\psi_{m2}}\right)}{s_2}\right)\right)\right\}\right] \quad (1)$$

Where:

θ_{s1} = saturated volumetric water content

θ_{s2} = volumetric water content related to air-entry value 2

β_1 = 0 when $\psi \leq \psi_{a1}$; β_1 = 1 when $\psi > \psi_{a1}$

β_2 = 0 when $\psi \leq \psi_{a2}$; β_2 = 1 when $\psi > \psi_{a2}$

ψ_{a1} = parameter related to air-entry value 1 (kPa)

ψ_{a2} = parameter related to air-entry value 2 (kPa)

C_r = input parameter according to Fredlung and Xing (1994) (kPa)

e_{rfc} = the complementary error function, $e_{rfc} = \int_{-\infty}^{x}, \frac{1}{\sqrt{2\pi}} exp\left(-\frac{x^2}{2}\right) dx$

ψ_{m1} = parameter related to suction at the inflection point 1

ψ_{m2} = parameter related to suction at the inflection point 2

θ_r = parameter related to volumetric water content at the residual condition

s_1 = parameter related to standard deviation 1

s_2 = parameter related to standard deviation 2

The subscripts 1 and 2 in the formula correspond to the dual-porosity soils' sub-curves 1 (macro pores) and 2 (microspores), respectively (Satyanaga et.al 2013). Basically there are so many equations for generating of bimodal SWCC and unsaturated permeability functions but each parameter in (Satyabaga et al., 2013) equations represents the physical properties of SWCC and unsaturated permeability.

The correlation between volumetric water content and negative water pressure in the soil is defined by the specific soil-water characteristic curve (SWCC). Many unsaturated soil parameters, such as porosity function and unsaturated shear strength, can be calculated using SWCC and (Goh et.al 2012) equations (Zhai et.al 2017). Hence both soil water characteristic curve (SWCC) and the permeability function were determined by Satyanga statistical method, and indeed the data best associated with the problem.

3.2 Bimodal unsaturated permeability

Experimental and field tests should be conducted for the determination of saturated permeability (k_s) and unsaturated permeability (k_w) functions for specified dual-porosity soils. In this study, for the unsaturated permeability function statistical method was used, which establishes the correlation between hydraulic conductivity and matric suction, is extremely crucial for seepage analysis in unsaturated soil water flow. On the other hand, since actual experimental testing is expensive and time-consuming, SWCC has been shown to have both unimodal and bimodal properties (Zhai et al. 2017). In this paper, the estimation method of Satyanaga et al. (2022) formula (1-2) and experimental test (Constant head for saturated permeability and unsaturated permeability based on the statistical method) were used to determine the permeability function of unsaturated fine grained and coarse grained soil shown in (figure.5). The following equation (2) presents the bimodal dual-mode permeability function.

$$k_w = (k_{s1} - k_{s2})\left(1 - erfc\,\frac{ln\left(\frac{\psi_{a1}-k_w}{k_{a1}-k_{m1}}\right)}{s_{k1}}\right) + (k_{s2})\left(1 - erfc\,\frac{ln\left(\frac{\psi_{a2}-k_w}{k_{a2}-k_{m2}}\right)}{s_{k2}}\right) \quad (2)$$

Where:

s_k = parameter related to geometric standard deviation of permeability function

k_m = parameter associated with matric suction within inflection point

ψ_a = parameter associated with air-entry value of soil obtained from water retention curve

k_w = coefficient of permeability for different suction

ψ = designated matric suction

k_s = measured saturated permeability from laboratory testing

The variables 1 and 2 in the equation, respectively, are related to soil macro-pores and micro-pores with dual-mode water retention curves.

3.3 Bimodal Unsaturated shear strength

Several investigations have been conducted to establish formulas for unsaturated soil shear strength. The majority of the calculations, however, are only applicable to specific soils with unimodal (single porosity) soil-water characteristic curves (SWCCs) (Rahardjo et.al 2019). To verify the suggested formula, numerous sets of unsaturated stabilized triaxial experiments were performed on statically crushed aggregate samples (sand and kaolin). In this study, a modified triaxial laboratory test was used to determine the shear strengths of the fine-grained soil and coarse grained soil. The dual-mode porosity soils' impactful cohesion c′, functional friction angle ϕ', and an angle that demonstrates the rate of changes in shear strength relative to an alteration in pore water pressure ϕ^b were determined using consolidated undrained-triaxle tests with Matric Suction measurements. The experimental values from the triaxial trial in the early phase were determined them by using the following mathematical equation (3-9) we found the total shear strength of the investigated soil.

$$\tau = c' + [(\sigma - u_a) + AEV1] \tan \phi' + [(u_a - u_w) - AEV1]\, b_1 \Theta\, k_1 \tan \phi' \quad (3)$$

$$k_1 = [\log (u_a - u_w) - \log AEV1]^{y} \quad (4)$$

$$b_1 = -0.245\ \{\ln [S_1 (Ip + 4.4)]\}^{2} + 2.114\{\ln [s1 (Ip + 4.4)]\} - 3.5 \quad (5)$$

$$\tau = c + (\sigma - ua) \tan \phi' + AEV2 \tan \phi^{b2} + [e \times (u_a - u_w) - (0.2 + fines) \times AEV2]\, b_2 \Theta^{k2} \tan \phi' \quad (6)$$

$$k_2 = [\log (u_a - u_w) - \log AEV2]^{y} \quad (7)$$

$$b_2 = -0.245\ \{\ln [S_2 (Ip + 4.4]\}^{2} + 2.114\{\ln [\ S^2 (Ip + 4.4)]\} - 3.522 \quad (8)$$

$$y = 0.502 \ln (Ip + 2.7) - 0.387 \quad (9)$$

Where:

τ = shear stress

σ = total normal stress

u_w = pore-water pressure

u_a = pore-air pressure

c'= impactful cohesion

$\sigma - u_a$ = net normal stress

$u_a - u_w$ = matric suction

ϕ'= friction angle

AEV_n = air-entry value of soil (kpa)

Ip=plasticity index

S_1 and S_2 = standard deviation related to sub-curves 1 and 2 from SWCC

y and b = fitting parameters.

Fines= percentage of fine soil.

Chapter 4 - Research Methodology

4.1. Laboratory testing

In this research work two sets of soils (60% sand with 40% kaolin as coarse-grained and 40 % sand with 60 % kaolin as fine-grained are used in laboratory and numerical analyses, the procedure and determination of soil physical and hydrological properties are based on ASTM standard.

Table 4-1 Laboratory tests based on ASTM standards

Test Name	ASTM Standard
Proctor method	ASTM D698-12(2021).
Atterberg Limits	ASTM D4318-17e1
Soil classification	ASTM D2487-00
Grain size distribution	ASTM D7928
Constant head	ASTM D2434-22
Shear strength (Triaxial)	ASTM D4767-11(2020)

4.1.1 Proctor method

Previous researches (Aragón et al., 2000) shows that the standard proctor method is a very widely used and accepted technique to examine how well-disturbed soils compact under a variety of soil water contents and typical dynamic stress. The moisture level at which the highest dry density is obtained is regarded as the optimum moisture content for fine- and coarse-grained soil. Hence, in this research work, the Proctor method was used to determine the maximum dry density of soil based on ASTM D698-12 (2021). For the compaction test to examine the compatibility of sand and kaolin with optimum water content for different percentage soil mixer, moisture content cans, a compaction hammer of 60 kN/m^3, Digital balance, Spray bottle, Metal spoon, Knife, Steel straightedge, and the oven was used shown in the following figure 4-1. A soil sample is compacted in a cylindrical mold with a defined height and weight for the standard proctor test. The soil specimen is compacted by a standardized hammer with 60KN/m3 weight in three layers, with each layer receiving a predetermined 25 number of blows. The number of strikes required is determined by the type of soil being examined as well as the amount of compaction energy required to attain the target density. The

mold is withdrawn when the last layer is compacted, and the soil sample is weighed and measured to determine its volume and maximum dry density.

However, the proctor approach has significant limitations. One of the key constraints is that it is a laboratory test and may not precisely represent the behavior of the soil in the field. Soil in the environment may be subjected to varying compaction strengths or water content, which might influence its qualities. Furthermore, the proctor test does not provide the impacts of time or loading history on soil parameters, which can be crucial in the engineering field.

Figure 4-1 The process of proctor test for determination of maximum dry density.

4.1.2 Specific gravity

The specific gravity of soil is an essential physical characteristic by which we can estimate its porosity, void ratio, and compaction rate. That's why these properties of the investigated soil specimen are very important for the design and assessment of the stability of slopes. Therefore, in this research work, the volumetric flask method is used, which is a more accurate technique that measures the amount of water that is evacuated by a particular mass of dry soil using a volumetric flask. The procedure of the test is that a fixed quantity of dry soil is prepared for the volumetric flask, which is then filled with water up to a defined mark. The water volume is then measured after the flask has been shaken to remove any tiny bubbles. The mass of the dry soil is divided by the difference between the volume of the flask and the volume of the water to determine the specific gravity of the soil. Later on, bulk density, dry density, and water content can be easily defined from specific gravity.

4.1.3. Index properties by Atterberg limit

The Atterberg limit is a very common method for determining the liquid limit (LL), plastic limit (PL), and plasticity index (PI). It was established by Albert Atterberg at the start of the 1900s and is currently widely used for the classification of soil (Zhao et al., 2008).

However, a study by (O'Kelly, 2015) shows that the Atterberg limit can't be applied to peat soil. In this research work, liquid limit and plastic limit tests were done based on ASTM D4318-17e1. For successful examination of sand and kaolin specimen properties, a soil mixer, moisture content cans, a spoon, electronic automatic Casa-Grande equipment, a roller, an oven, and a digital balance are necessary equipment. Later on, using these properties (LL, PL, SL, and PI), we can easily define the investigated soil classification. The process of Atterbeg limit is shown in the following figure 4-2.

The liquid limit (LL), plastic limit (PL), shrinkage limit (SL), and plasticity index (PI) are the four Atterberg limits that are used to anticipate how soils would behave in certain situations. These limits were established by conventional laboratory experiments. It allows engineers and geologists to design structures that are secure and stable while also ensuring that soils are used sustainably and responsibly by understanding the Atterberg limitations.

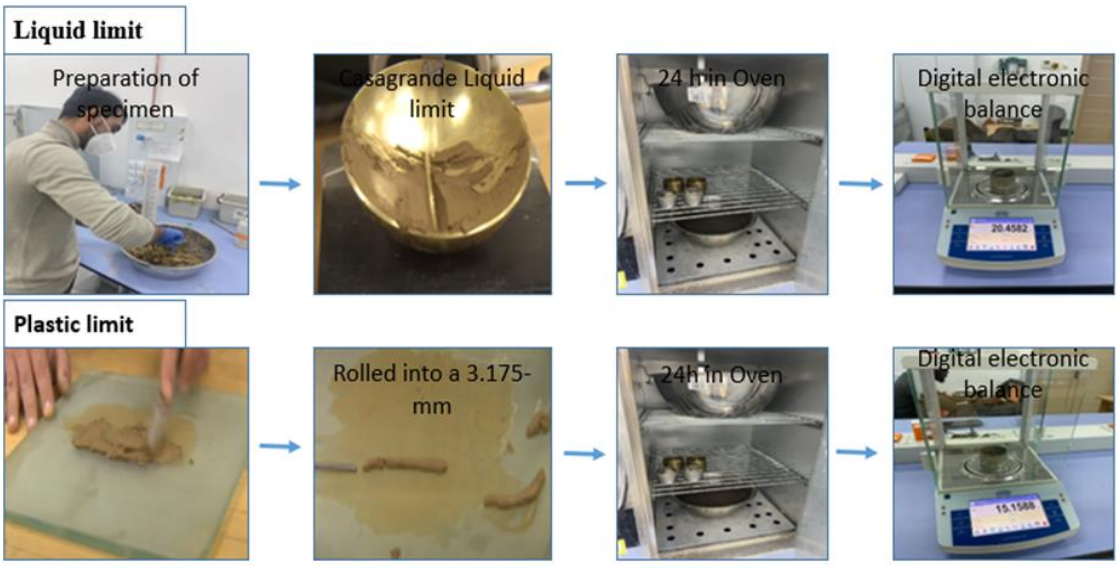

Figure 4-2 The process of Atterberg limit for determination of LL, PL and PI

4.1.4 Gran size distribution (GSD)

As it is known, fine-grained soil particle size distribution can't be determined by sieve analysis. Therefore, it was necessary to do hydrometer analyses, which are a very simple and accurate way to determine the grain size distribution from 0.075mm to 0.001mm for fine-grained soil, and for soil with a particle size of more than 0.075 mm, sieve analysis was used. For the creation of a complete gradation grain size distribution curve hydrometer analyses were combined with sieve analyses. For the determination of the GSD Mixer (blender) balance control, cylinder, Hydrometer (152H model preferably, dispersing agent (sodium silicate (NaSiO3), sedimentation cylinder (1000 mL) thermometer, beaker, timing device and graduated 1000 mL cylinder for control jar were used.

In this experiment, soil particles are suspended in water, and the rate at which the various-sized particles settle is measured. The obtained information is then utilized to categorize the soil using a standardized approach, or the Unified Soil Classification System (USCS). The GSD test was based on ASTM D7928, as shown in Figure 4-3. Additionally, soil classification was carried out based on the Unified Soil Classification System (USCS) according to ASTM D2487-00. Additionally, to acquire a more thorough PSD of a soil specimen, these techniques are frequently combined in practice. To measure the larger particle sizes, for instance, sieve analysis might be employed, whereas hydrometer analysis might be used to assess the smaller particle sizes. A more accurate depiction of the PSD of the soil sample can then be made by combining the results.

Figure 4-3 Sieve and hydrometer analyses

4.1.5 Saturated permeability Using Constant head

An essential element of hydrogeology is the constant head saturated permeability, which is used to calculate the rate of groundwater flow through a porous media. (Bear, J. 1979). For the determination of saturated permeability, a constant head permeability test was performed. The process of constant head permeability means that water is forced through a spherical soil sample column as part of the steady flow permeability test while the pressure differential is maintained at a fixed level. The test was based on ASTM D2434-22, shown in the following figure 4-4. The testing device has an output reservoir and a customizable constant head reservoir that allow a steady head to be maintained throughout the test. De-aired water at a consistent temperature is utilized for testing. Another feature of the permeability cell is a loading piston that may be used to deliver consistent axial stress to the material throughout the test. In this study, the unsaturated permeability of fine and coarse-grained soil is frequently assessed using the falling head permeability test. It allows us to understand how water moves through an aquifer's unsaturated zone, the region above the water table (Chapuis et al., 2006). However, its time consumable and expensive therefore for accurate result statistical method was used.

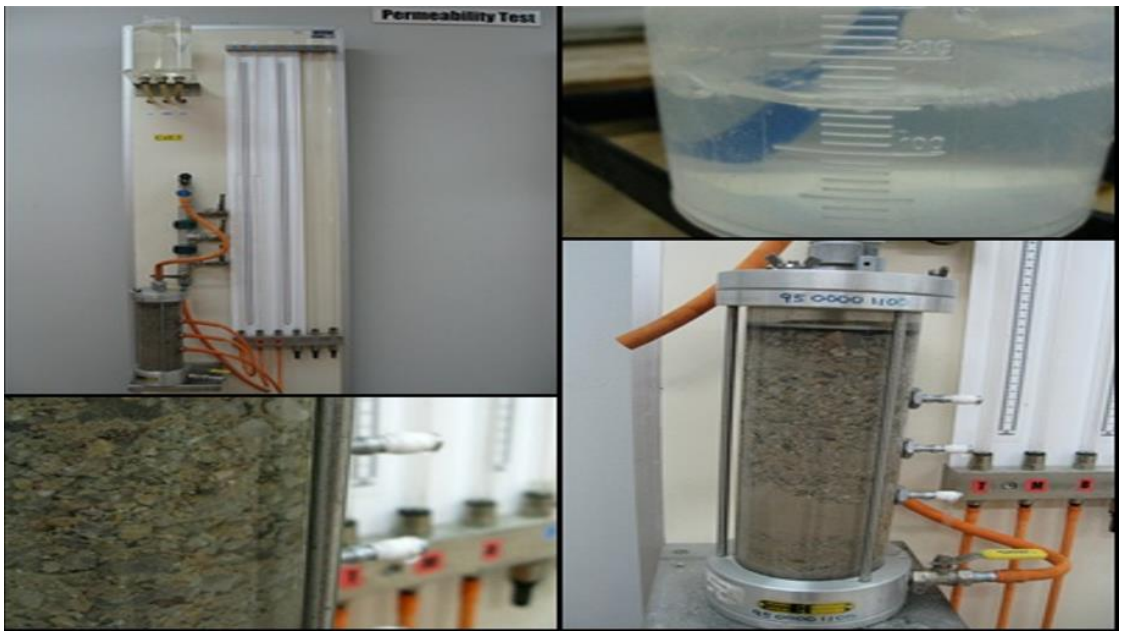

Figure 4-4 Constant Head Permeability Test

4.1.6 Shear strength Using Triaxial test.

The capacity of unsaturated soil to withstand deformation under load is known as shear strength. It is influenced by several variables, such as pore water pressure, moisture content, and soil composition in different layers. Due to the lack of water in the soil matrix, which lessens the cohesion and interlocking forces between the soil particles, unsaturated soil generally has a lower shear strength than saturated soil. However, the shear strength can also be impacted by the presence of water in unsaturated soil (Kim & Borden, 2011). Therefore, for the determination of shear strength properties, a consolidated undrained test was used. For the triaxial test, the soil specimen was prepared with a 50 mm diameter and 100 mm height, the soil sample was covered vertically by a thin rubber membrane to encapsulate the specimen, and then the cylindrical soil sample was subjected to radial stresses (constricting pressure) and gradually increasing longitudinal stresses, or axial displacements, during the conventional triaxial test. The test has three main stages, including saturation, consolidation, and shearing. The test was performed based on ASTM D4767-11 (2020), as shown in the following figure.4-5.

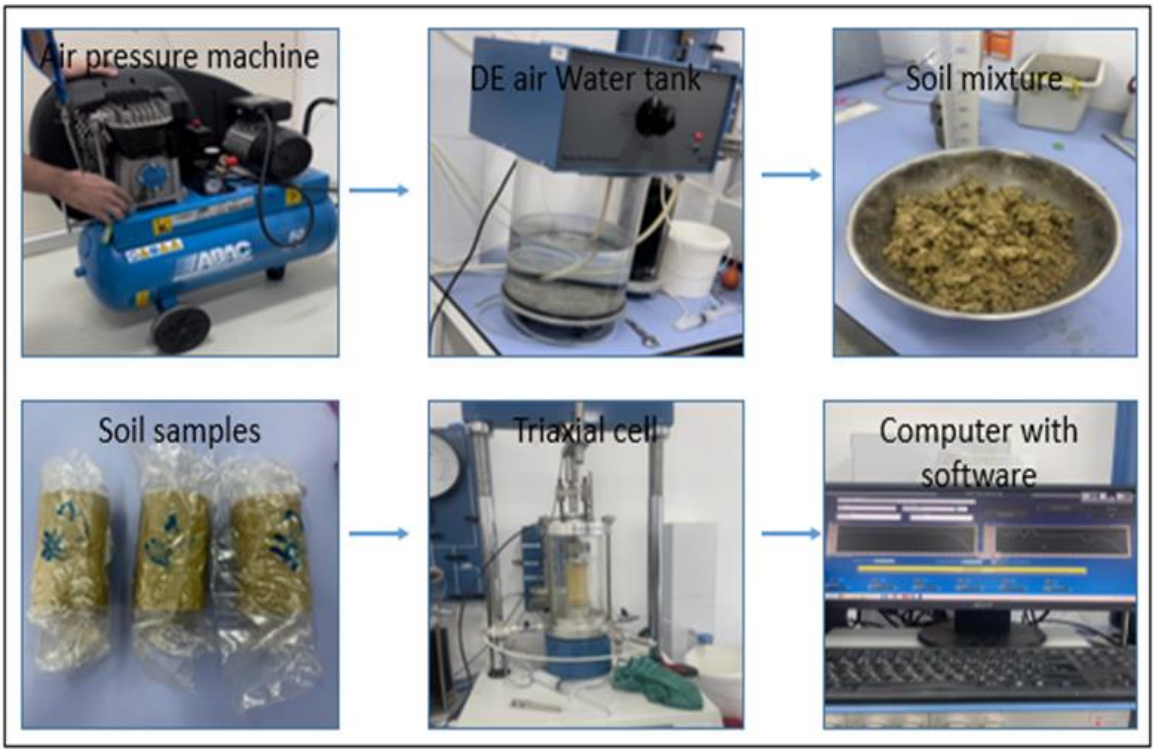

Figure 4-5The process consolidated undrained triaxial test

4.1.7 SWCC of fine grained (MH) and coarse grained (SM) soil.

In this study, the SWCC of the investigated specimen was obtained using Hyprop. The Hyprop test is based on the evaporation method developed by Wind (1966) and simplified by Schindler (1980). Specimen for Hyprop was prepared using a 250cm^3 metal ring, which had a diameter of 8 cm and a height of 5 cm. The soil was divided into 3 portions of equal mass and compacted into 3 layers in the metal ring using a tamper. The investigated soil for fine-grained (MH) soil consisted of 40% sand and 60% kaolin and for coarse-grained (SM) soil 60% sand and 40% kaolin compacted at dry optimum with a dry density for (MH) 1.59 Mg/m^3 and water content of 22.8 % for (SM) with a dry density of 1.84 Mg/m^3 and water content of 15% following a study by (Satyanaga et al, .2013

The working procedure of Hyprop is based on a continuous evaporation process over time. There are a few steps to conducting the SWCC test using Hyprop. The first step of using Hyprop is degassing the ceramic disc. Two basic methods can be utilized concerning this step: using syringes and using Hyprop degassing equipment. The second step is a saturation of the soil specimen; the soil should be saturated for at least 24 hours. The third step is connecting the Hyprop apparatus to electricity and linking it with a computer. While on the computer, it's necessary to install two software, which are Hyprop View and Hyprop Fit. The value we get from testing will be shown in the Hyprop view. Then we can take those values to Hyprop Fit to plot the SWCC for the particular soil. The process of the Hyprop test is shown in figures 4–6.

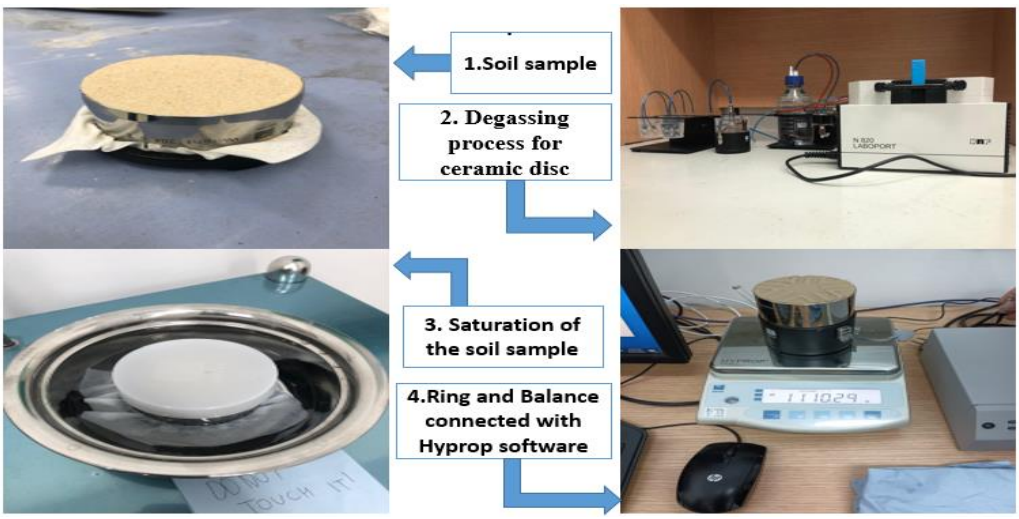

Figure 4-6 The process of Hyprop test for SWCC and unsaturated permeability

4.2 Numerical Analyses

An essential component of geotechnical engineering is slope stability analysis, which helps engineers to analyze the risk of slope failure and determine the integrity of a slope. In regions with steep slopes, like mountainous areas in the southeastern parts of Kazakhstan, slope failures can have serious repercussions, including loss of life and destruction of properties. This makes slope stability analysis particularly crucial in these situations. SEEP/W and SLOPE/W, two software tools created by Geo-Slope International Ltd. (2004–2012), are frequently used for slope stability analysis. Hence in this study, seepage and stability of dual-porosity soil slopes (fine and coarse-grained soil) with slope angles of 27, 35, 45, 60, and 80 degrees with slope heights of 10 m, 20 m, and 30 m were considered to analyze the impact of heavy rainfall and groundwater table on the factor of safety and pore water pressure. While a combination of 24 days starts from the initial time to 12 rainy days circumstances according to (Chepelianskaia et.al 2022; Beketova et al., 2019 and Weather and Climate, 2010), then 12 extra days without precipitation as dray periods were used to determine the factor of safety and pore water pressure.

4.2.1 Position of the ground-water table

The position of the ground water table depends on the region, geology, and climate, the groundwater table is naturally nearer the surface in areas with heavy rainfall or permeable soil structure. Thus groundwater table is often deeper in locations with low rainfall or impermeable soil structure. Previous research (Pradel, 2020) shows that the stability of slopes can be significantly impacted by the location of the groundwater level. The pressure that is applied by water on the slope surface when the groundwater table is high might increase the forces pushing on it. This could weaken the slope's stability and raise the probability of failure. On the other hand, the slope's soil may become dry and lose its cohesiveness when the groundwater level is insufficient, resulting in a greater vulnerability to erosion. In this study, the groundwater table was located 3–10 m below the ground surface, as suggested in previous research by (King et.al 1999). For soil slope in Kazakhstan, the parametric studies by (King et al. 1999) indicated that the groundwater table position within gap-graded soil is commonly observed at a deeper depth compared to that within well-graded or poorly-graded soil (King et.al 1999).

4.2.2 Seepage analyses using Seep/W

Seep/W can represent intricate geological and hydrological variables for complex geometries which is one of the primary characteristics of slope stability analyses. The software

helps to define heterogeneity, anisotropy, and changeable permeability as well as initial boundary conditions and evaluate the outcomes of various situations. Moreover, Seep/W has tools for examining slope and embankment stability as well as the relationship between groundwater and beneath infrastructure. SEEP/W is designed based on the unsteady state seepage equation for water within unsaturated soil zone such as the flow law of water or Darcy's law, Richards's equation, and Laplace's equations (GEO-SLOPE International Ltd.2004-2012). Presented in the following equations (10a-10b, 11, 12 and 13).

The unsteady seepage equation is incorporated into SEEP/W analyses (Fredlund et al. 2012):

$$\frac{d}{dx}\left(k_w \frac{dh_w}{dx}\right) + \frac{d}{dy}\left(k_w \frac{dh_w}{dy}\right) = m_2^w \rho_w g \frac{dh_w}{dt} \quad (10)$$

Where,

dx, dy = dimensions in the x-, y-directions, respectively,

m_2^w = water storage modulus,

h_w = hydraulic head (gravitational plus pore-water pressure head),

k_w = major coefficient of permeability with respect to water as a function of matric suction which varies in all directions due to the isotropic condition of soil,

dt = time derivative,

ρ_w = density of water,

g = gravitational acceleration.

Additionally, to model hydraulic conductivity and study the seepage analyses of slope stability, seep/w developers use these equations in conjunction with numerical techniques and finite element analysis. This allows them to visualize complicated geotechnical and environmental mechanisms and improve their design concepts for better efficiency and lower risk. Hence, in this research work for numerical modeling of the dual-porosity soil slope, the simulation software SEEP/W (Geostudio International Pte. Ltd., 2004a) was used to conduct two-dimensional seepage evaluations in Kazakhstan's Almaty region.

In this study, 29 sets of numerical analyses were conducted for dual-porosity soil with different slope geometries and different soil properties. The soil-water characteristic curve (SWCC) and hydraulic conductivity function (kw) were taken from experimental work in a laboratory. For the slope geometry, three main boundary conditions were assigned. The circumstances along

the constant left-head and right-head vertical borders were established as groundwater-level head boundaries; thus, the upper boundary was designated as a flux boundary (rainfall), whereas the bottom border was designated as a no-flow barrier or h_p=0. Therefore, according to the available data, the groundwater table can be assumed to be between 3 m and 10 m below the slope surface (King et.al 1999). For the flux boundary condition (q_x), the first 12 days of prolonged heavy precipitation with a daily rainfall intensity of more than 20 mm/day were assigned to the model according to (Chepelianskaia et.al 2022). A comprehensive numerical model from seepage analyses is shown in figure 4–7.

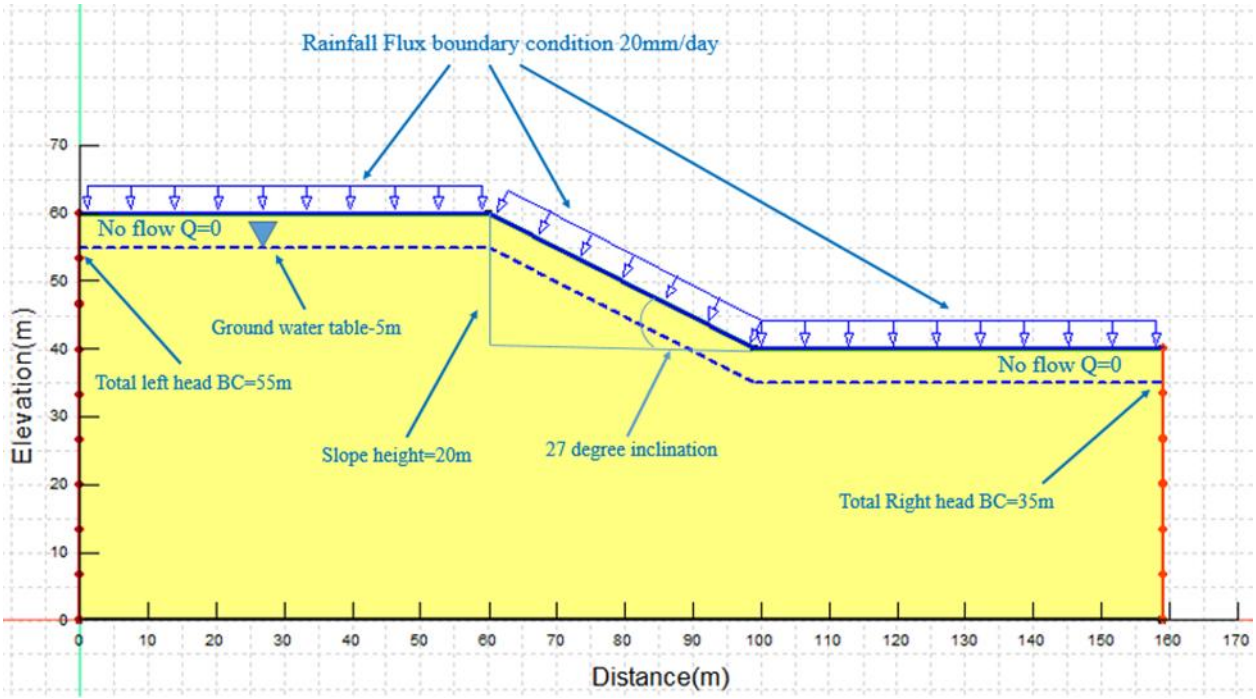

Figure 4-7Numerical model for seepage analyses or seep/w with a slope height of 20 m and slope degree of 27-degree.

4.2.3. Slope stability analyses using Slope/W

Slope/w was used for the slope stability analyses based on the Morgenstern-Price method because this method can satisfy both force and moment equilibrium. The Morgenstern-Price method is presented in equation (12). After seepage analyses, the same model was generated from seep/w to slope/w, which is also known as limit equilibrium. The slope stability analyses were performed with the incorporation of shear strength parameters taken from experimental work in the laboratory. Soil shear strength properties and grain Grain-size distribution properties are shown in (table 4-5).

After all setups Grid and radius methods are both used to create the slip surface for the investigated slope, the numerical model for 1 set of slope stability is shown in figure 4-8.

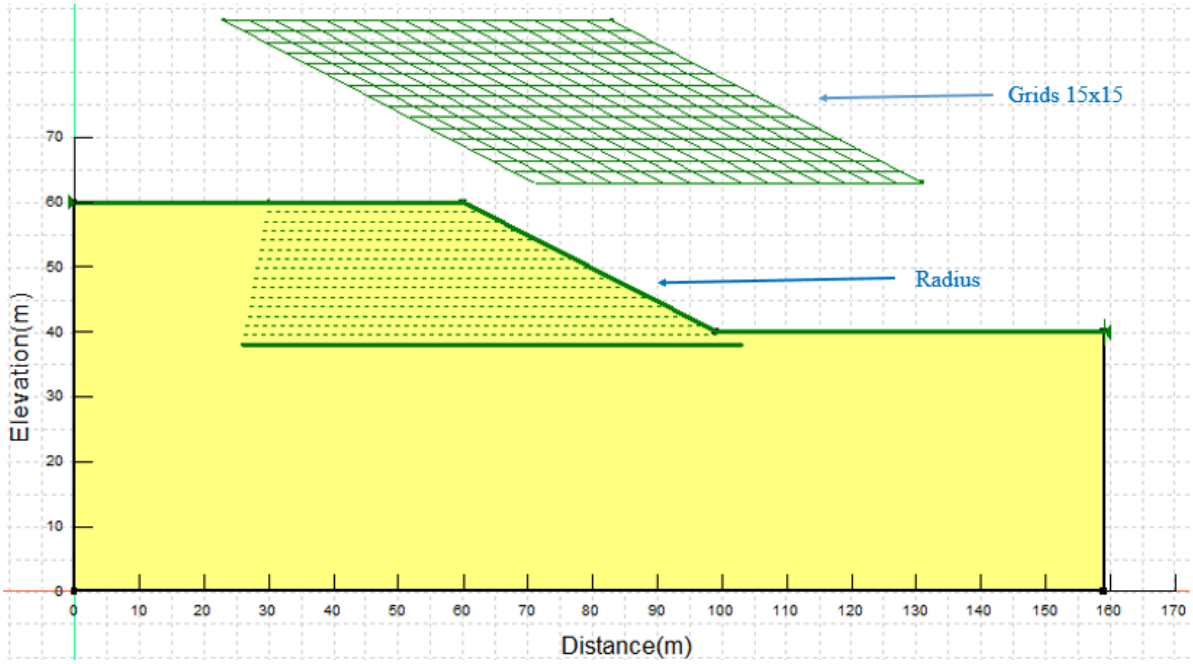

Figure 4-8Numerical model for slope stability analyses or slope/w with a slope height of 20 m and slope degree of 27-degree

The following (11–12) constitutive formulas are mathematical representations of the relationships between the stress state variables and the shear strength or volume change of unsaturated soils. In other words, they are used to characterize the mechanical behavior of unsaturated soils in terms of seepage and slope stability issues (Rahardjo et.al 2012).

Moment equilibrium equation;

$$Fm = \frac{\Sigma\left[Ć\beta R + \left\{N - uw\beta\frac{\tan\phi^b}{\tan\phi'}\right\}R\tan\phi'\right]}{\Sigma Wx - \Sigma Nf} \quad (11)$$

Force equilibrium equation;

$$Ff = \frac{\Sigma\left[Ć\beta\cos\alpha + \left\{N - uw\beta\frac{\tan\phi^b}{\tan\phi'}\right\}\tan\phi'\cos\alpha\right]}{\Sigma N\sin\alpha} \quad (12)$$

Where:

N = the sum of all ordinary force acting on the bottom of the slice.

β = the sloping length across a slice's edge

α = the angle between the parallel to the middle from each slice's bottom as well as the horizontal

f = the distance, measured perpendicularly, that the normal force is displaced from the origin of spin or the center of moments.

uw = pore-water pressure

x = the horizontal distance between each slice's midline and the center of spinning or the center of moments.

ϕ' = effective angle of internal friction

ϕ^b = angle representing the rate of improvement in shear strength with respect to matric suction

R = radius for round slip surface or moment arm linked with organized shear force, Sm, for any slip surface shape.

Chapter 5 - RESULTS

5.1 Result from laboratory

5.1.1 Index properties of unsaturated soil

A combination of 40 percent sand 60 percent kaolin as fine-grained soil and 60 percent sand with 40 percent kaolin as coarse-grained soil were prepared to generate the bimodal characteristics of the soil. The index properties of the investigated soils are shown in the table.5-1

Table 5-1 Summary of index properties of fine grained (MH) and coarse grained SM soil.

Index Properties	60%sand-40%kaolin	40%sand-60%kaolin
Specific gravity, Gs	2.62	2.60
Liquid Limit, LL (%)	41.2	48.9
Plastic Limit, PL (%)	24.8	28.2
Plasticity Index, PI (%)	16.4	20.7
Void Ratio, e	0.42	0.64
Dry density, ρd (Mg/m^3)	1.94	1.65
Water content, w (%)	10	18
Sand (%)	60.0	40.0
Silt (%)	32.8	52.4
Clay (%)	7.2	7.6
Soil classification according to USCS	SM	MH

5.1.2 Result from Proctor method

For the determination of the soil compaction curve, the proctor method was used, Figure 5-1 shows the correlation between soil water content and maximum dry density for various compaction efforts or energy consumption. For silty sand, the maximum dry density is 1.65 Mg/m3 with 18% water content, whereas for sandy silt soil to reach 95% of moisture content**,** the maximum dry density is 1.94 Mg/m3 with 10% water content. As a result, it shows that the dry density of silty sand soil is always lower than that of sandy silt soil.

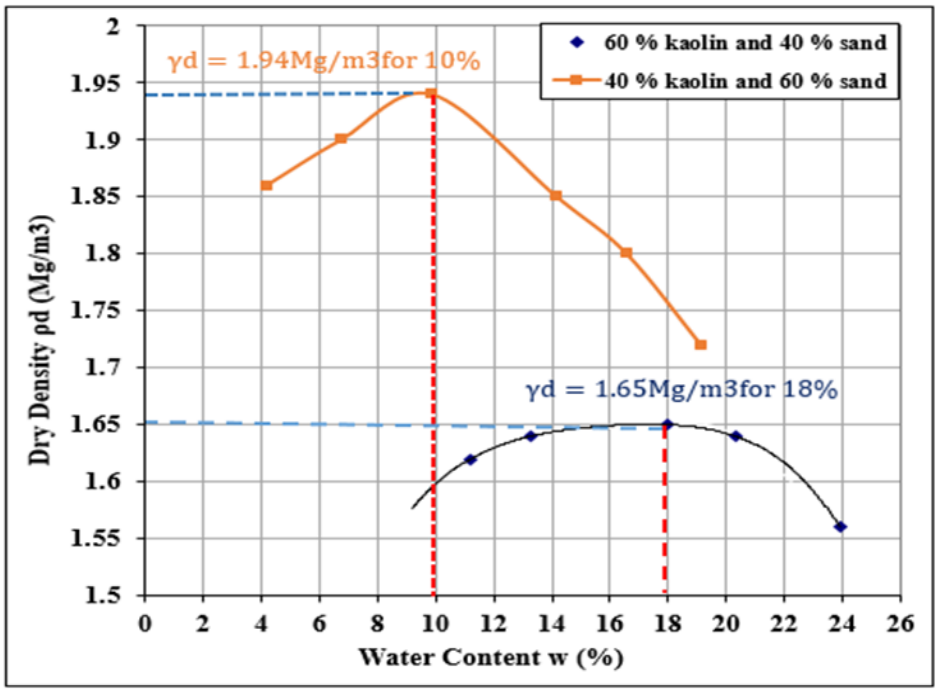

Figure 5-1 Compaction curve of fine and coarse grained soil

5.1.3 Particle size distribution (PSD)

For the classification of soil, the PSD method was used. Data from the sieve and hydrometer tests are shown in the following figure 5-2. Based on their size, soil particles are divided into three main groups: sand, silt, and clay. The biggest particles are coarse sand, which generally ranges in size from 0.07 to 4.75 mm. whereas fine sand particles are smaller and range in size from 0.002 mm to 0.425 mm, the tiniest particles of the analysis are clay particles with a diameter of less than 0.002 mm.

For determination of the coefficient of uniformity (Cu) and coefficient of curvature (Cc) for the investigated soil the data was taken from the following (tables 3-4) and figure 5-2.

Table 5-2 particle size of Sandy silt soil

Diameter	Size(mm)
D60	0.35
D30	0.005
D10	0.0018

Table 5-3 Particle size of silty sand soil

Diameter	Size(mm)
D60	0.15
D30	0.0028
D10	0.0013

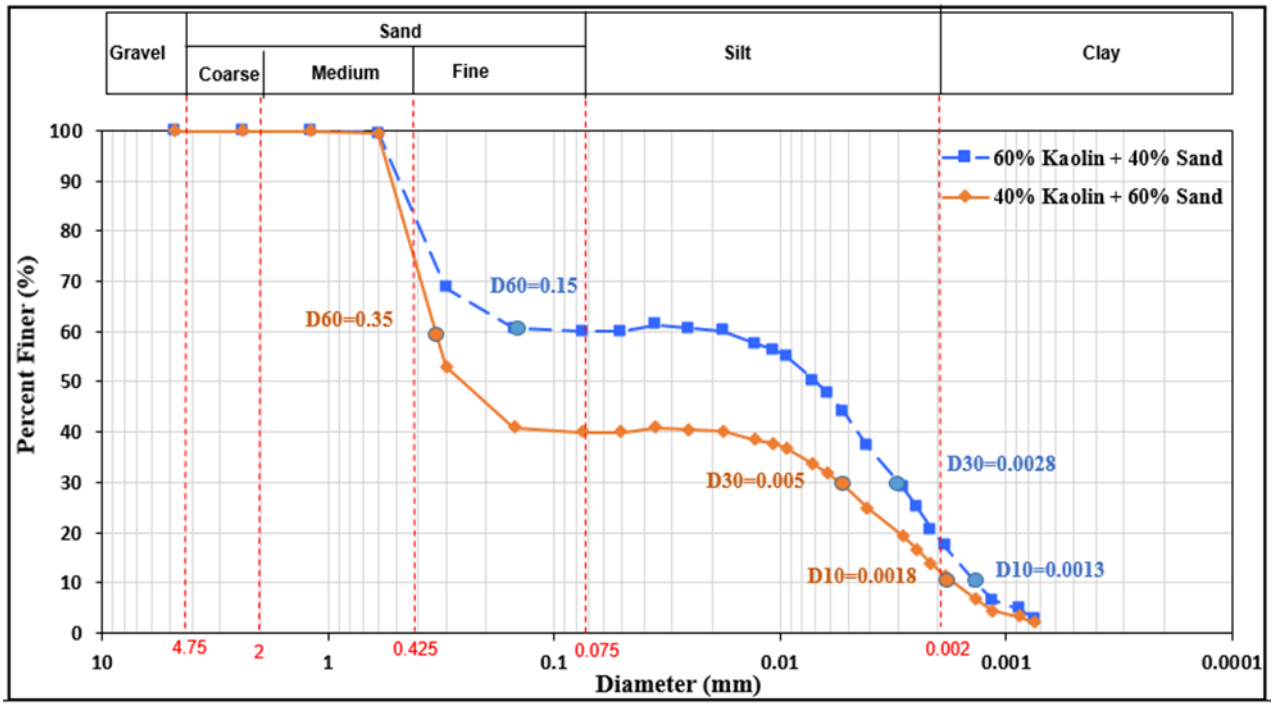

Figure 5-2 Particle size distribution curve of the soils

$$cu = \frac{D60}{D10} \tag{13}$$

$$CC = \frac{(D30)^2}{D10xD60} \tag{14}$$

$$cu = \frac{0.35}{0.0018} = 194.4$$

$$CC = \frac{(0.005)^2}{0.0018x0.005} = 0.039$$

$$cu = \frac{0.15}{0.0028} = 53.57$$

$$CC = \frac{(0.005)^2}{0.0018x0.005} = 0.128$$

For the classification of soil by the USCS system, soil texture is defined as the relative distribution of sand, silt, and clay particles in a soil specimen. Sandier soils are ones that have a large percentage of sand grains, whereas clavier soils contain a large percentage of kaolin particles. After consideration of all index and PSD properties, both soils are classified as gap-graded soils. Furthermore, soil with 60% kaolin and 40% sand is defined as fine-grained or "silty sand" (MH). whereas soil with 60% sand and 40% kaolin is defined as coarse-grained or "sand silty" (SM) soil.

5.1.4 Soil water characteristic curve SWCC

For the determination of the graphical correlation between volumetric water content and soil suction, laboratory tests and statistical methods were used. It is a crucial tool for comprehending the soil suction in relation to water infiltration into the slope surface and soil structure. The soil-water characteristic curve (SWCC) of bimodal soil is shown in Figure 5-3. The results indicate that the SWCC data from the experimental work in a laboratory has bimodal characteristics and should be best fitted using (Satyanaga, 2021) bimodal mathematical function and Yarifudin and Satyanaga, 2021). Figure 4-3 presents all physical parameters of SWCC with respect to saturated and residual volumetric water content, residual suction, and air entry value (AEV1 and AEV2), which are defined based on (Satyanaga, 2013) best-fitting statistical method.

Overall, the finding from SWCC demonstrates that for silty sand with a volumetric water content of θs1=0.520 the first air entry (AEV1) happened when the soil suction increased to 1 kpa; however, the (AEV1) for sandy silt soil happened when θs1=0.282 with the same suction. Furthermore, this curve represents how the soil stores water at various degrees of wetness. The

Moreover, the second air entry value (AEV2) of silty sand soil with saturated volumetric water content θs2=0.400 happened after the soil suction increased to 10 kpa, while for sandy silt soil, with θs2=0.234 was constant until the soil suction increased to 20kpa. Overall, the finding from SWCC demonstrates how the soil stores water at various degrees of wetness. The best-fitting parameters for the SWCC are shown in Tables (5-4) and (5-5).

Table 5-4Best fitting parameters for silty sand bimodal soil SWCC.

Descriptions	Parameters	value
Saturated volumetric water content	θ_{s1}	0.520
parameter of volumetric water content at residual condition	θ_{r1}	0.400
Parameter related to air-entry value AVE-1 (kpa)	Ψ_{a1}	1.000
Parameter related to suction at the inflection point 1	Ψ_{m1}	1.500
Standard deviation related to sub-curves 1 and 2 in SWCC	σ_1	0.500
Saturated volumetric water content	θ_{s2}	0.400
Parameter related to air-entry value AEV-2 (kPa)	ψ_{a2}	10.000
Parameter related to suction at the inflection point 2	ψ_{m2}	85.000
Standard deviation related to sub-curves 1 and 2 in SWCC	σ_2	2.200
Curve fitting parameter related to residual matric suction	ψ_{r2}	1500.000
Parameter of volumetric water content at residual condition	θ_{r2}	0.000
Coefficient of determination	R^2	1.0000

Table 5-5 Best fitting parameters for sandy silt bimodal soil SWCC.

Descriptions	Parameters	value
Saturated volumetric water content	θ_{s1}	0.282
parameter of volumetric water content at residual condition	θ_{r1}	0.25
Parameter related to air-entry value AVE-1 (kpa)	Ψ_{a1}	3.00
Parameter related to suction at the inflection point 1	Ψ_{m1}	4.00
Standard deviation related to sub-curves 1 and 2 in SWCC	σ_1	0.360
Saturated volumetric water content	θ_{s2}	0.234
Parameter related to air-entry value AEV-2 (kPa)	ψ_{a2}	25.00
Parameter related to suction at the inflection point 2	ψ_{m2}	100.00
Standard deviation related to sub-curves 1 and 2 in SWCC	σ_2	1.00
Curve fitting parameter related to residual matric suction	ψ_{r2}	600.00
Parameter of volumetric water content at residual condition	θ_{r2}	0.050
Coefficient of determination	R^2	0.9818

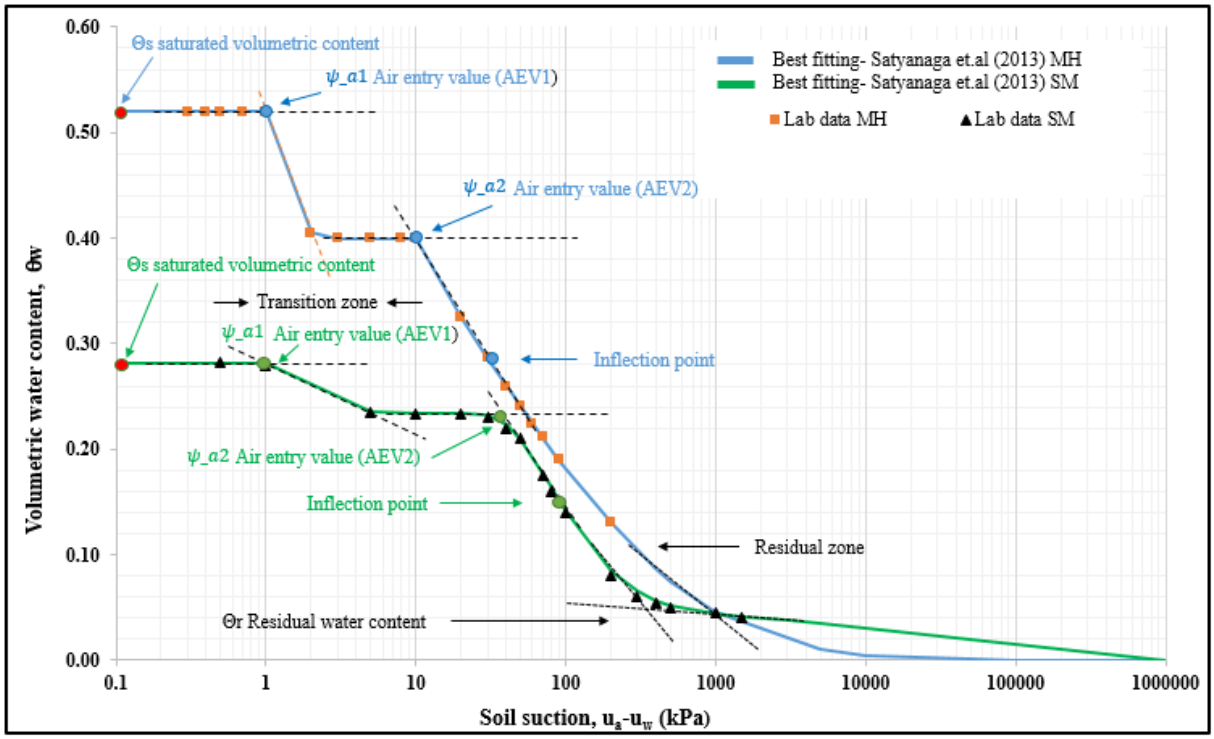

Figure 5-3Bimodal soil water characteristic curve (SWCC) fitted using Satyanaga (2021) mathematical function

5.1.5 Unsaturated permeability function

For the determination of saturated permeability (ks) constant head method was used, while for unsaturated permeability, the statistical method was used. The unsaturated permeability (k_W) of the fine-grained and coarse-grained bimodal soils is presented in Figure 5-4. The unsaturated permeability of the investigated soil was obtained using a statistical method following the procedures explained by (Satyanaga et al., 2022), especially for determining unsaturated permeability for soils with bimodal characteristics. First, results from the experimental work on permeability testing indicated that the saturated permeability of the investigated sandy silt soil is 7.00E-5 m/s, while for silty sand soil, it is 6.47E-7m/s Secondly, the findings from the Hyprop test demonstrated that the soil specimen is saturated until suction is around 1 kPa. Then the suction increased to 10 kPa, and permeability for fine-grained soil dramatically approached 9E-7 m/s for silty sand soil. However, sandy silt soil is 1.29E-8 m/s due to air in the soil pores, and its equivalent to the air entry value (AEV2).

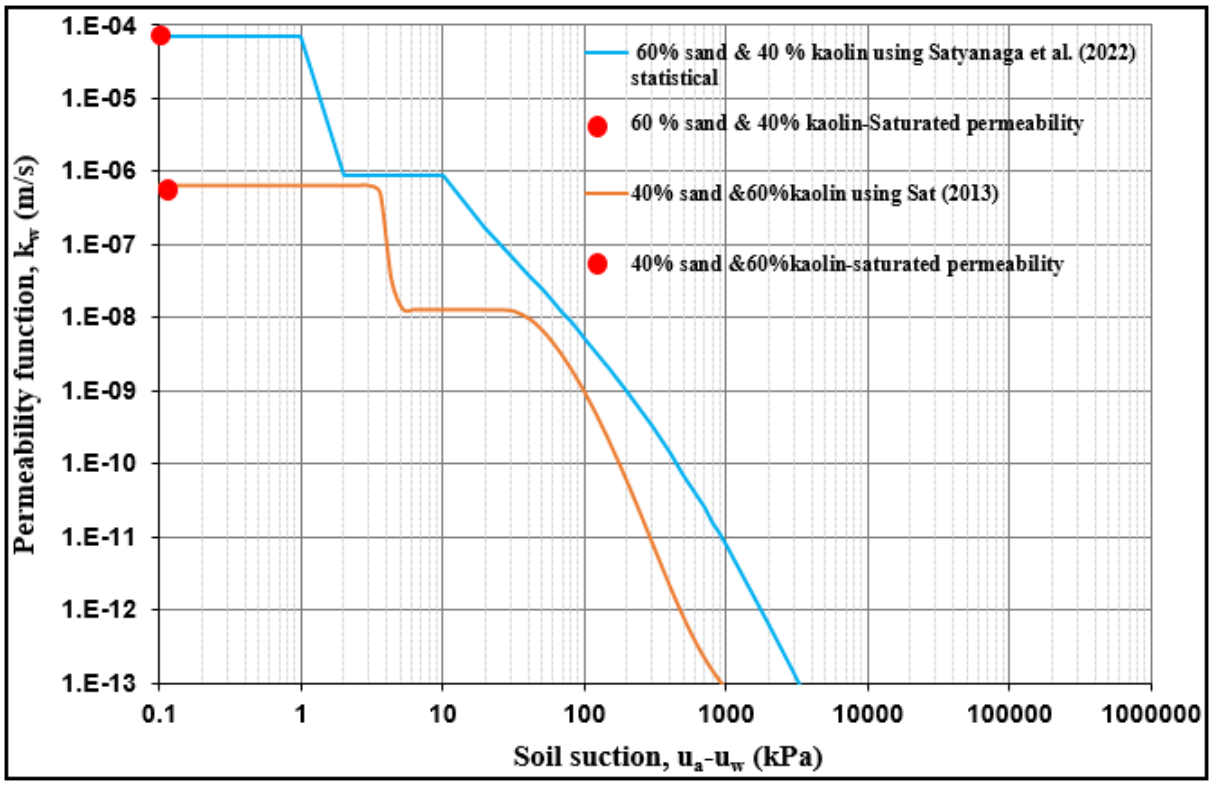

Figure 5-4Bimodal soil permeability function based on Statistical method

5.1.6 Result from Unsaturated soil shear strength

For the unsaturated shear strength modified triaxial test was used to find the unsaturated shear strength properties of fine (MH) and coarse-grained (SM) soil for seepage and slope stab**ility analyses, shown in (tables** 5-6 and 5-7).

Table 5-6Coarse grained soil (SM) shear strength data for slope stability.

Description	Symbol	value	unit
cohesion	c'	8	kPa
friction angle	ϕ′	31	degree
Unit weight	γ	18	kN/m3
Phb	ϕ^b	15.5	degree

Table 5-7 Fine grained soil (MH) shear strength data for slope stability.

Description	Symbol	value	unit
cohesion	c'	2	kPa
friction angle	ϕ′	32	degree
Unit weight	γ	19	kN/m3
Phb	ϕ^b	16	degree

(Tables 5-7 and 5-6) indicate the most important parameters for stability analysis of the slope, such as unit weight, internal friction angle, cohesion, and dilation angle, all of which were obtained through the shear strength test, along with other important characteristics.

5.2 Result from seepage and slope stability

5.2.1 Factor of safety and pore water pressure for fine grained soil (MH).

The reduction in the factor of safety for silty sand (MH) slopes with different angles and heights under rainfall loading is shown in figures 5-5, 5-6, 5-7, 5-8, and 5-9). Figures 5–5 and 5-8 indicate that the initial factor of safety of the slope with a 10 m height and a 27-degree inclination is FoS = 1.92 > 1.25 before rainfall starts. This initial factor of safety reduces to FoS = 0.85 >< 1.25 for a slope with the same height but an 80-degree inclination. Secondly, Figures 5–6 and 5–9 present another slope with a 20-meter height and a 27-degree inclination that had the initial factor of safety FoS = 1.3 > 1.25 before precipitation began; this factor of safety dropped to FoS= 0.60<1.25 for slope with the same height but an 80-degree inclination. Additionally, figures 5-7, 5-8, and 5-9 indicate the factor of safety for a slope with a 30 m height and a 27-degree angle with the same mechanical properties: the factor of safety FoS = 1.29 > 1.25 before a rainfall event. As a result, it shows that factors of safety and slope geometry directly relate to each other. For the investigated slope, the factor of safety decreased to FoS= 0.46<1.25 with the same slope's height but an alteration of slope geometry. The decrease in factor of safety for steeper slopes is sharp when the slope angle changes from 27 degrees to 60 degrees. However, the changes start to be gradual when the slope angle changes from 60 degrees to 80 degrees. It can be attributed to slope failure or landside erosion. On the other

hand, we can demonstrate that without live or natural loads, slope geometry can directly impact the stability of dual-porosity soil slopes.

(Figures 5-5, 5-6, 5-7, 5-8, and 5-9) show the minimum factor of safety of the slope after 12 days of continuous precipitation. For the slope with 10m height and 27 degrees, the factor of safety FoS = 1.71 > 1.25 after experiencing 12 days of rainfall reduced to FoS=0.77<1.25 with the same height but numerous alterations of slope geometry (80 degrees). For the second slope with 20m height and 27 degrees, the factor of safety FoS is 1.26 > 1.25 after 12 days of heavy rainfall, reducing to FoS=0.56<1.25. Additionally, for the slope with a 30 m height and a 27-degree angle, the factor of safety is FoS = 1.49 > 1.25, and it declines to FoS=0.48<1.25 due to the rainfall infiltration and inclinations of the slope geometry. Hence, this decrease in the factor of safety can be linked to a decrease in the shear strength of the soil due to the matric suction. It has been shown that with the inclination of slope geometry during 12 days of rain and 12 recovery days, the factor of safety approaches a small value utilizing FoS<1. As mentioned by Prof Kim, FoS = 1 is the actual boundary between a fail and a non-fail but the previous study by (Abramson et al, .1996) suggested using FoS=1.25. Hence slope with 10m, 20m, and 30m height and inclination of the slope angles from 45-degree to 80-degrees can't be stable under applied loads. It's observed that the factor of safety can be different at numerous heights and angles of the dual porosity soil slope.

(Figures 5-10 and 5-11) illustrates that prolonged precipitation and infiltration within the soil surface decrease the pore water pressure from highly negative to low negative values and factor of safety from FoS=1.92 to FoS<1 or FoS<1.25 For the slope height 10m and 20m with 27-degree the pore water pressure at t = 0 was a negative 49 kpa or 65%, dropping to negative 14kpa or 70% after 12 days of rainfall infiltration. However, the pore water pressure values somehow remain the same at the depth range of (27 m-54) respectively. Additionally, it indicates that the height of the slope and the inclination of the slope's angles can directly impact pore water pressure.

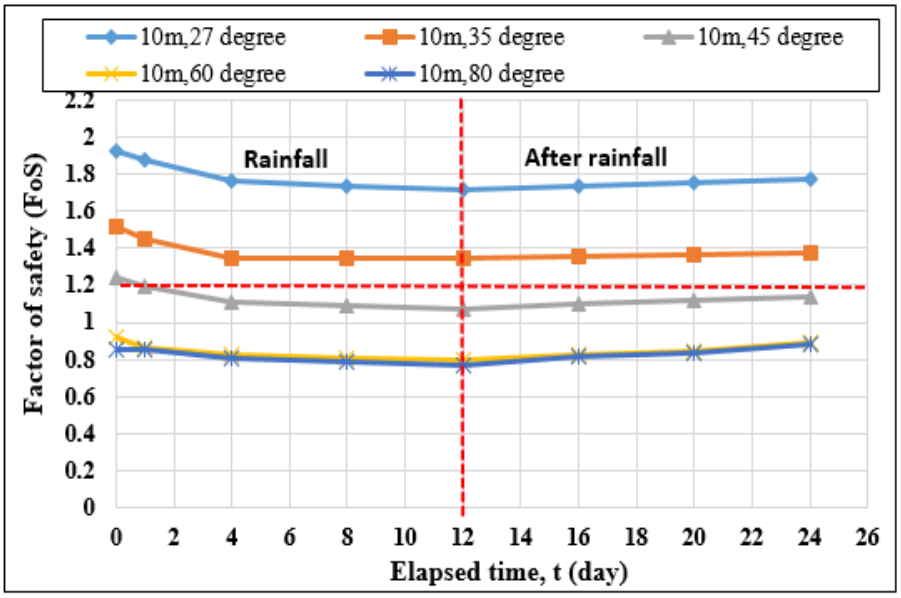

Figure 5-5 Factor of safety (FoS) for fine grained soil, (10m with 27º,35º,45º,60º and 80º degrees)

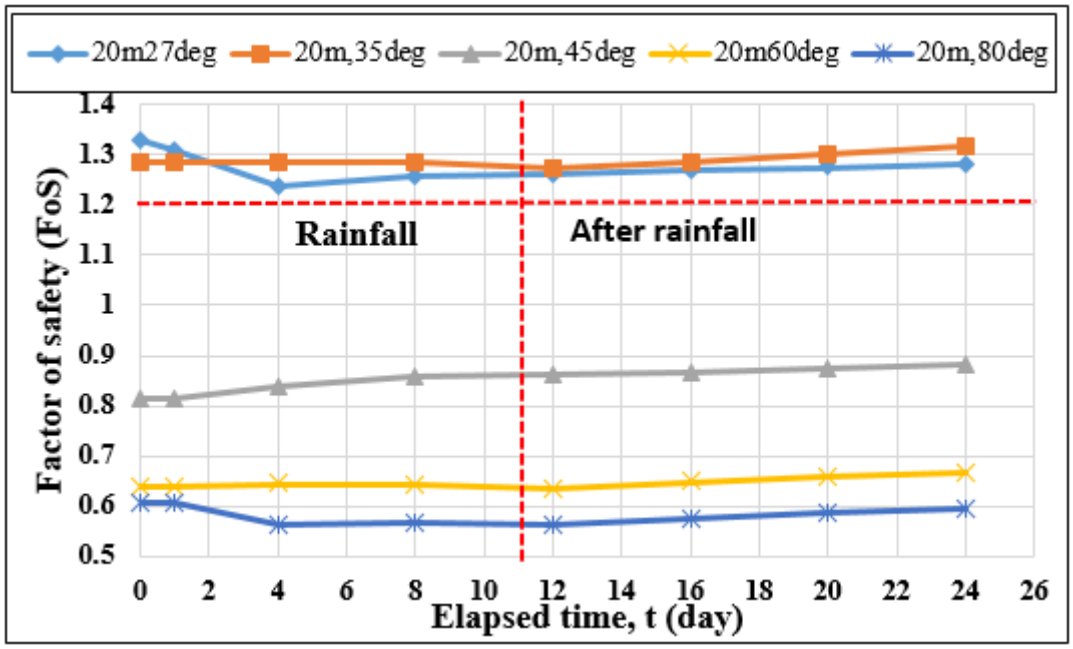

Figure 5-6 Factor of safety (FoS) for fine grained soil, (20m with 27º,35º,45º,60º and 80º degrees)

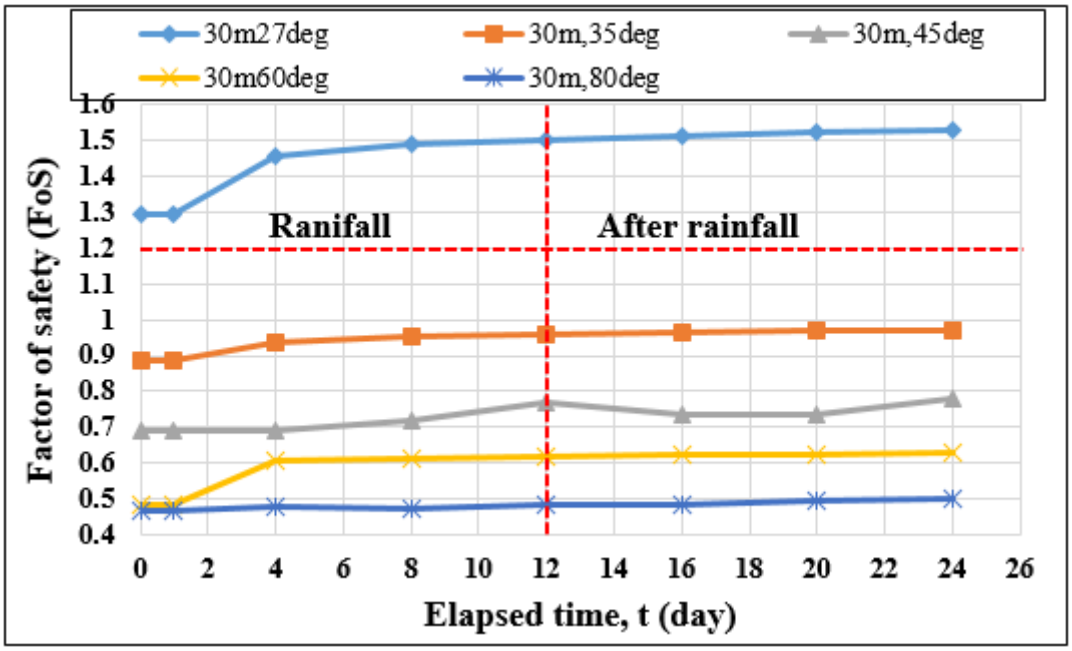

Figure 5-7 Factor of safety (FoS) for fine grained soil, (30m with 27º,35º,45º,60º and 80º degrees)

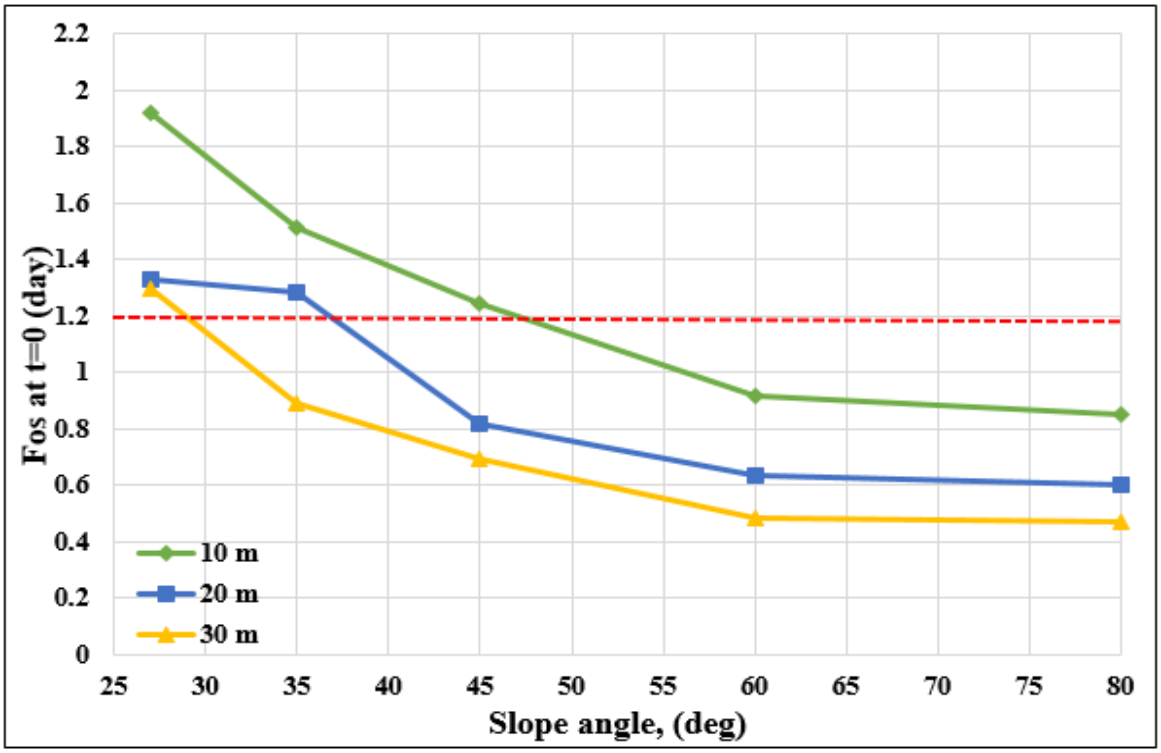

Figure 5-8 Changes in Factor of safety (FoS) during 20mm/day rainfall for 10m 20m and 30m height with 27º,35º 45º,60º and 80º degrees) t=0

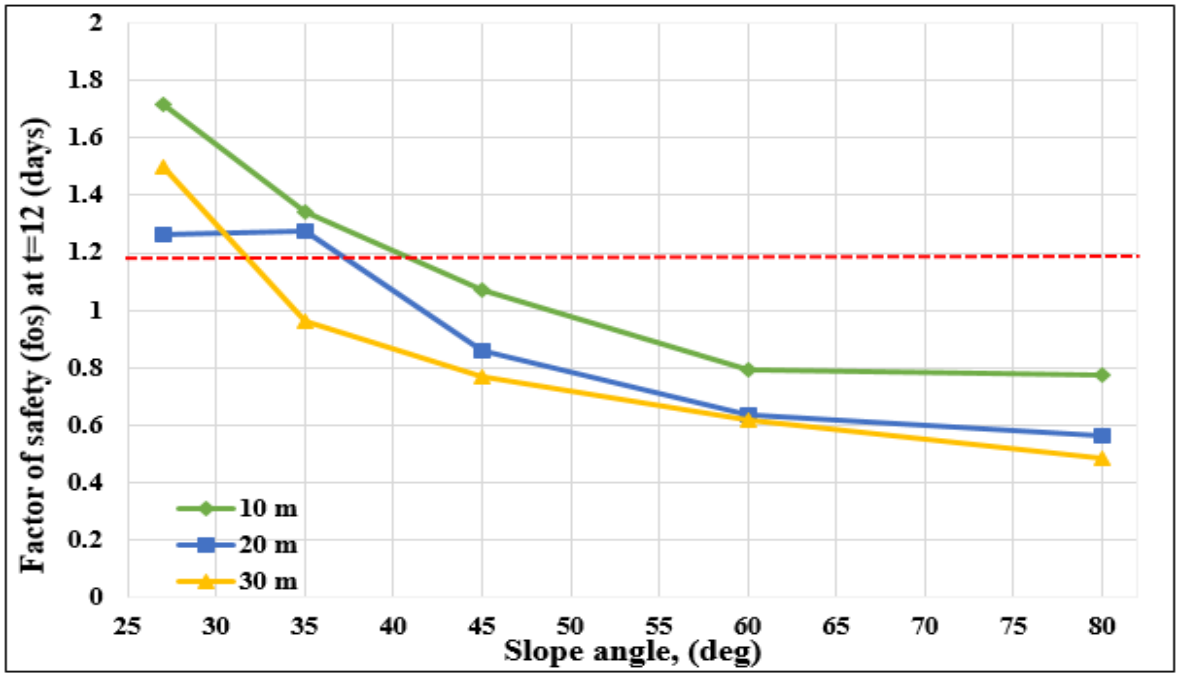

Figure 5-9 Changes in Factor of safety (FoS) after20mm/day rainfall for 10m 20m and 30m height with 27º,35º 45º,60º and 80º degrees) t=12

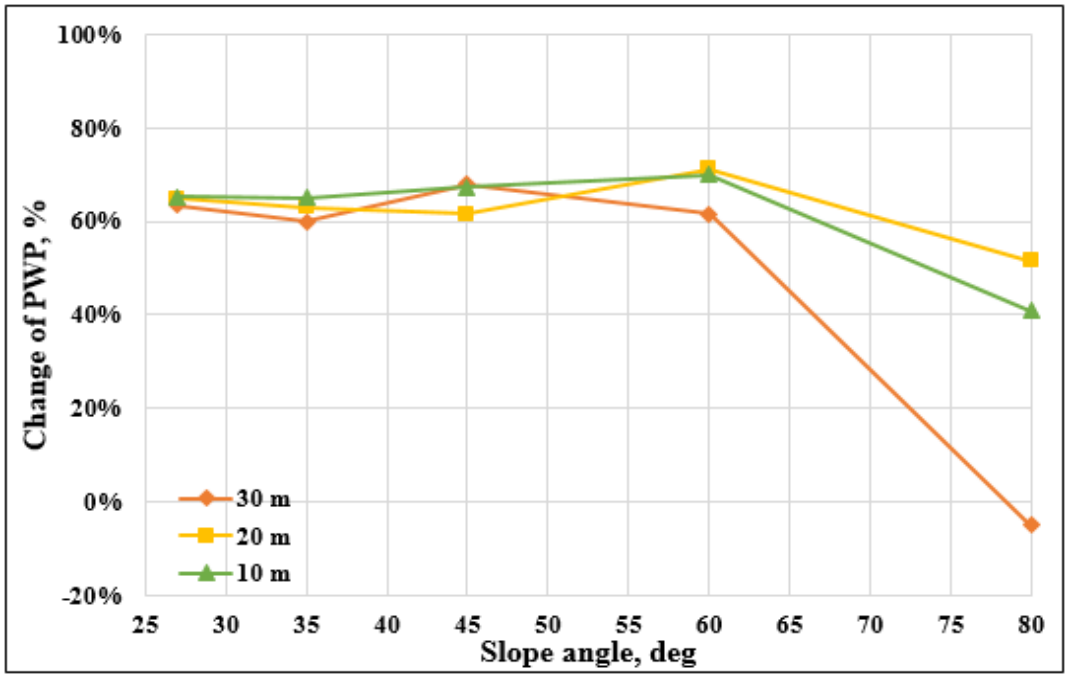

Figure 5-10 **Change in** *pore water pressure vs vs slope with different height and angles after 20mm/day rainfall at t=12 days*

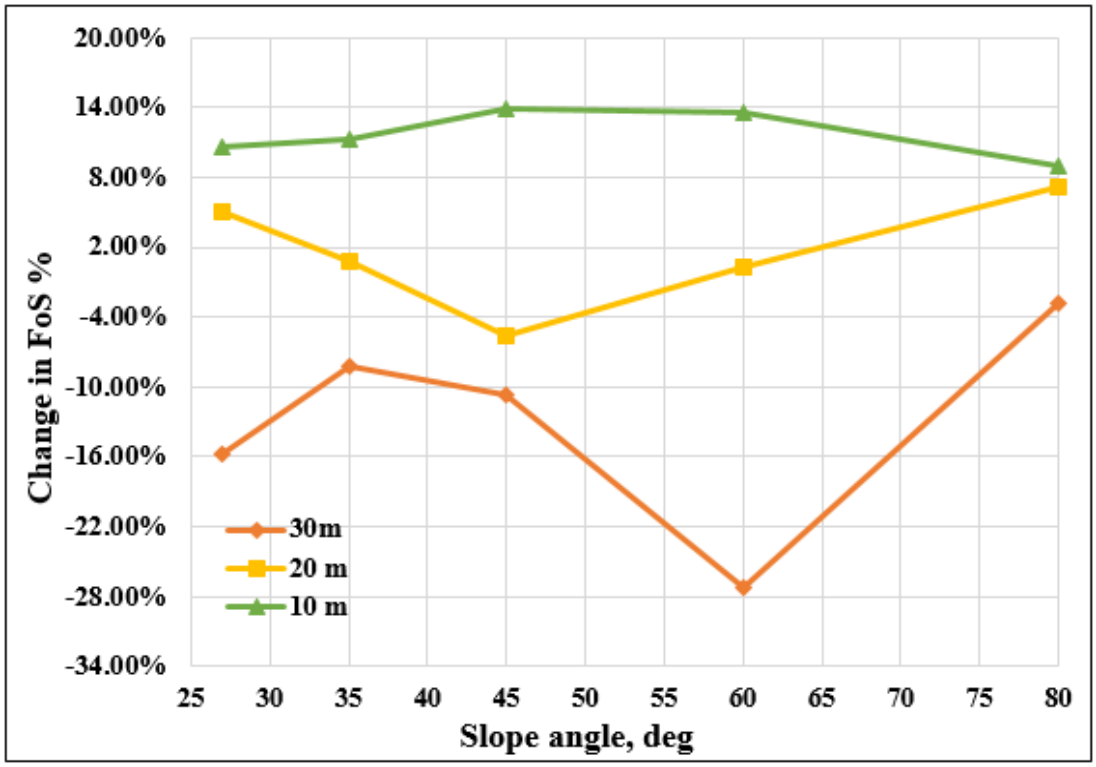

Figure 5-11 Change in factor of safety vs slope with different height and angles after 20mm/day rainfall at t=12 days

5.2.2 Factor of safety and pore water pressure for coarse grained soil (SM)

The deterioration in the factor of safety for sandy silt (SM) soil slopes at various angles and heights and under 20 mm/day precipitation is represented in (Figures 5-12, 5-13, 5-14, 5-15, and 5-17). Figures 5-12 and 5-13 show that for a slope with a 10 m height and a 27-degree incline, the initial factor of safety FoS = 2.17 > 1.25 before prolonged precipitation, whereas for a slope at the same height but an inclination of 45 degrees, the initial factor of safety drops to FoS = 1.45 > 1.25. Secondly, (Figures 5–13, and 5–14) show another slope with a 20-meter height and a 27-degree incline that had an initial factor of safety of FoS = 1.35 > 1.25 before precipitation started. However, the factor of safety was reduced to FoS=0.97<1.25 for the same investigated slope but with an inclination of 45 degrees.

Moreover, (figures 5-12, 5-13, 5-14, and 5-15) depict the slope's lowest safety factor for t = 12 days of nonstop precipitation. The factor of safety FoS=1.21<1.25 for the slope with a 10 m height and a 27-degree angle after 12 days of rainfall was reduced to FoS=0.84<1.25 with the same height but an inclination of slope geometry from 27 to 45 degrees. For the second slope geometry with a 20-meter height and a 27-degree angle, the factor of safety

FoS=0.91<1.25 which demonstrates that the slope is not stable. However, after 12 days of heavy rainfall and an inclination of the slope angle from 27 to 45, it was reduced to FoS=0.59<1.25.

Additionally, figures 5–16 represent that the pore water pressure was negative 49 kpa, or 100%, for the slope heights of 10 m with a slope angle of 27, 35, and 45 degrees at t = 0 time. After 12 days of rainwater infiltration, it decreases to 0 kpa, or 0%. However, for slope with a height of 20 m and a slope angle of 27 degrees at t = 0 time PWP was 49kpa or 100% while after inclination of slope angles and rainfall infiltration, it reduced to 1.6kpa or 104% and 2.99kpa or 107% in row for each angle.

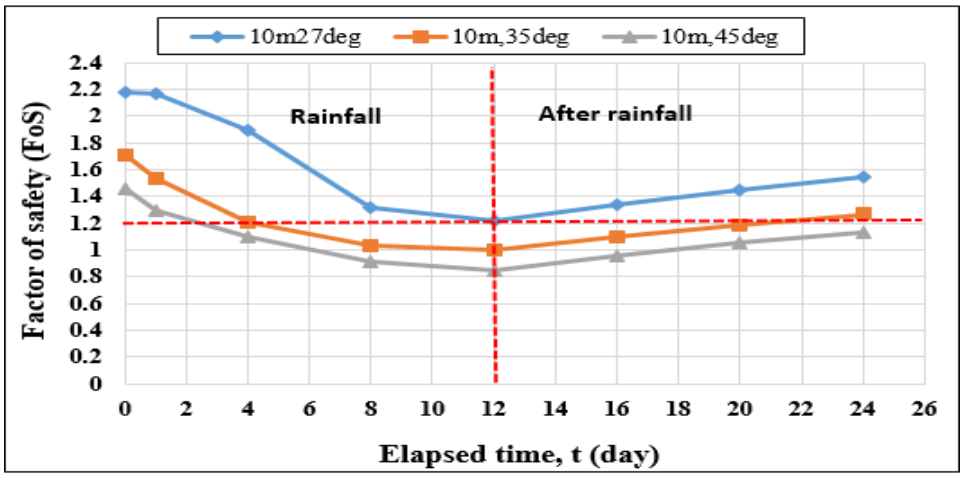

Figure 5-12 Factor of safety (FoS) for coarse grained soil, (10m with 27⁰,35⁰ and 45⁰ degrees)

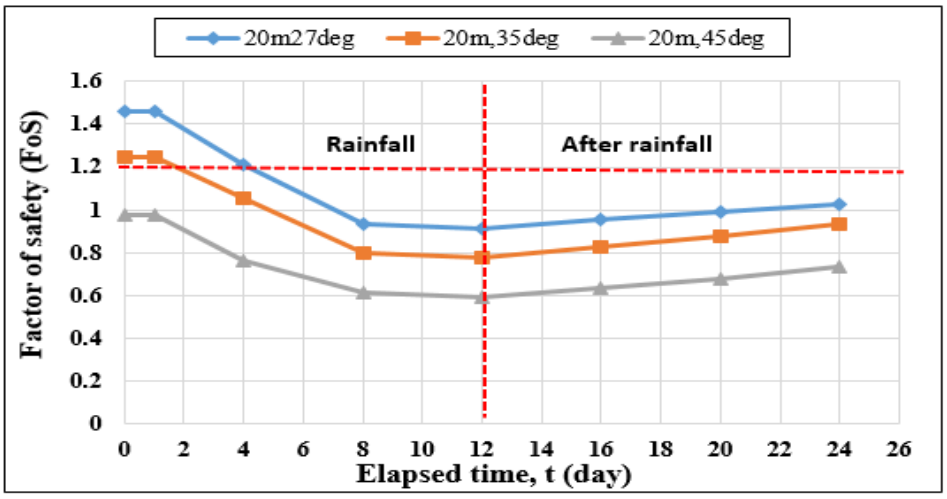

Figure 5-13 Factor of safety (FoS) for coarse grained soil, (10m with 27⁰,35⁰ and 45⁰ degrees)

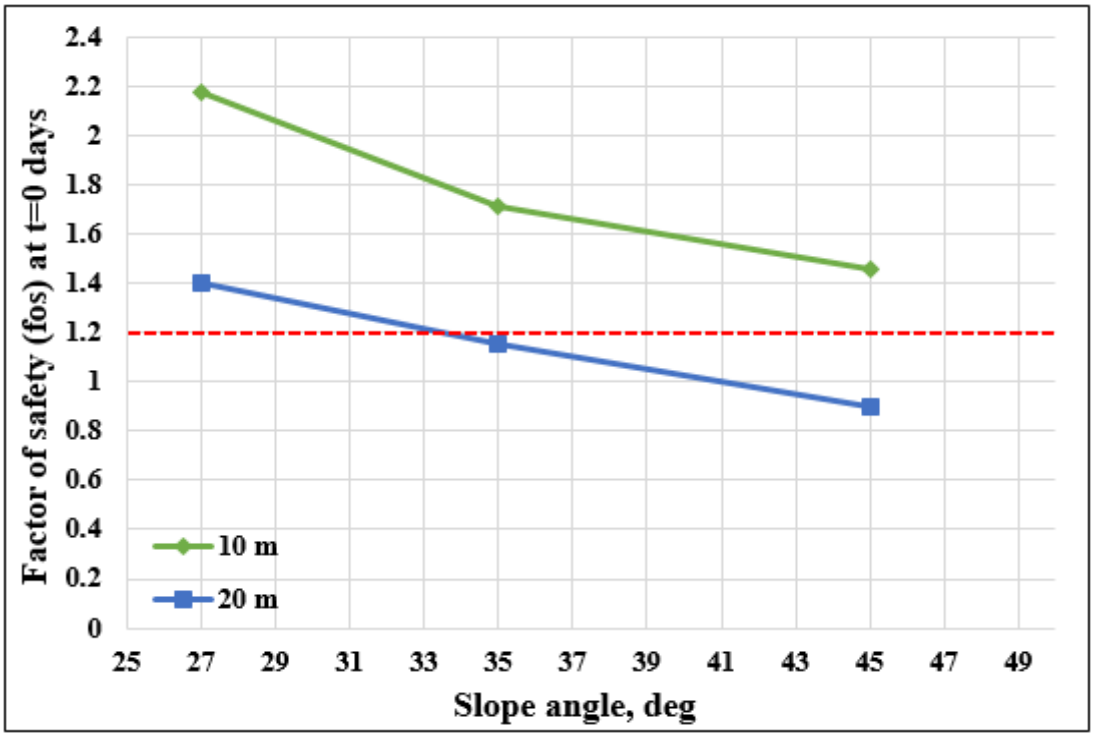

Figure 5-14 Changes in Factor of safety (FoS) during 20mm/day rainfall for 10m and 20m height with 27º,35º and 45ºdegrees at t=0

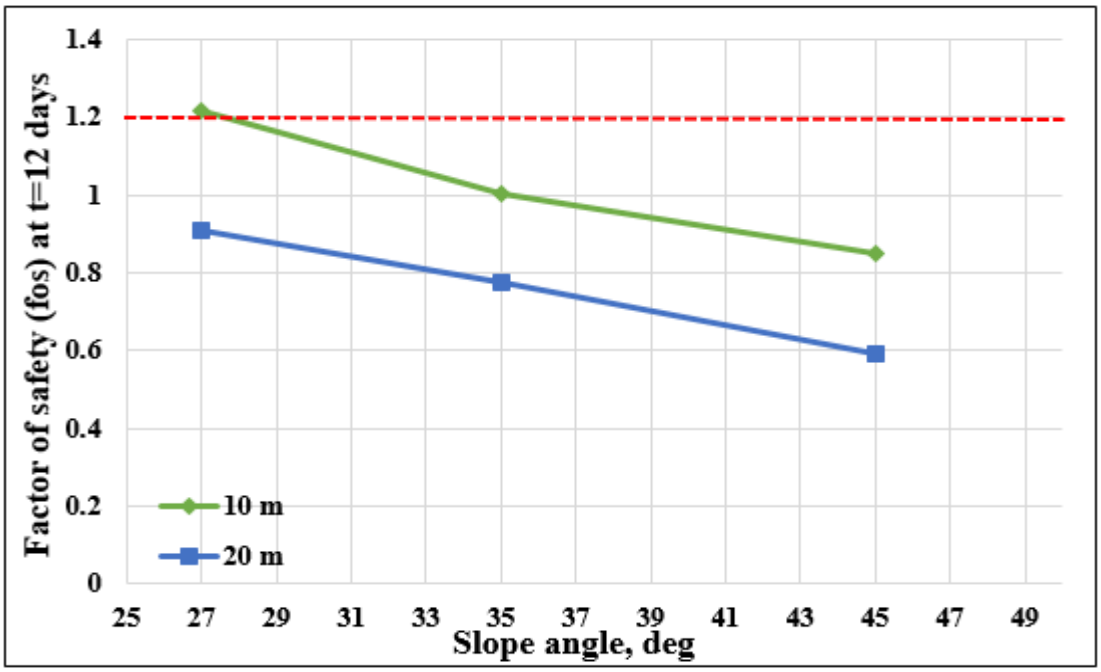

Figure 5-15 Changes on factor of safety (FoS) after 20mm/day rainfall for 10m and 20m height with 27,35 and 45 degrees at t=12 days

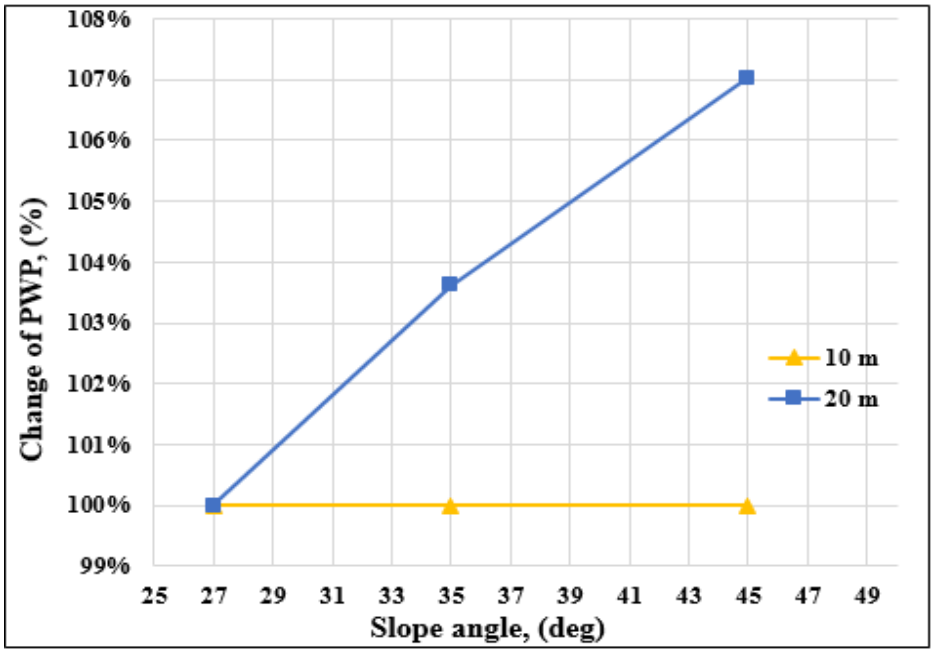

Figure 5-16* Change in *pore water pressure vs slope with different height and angles after 20mm/day rainfall at t=12 days

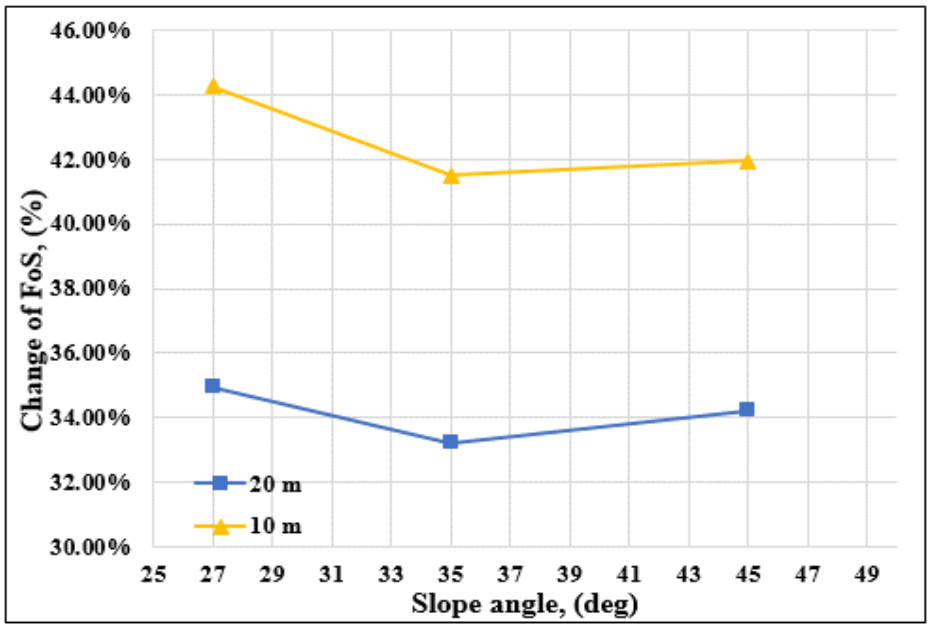

Figure 5-17 Changes in Factor of safety (FoS) during 20mm/day rainfall for 10m and 20, height with 27⁰,35⁰ and 45⁰degrees

Chapter 6 - DISCUSSION

In this research, laboratory experiments and numerical analyses illustrate a very clear relationship between the factors of safety and pore water pressure. The results show that slope geometry, soil properties, continuous precipitation intensity, and duration have significant impacts on the slope's stability. This finding from the numerical analyses and laboratory tests indicates that the primary cause of the landslide is the decrease in shear strength caused by an increase in soil moisture content and a decrease in matric suction.

Findings from the laboratory Hyprop test show that after rainfall infiltration to the slope surface, the saturated volumetric water content of both soils is constant ($\theta s1=520$ for silty sand soil and $\theta s1=282$ for sandy silt soil), while after continuing the evaporation process with time, the soil suction increased to 1 kpa and the first air entry happened, as shown in figures 12–13. The soil has bimodal properties, which is why after the soil suction increased to 10 kpa, the second air entry value (AEV2) happened for silty sand soil at $\theta s1=400$, while for sandy silt it was twice of that soil suction at $\theta s1=234$. It illustrates that sandy silt soil has higher permeability and allows water to pass through slope surfaces compared to silty sand soil. Secondly, from other laboratory tests, classification of the soil was done as silty sand (MH) and sandy silt (SM). Additionally, the physical and engineering properties of both soil are somehow similar but silty sand is stickier compare to sandy silt.

A key criterion for identifying whether a slope is stable or probable for failure is the factor of safety for slope stability analysis. When the slope's factor of safety is greater than 1, it means that the forces preventing failure are stronger than the forces generating it, but when it is less than 1, it means that breakdown is possible for the investigated slope. Previous studies by (Abramson et al, .1996) indicate that for the stability of a slope, Fos =1.25 is acceptable, while most of the time for stability analyses, slopes are assumed to be safe when the factor of safety is between 1.5 and 2.5. Nevertheless, a higher factor of safety might be necessary in some situations or locations, such as in regions with essential infrastructure or high danger zones.

Findings from Numerical analyses indicates that rainfall intensity, groundwater table, slope geometry, and soil properties are highly considerable to the landslide and other environmental hazards; therefore, in this study it was observed that for the slope made of silty sand initial state t = 0, the factor of safety is FoS=1.92 with a pore-water pressure of negative 49 kpa the slope is still stable, but after 12 days of rainfall intensity and inclinations of slope geometries, the factor of safety declined to less than $FoS=0.48<1.25$ and the pore water pressure

converged from negative high to negative low, respectively while for the slope made sandy silty soil for the initial time t=0 FoS= 2.17 with PWP 49kpa but after 12 days of continues prolong precipitation and slope degree inclination from 27-45 FoS decreased to FoS=0.9< 1.25 it shows that for sandy silty soil the changes in pore water pressure and factor of safety are more faster than compare to silty sand soil

Secondly, for slope heights of 10–20 m and inclinations of slope geometries from 27–80 degrees made of silty sand, only slopes with 20m height and 27–35 degrees and 10m height with 27–45 degrees are stable, while for slopes made of sandy silt soil, only slopes with 10–20 m height and 27–35 degrees are safe before rainfall events. Additionally, for the slope heights of 10m and 20m, with alteration of slope angles from 27-80 degrees made of silty sand soil experienced 12 days of 20mm/day rainfall only 10m, 20m with 27 degrees is stable while the same geometry with sandy silt soil can be stable only with 10m height and 27 degrees. It indicates that for the stability of the slopes silty sand (MH) or fine-grained soils are more stable than sandy silt soil (SM) or coarse-grained soil. However, the factor of safety for the initial time t=0 sandy silt is higher than silty sand but after rainfall can decrease dramatically. Overall it illustrates that sandy silt soil has large pores and it allows rainfall water infiltration very fast to the slope surface and causes slope failure. Hence slope geometry, rainfall intensity and duration, groundwater table, and geotechnical structure of the soil are important factors in slope stability analysis and can cause slope failure.

Chapter 7 - CONCLUSION

According to the analysis's findings, the slope geometry (heights and angles) potentially influences the factors of safety and pore water pressure and causes the failure of a dual-porosity soil slope. Additionally, it shows that prolonged precipitation directly impacts factors of safety and pore water pressure. Overall, the summarization of the current study is as follows, and only it can be limited to dual-porosity fine-grained (MH) and coarse-grained (SM) soil slopes: Finding from laboratory tests shows that silty sand and sandy silt soil has bimodal properties. Silty sand soil has the same first air entry value (AEV1) as compared to sandy silt soil with different saturated volumetric water content. The second air entry value (AEV2) of silty sand soil is 10 kpa which is lower than AEV2 of sandy silt soil (30kpa).

1. Silty sand soil has a higher permeability as compared to sandy silt soil.
2. Results from numerical analyses indicate that slope angles play an important role in the stability of dual porosity soil slopes. Prior to rainfall, the gentlest slope (27-degree inclination) has the highest FoS (1.92 for silty sand and 2.17 for sandy silt) as compared to other slope angles. The steepest slope angle that can be constructed under a dry period is 45 degrees where the FoS is 1.25 for silty sand and FoS=1.45 for sandy silt. All these FoS are higher or equal to the minimum criteria for stable slope (FoS = 1.25)
3. Findings from the numerical simulation shows that rainfall intensity and its duration is an important factor in slope stability analysis. After extreme rainfall the gentlest slope with an angle of 45 degrees has a minimum FoS=1.07 for silty sand soil thus the same geometry made of sandy silt soil has a minimum FoS=0.84. The high factor of safety for silty sand soil indicates that it’s more stable against rainfall intensity and duration compared to sandy silt soil slope. However, for the current factor of safety with the same geometries and rainfall infiltration, both investigated slopes are not safe. The steepest slope angle that can be stable under 12 days of 20mm/day rainfall is 27-35 degrees where the minimum is FoS= 1.27 for silty sand soil while for sandy silt soil minimum is FoS= 1.21. Only less than 27 degrees is acceptable for the minimum criteria of stable slope (FoS=1.25).
4. Result from numerical simulation determined that the stability of slopes comprised of two distinct soil types silty sand and sandy silt under various environmental circumstances. It contrasts the factor of safety (FoS) of slopes with different heights, angles, and rainfall intensities before and after the changes. The results suggest that

slopes composed of silty sand soil have a greater factor of safety and are more stable against rainfall water compared to those built of sandy silt soil. Moreover, it implies that compared to taller slopes, slopes with lesser heights and angles have a better factor of safety and they are more stable. Also, the greatest factor of safety for the silty sand soil slope was FoS=1.92 which reduced to FoS=0.48 after 12 days of continuous precipitation, whereas the sandy silt soil slope had the maximum factor of safety FoS=2.17, which dropped to FoS=0.8 under defined conditions. It indicates that slopes built of sandy silt soil with heights larger than 10m and inclination angles greater than 27 degrees cannot be stable under the same conditions, those made of silty sand soil can have the stable factor of safety with 10m and 20m height and inclination of angles between 27 and 35 degrees under minimum criteria of the factor of safety Fos=1.25.

5. Findings from seepage and slope stability analyses indicate that pore water pressure and soil shear strength have direct impacts on each other and can affect the stability of dual-porosity soil's slope. For the initial state of the slope t = 0 days, the pore-water pressure is negative 49 kpa, which shows that the slope has enough shear strength. However, after 12 days of rainfall intensity and inclinations of slope geometries, the pore water pressure converged from negative high to negative low, respectively, and dual-porosity soil (silty sand and sandy silt) lost its shear strength. However, according to the soil geotechnical structure, Silty sand soil somehow keeps pore water pressure but sandy silt soil pore water pressure decrease from 49kpa to 0 kpa.

LIST OF REFERENCES

"Test method for consolidated undrained triaxial compression test for cohesive soils" (22AD). Available at: https://doi.org/10.1520/d4767-11r20.

"Test method for consolidated undrained triaxial compression test for cohesive soils" (22AD). Available at: https://doi.org/10.1520/d4767-11r20.

Abramson, L., Boyce, G., Lee, T., and Sharma, S., 1996, Slope Stability and Stabilization Methods, Wiley, ISBN 0471106224.

Abramson, L., Boyce, G., Lee, T., and Sharma, S., 1996, Slope Stability and Stabilization Methods, Wiley, ISBN 0471106224.

Aragón, A., García M.G., Filgueira, R. R., & Pachepsky, Y. A. (2000). Maximum compactibility of Argentine soils from the Proctor test; *Soil and Tillage Research*, *56*(3-4), 197–204. https://doi.org/10.1016/s0167-1987(00)00144-6

Aragón, A., García M.G., Filgueira, R. R., & Pachepsky, Y. A. (2000). Maximum compactibility of Argentine soils from the Proctor test; *Soil and Tillage Research*, *56*(3-4), 197–204. https://doi.org/10.1016/s0167-1987(00)00144-6

ASTM D2434-22 (no date) *ANSI Webstore*. Available at: https://webstore.ansi.org/standards/astm/astmd243422 (Accessed: March 5, 2023).

ASTM D2434-22 (no date) *ANSI Webstore*. Available at: https://webstore.ansi.org/standards/astm/astmd243422 (Accessed: March 5, 2023).

Baimakhan, A., Seinassinova, A., Baimakhan, R., Rysbayeva, A. and Moldakunova, N. (2020). Determining the Physical and Mechanical Properties of Two-Phase Soil for Landslide Slopes of the Northern Tien Shan. *International Journal of Engineering Research and Technology*, 13(4), p.699. doi:10.37624/ijert/13.4.2020.699-705.

Baimakhan, A., Seinassinova, A., Baimakhan, R., Rysbayeva, A. and Moldakunova, N. (2020). Determining the Physical and Mechanical Properties of Two-Phase Soil for Landslide Slopes of the Northern Tien Shan. *International Journal of Engineering Research and Technology*, 13(4), p.699. doi:10.37624/ijert/13.4.2020.699-705.

Bear, J. (2012). Hydraulics of Groundwater ([edition unavailable]). Dover Publications. Retrieved from https://www.perlego.com/book/110730/hydraulics-of-groundwater-pdf (Original work published 2012)

Bear, J. (2012). Hydraulics of Groundwater ([edition unavailable]). Dover Publications. Retrieved from https://www.perlego.com/book/110730/hydraulics-of-groundwater-pdf (Original work published 2012)

Beketova, a., berdenov, z., ataeva, g., safarov, r., shomanova, z. And herman, g.v. (2019). Geochemical monitoring of industrial center for development of recreational areas (on the example of khromtau-don industrial hub, kazakhstan). *Geojournal of tourism and geosites*, 27(4), pp.1449–1463. Doi:10.30892/gtg.27428-447.

Beketova, a., berdenov, z., ataeva, g., safarov, r., shomanova, z. And herman, g.v. (2019). Geochemical monitoring of industrial center for development of recreational areas (on the example of khromtau-don industrial hub, kazakhstan). *Geojournal of tourism and geosites*, 27(4), pp.1449–1463. Doi:10.30892/gtg.27428-447.

Brocca, L., Pellarin, T., Crow, W. T., Ciabatta, L., Massari, C., Ryu, D., Su, C.-H., Rüdiger, C., & Kerr, Y. (2016). Rainfall estimation by inverting Smos Soil Moisture Estimates: A comparison of different methods over Australia. *Journal of Geophysical Research: Atmospheres*, *121*(20). https://doi.org/10.1002/2016jd025382

Brocca, L., Pellarin, T., Crow, W. T., Ciabatta, L., Massari, C., Ryu, D., Su, C.-H., Rüdiger, C., & Kerr, Y. (2016). Rainfall estimation by inverting Smos Soil Moisture Estimates: A comparison of different methods over Australia. *Journal of Geophysical Research: Atmospheres*, *121*(20). https://doi.org/10.1002/2016jd025382

Chapuis, R.P. *et al.* (2006) *Falling-head permeability tests in an unconfined sand aquifer*, *Geotechnical Testing Journal*. ASTM International. Available at: https://www.astm.org/gtj100067.html (Accessed: 2022).

Chapuis, R.P. *et al.* (2006) *Falling-head permeability tests in an unconfined sand aquifer*, *Geotechnical Testing Journal*. ASTM International. Available at: https://www.astm.org/gtj100067.html (Accessed: 2022).

Childs, E. C., & George, N. C. (1950). The permeability of porous materials. *Proceedings of the Royal Society of London. Series A. Mathematical and Physical Sciences*, *201*(1066), 392–405. https://doi.org/10.1098/rspa.1950.0068

Childs, E. C., & George, N. C. (1950). The permeability of porous materials. *Proceedings of the Royal Society of London. Series A. Mathematical and Physical Sciences*, *201*(1066), 392–405. https://doi.org/10.1098/rspa.1950.0068

Fredlund, D. G., & Xing, A. (1994). Equations for the soil-water characteristic curve. *Canadian Geotechnical Journal*, *31*(4), 521–532. https://doi.org/10.1139/t94-061

Fredlund, D. G., & Xing, A. (1994). Equations for the soil-water characteristic curve. *Canadian Geotechnical Journal*, *31*(4), 521–532. https://doi.org/10.1139/t94-061

Fredlund, D. G., Rahardjo, H., & Fredlund, M. D. (2012). Unsaturated soil mechanics in engineering practice. https://doi.org/10.1002/9781118280492

Fredlund, D. G., Rahardjo, H., & Fredlund, M. D. (2012). Unsaturated soil mechanics in engineering practice. https://doi.org/10.1002/9781118280492

Fredlund, D.G. and Rahardjo, H. (1993). *Soil Mechanics for Unsaturated Soils*. Hoboken, NJ, USA: John Wiley & Sons, Inc. doi:10.1002/9780470172759.
Fredlund, D.G. and Rahardjo, H. (1993). *Soil Mechanics for Unsaturated Soils*. Hoboken, NJ, USA: John Wiley & Sons, Inc. doi:10.1002/9780470172759.
Fredlund, D.G. and Xing, A. (1994) "Equations for the soil-water characteristic curve," *Canadian Geotechnical Journal*, 31(4), pp. 521–532. Available at: https://doi.org/10.1139/t94-061.
Fredlund, D.G. and Xing, A. (1994) "Equations for the soil-water characteristic curve," *Canadian Geotechnical Journal*, 31(4), pp. 521–532. Available at: https://doi.org/10.1139/t94-061.

Huyghe, J. M., Nikooee, E., & Hassanizadeh, S. M. (2017). Bridging effective stress and soil water retention equations in deforming unsaturated porous media: A thermodynamic approach. *Transport in Porous Media, 117*(3), 349–365. https://doi.org/10.1007/s11242-017-0837-9
Huyghe, J. M., Nikooee, E., & Hassanizadeh, S. M. (2017). Bridging effective stress and soil water retention equations in deforming unsaturated porous media: A thermodynamic approach. *Transport in Porous Media, 117*(3), 349–365. https://doi.org/10.1007/s11242-017-0837-9

Kim, W.S. and Borden, R.H. (2011) "Influence of soil type and stress state on predicting shear strength of unsaturated soils using the soil-water characteristic curve," *Canadian Geotechnical Journal*, 48(12), pp. 1886–1900. Available at: https://doi.org/10.1139/t11-082.
Kim, W.S. and Borden, R.H. (2011) "Influence of soil type and stress state on predicting shear strength of unsaturated soils using the soil-water characteristic curve," *Canadian Geotechnical Journal*, 48(12), pp. 1886–1900. Available at: https://doi.org/10.1139/t11-082.
King, S.A., Khalturin, V.I. and Tucker, B.E. eds., (1999). *Seismic Hazard and Building Vulnerability in Post-Soviet Central Asian Republics*. Dordrecht: Springer Netherlands. doi:10.1007/978-94-017-2971-0.
King, S.A., Khalturin, V.I. and Tucker, B.E. eds., (1999). *Seismic Hazard and Building Vulnerability in Post-Soviet Central Asian Republics*. Dordrecht: Springer Netherlands. doi:10.1007/978-94-017-2971-0.
Kristo, C., Rahardjo, H. and Satyanaga, A. (2017). Effect of variations in rainfall intensity on slope stability in Singapore. *International Soil and Water Conservation Research*, 5(4), pp.258–264. doi: 10.1016/j.iswcr.2017.07.001.
Kristo, C., Rahardjo, H. and Satyanaga, A. (2017). Effect of variations in rainfall intensity on slope stability in Singapore. *International Soil and Water Conservation Research*, 5(4), pp.258–264. doi: 10.1016/j.iswcr.2017.07.001.

Lai, C., Chen, X., Wang, Z., Xu, C.-Y. and Yang, B. (2017). Rainfall-induced landslide susceptibility assessment using random forest weight at basin scale. *Hydrology Research*, 49(5), pp.1363–1378. doi:10.2166/nh.2017.044.
Lai, C., Chen, X., Wang, Z., Xu, C.-Y. and Yang, B. (2017). Rainfall-induced landslide susceptibility assessment using random forest weight at basin scale. *Hydrology Research*, 49(5), pp.1363–1378. doi:10.2166/nh.2017.044.
Leong, E.C., Rahardjo, H. and Satyanaga, A. (2011). *Unsaturated soil mechanics for slope stabilization*. [online] dr.ntu.edu.sg. Available at: https://hdl.handle.net/10356/93993 [Accessed 19 Nov. 2022].
Leong, E.C., Rahardjo, H. and Satyanaga, A. (2011). *Unsaturated soil mechanics for slope stabilization*. [online] dr.ntu.edu.sg. Available at: https://hdl.handle.net/10356/93993 [Accessed 19 Nov. 2022].

MUIR WOOD, D., MAEDA, K., & NUKUDANI, E. (2010). Modelling mechanical consequences of erosion. *Géotechnique*, *60*(6), 447–457. https://doi.org/10.1680/geot.2010.60.6.447
MUIR WOOD, D., MAEDA, K., & NUKUDANI, E. (2010). Modelling mechanical consequences of erosion. *Géotechnique*, *60*(6), 447–457. https://doi.org/10.1680/geot.2010.60.6.447
Ng, C. W., Zhan, L. T., Bao, C. G., Fredlund, D. G., & Gong, B. W. (2003). Performance of an unsaturated expansive soil slope subjected to artificial rainfall infiltration. *Géotechnique*, *53*(2), 143–157. https://doi.org/10.1680/geot.2003.53.2.143
Ng, C. W., Zhan, L. T., Bao, C. G., Fredlund, D. G., & Gong, B. W. (2003). Performance of an unsaturated expansive soil slope subjected to artificial rainfall infiltration. *Géotechnique*, *53*(2), 143–157. https://doi.org/10.1680/geot.2003.53.2.143
O'Kelly, B. C. (2015). Atterberg limits are not appropriate for peat soils. *Geotechnical Research*, *2*(3), 123–134. https://doi.org/10.1680/jgere.15.00007
O'Kelly, B. C. (2015). Atterberg limits are not appropriate for peat soils. *Geotechnical Research*, *2*(3), 123–134. https://doi.org/10.1680/jgere.15.00007

Olga Chepelianskaia., Madhurima Sarkar, Swais good. Climate Change Consultant to ESCAP Kazakhstan - Climate Change and Disaster Risk Profile. *2022, volume 1-19, United nation (ESCAP).*
Olga Chepelianskaia., Madhurima Sarkar, Swais good. Climate Change Consultant to ESCAP Kazakhstan - Climate Change and Disaster Risk Profile. *2022, volume 1-19, United nation (ESCAP).*

Pradel, D. (2020) "Numerical modelling for Slope Stabilizations in modern geotechnical practice," *Understanding and Reducing Landslide Disaster Risk*, pp. 65–79. Available at: https://doi.org/10.1007/978-3-030-60706-7_4.

Pradel, D. (2020) “Numerical modelling for Slope Stabilizations in modern geotechnical practice,” *Understanding and Reducing Landslide Disaster Risk*, pp. 65–79. Available at: https://doi.org/10.1007/978-3-030-60706-7_4.

Qian, Z., & Rahardjo, H. (2016). Application of fitting parameters in best fit equation. *E3S Web of Conferences*, *9*, 10008. https://doi.org/10.1051/e3sconf/20160910008
Qian, Z., & Rahardjo, H. (2016). Application of fitting parameters in best fit equation. *E3S Web of Conferences*, *9*, 10008. https://doi.org/10.1051/e3sconf/20160910008
Rahardjo, H., Kim, Y. and Satyanaga, A. (2019). Role of unsaturated soil mechanics in geotechnical engineering. *International Journal of Geo-Engineering*, 10(1). doi:10.1186/s40703-019-0104-8
Rahardjo, H., Kim, Y. and Satyanaga, A. (2019). Role of unsaturated soil mechanics in geotechnical engineering. *International Journal of Geo-Engineering*, 10(1). doi:10.1186/s40703-019-0104-8
Rahardjo, H., Ong, T. H., Rezaur, R. B., & Leong, E. C. (2007). Factors Controlling Instability of Homogeneous Soil Slopes under Rainfall. Journal of Geotechnical and Geoenvironmental Engineering, 133(12), 1532–1543. doi:10.1061/(asce)1090-0241(2007)133:12(1532).
Rahardjo, H., Ong, T. H., Rezaur, R. B., & Leong, E. C. (2007). Factors Controlling Instability of Homogeneous Soil Slopes under Rainfall. Journal of Geotechnical and Geoenvironmental Engineering, 133(12), 1532–1543. doi:10.1061/(asce)1090-0241(2007)133:12(1532).
Rahardjo.H, Satyanaga. A and Leong E. C. (2012). Unsaturated Soil Mechanics for Slope Stabilization. *Geotechnical Engineering Journal of the SEAGS & AGSSEA* Vol. 43 No.1 March 2012 ISSN 0046-5828
Rahardjo.H, Satyanaga. A and Leong E. C. (2012). Unsaturated Soil Mechanics for Slope Stabilization. *Geotechnical Engineering Journal of the SEAGS & AGSSEA* Vol. 43 No.1 March 2012 ISSN 0046-5828

Russell, A. R. (2010). Water retention characteristics of soils with double porosity. *European Journal of Soil Science*, *61*(3), 412–424. https://doi.org/10.1111/j.1365-2389.2010.01237.x
Russell, A. R. (2010). Water retention characteristics of soils with double porosity. *European Journal of Soil Science*, *61*(3), 412–424. https://doi.org/10.1111/j.1365-2389.2010.01237.x

Satyanaga, A., Bairakhmetov, N., Kim, J.R. and Moon, S.-W. (2022). Role of Bimodal Water Retention Curve on the Unsaturated Shear Strength. *Applied Sciences*, 12(3), p.1266. doi:10.3390/app12031266.

Satyanaga, A., Bairakhmetov, N., Kim, J.R. and Moon, S.-W. (2022). Role of Bimodal Water Retention Curve on the Unsaturated Shear Strength. *Applied Sciences*, 12(3), p.1266. doi:10.3390/app12031266.

Satyanaga, A., Rahardjo, H., Leong, E.-C. and Wang, J.-Y. (2013). Water characteristic curve of soil with bimodal grain-size distribution. *Computers and Geotechnics*, 48, pp.51–61. doi: 10.1016/j.compgeo.2012.09.008.

Satyanaga, A., Rahardjo, H., Leong, E.-C. and Wang, J.-Y. (2013). Water characteristic curve of soil with bimodal grain-size distribution. *Computers and Geotechnics*, 48, pp.51–61. doi: 10.1016/j.compgeo.2012.09.008.

Satyanaga, A., Rahardjo, H., Leong, E.-C. and Wang, J.-Y. (2013). Water characteristic curve of soil with bimodal grain-size distribution. *Computers and Geotechnics*, 48, pp.51–61. doi: 10.1016/j.compgeo.2012.09.008.

Satyanaga, A., Rahardjo, H., Leong, E.-C. and Wang, J.-Y. (2013). Water characteristic curve of soil with bimodal grain-size distribution. *Computers and Geotechnics*, 48, pp.51–61. doi: 10.1016/j.compgeo.2012.09.008.

Standard test method for consolidated undrained triaxial compression test for cohesive soils. ASTM International - Standards Worldwide. (n.d.). Retrieved 2023, from https://www.astm.org/d4767-11r20.html

Standard test method for consolidated undrained triaxial compression test for cohesive soils. ASTM International - Standards Worldwide. (n.d.). Retrieved 2023, from https://www.astm.org/d4767-11r20.html

Standard test method for sieve analysis of fine and coarse aggregates. ASTM International - Standards Worldwide. (n.d.). Retrieved June 3, 2022, from https://www.astm.org/c0136_c0136m-19.html

Standard test method for sieve analysis of fine and coarse aggregates. ASTM International - Standards Worldwide. (n.d.). Retrieved 2022, from https://www.astm.org/c0136_c0136m-19.html

Standard test method for sieve analysis of fine and coarse aggregates. ASTM International - Standards Worldwide. (n.d.). Retrieved June 3, 2022, from https://www.astm.org/c0136_c0136m-19.html

Standard test method for sieve analysis of fine and coarse aggregates. ASTM International - Standards Worldwide. (n.d.). Retrieved 2022, from https://www.astm.org/c0136_c0136m-19.html

Standard test methods for laboratory compaction characteristics of soil using standard effort (12,400 ft-lbf/FT3 (600 kN-m/m3)). ASTM International - Standards Worldwide. (n.d.). Retrieved 2022, from https://www.astm.org/d0698-12r21.html

Standard test methods for laboratory compaction characteristics of soil using standard effort (12,400 ft-lbf/FT3 (600 kN-m/m3)). ASTM International - Standards Worldwide. (n.d.). Retrieved 2022, from https://www.astm.org/d0698-12r21.html

Standard test methods for liquid limit, plastic limit, and plasticity index of Soils. ASTM International - Standards Worldwide. (n.d.). Retrieved 2022, from https://www.astm.org/d4318-17e01.html

Standard test methods for liquid limit, plastic limit, and plasticity index of Soils. ASTM International - Standards Worldwide. (n.d.). Retrieved 2022, from https://www.astm.org/d4318-17e01.html
Standard test methods for measurement of hydraulic conductivity of coarse-grained soils. ASTM International - Standards Worldwide. (n.d.). Retrieved 2023, from https://www.astm.org/d2434-22.html
Standard test methods for measurement of hydraulic conductivity of coarse-grained soils. ASTM International - Standards Worldwide. (n.d.). Retrieved 2023, from https://www.astm.org/d2434-22.html
Think Hazard, (2020) *Almatinskaya region, Alamty Kazakhstan- landsliding risks* , *Think Hazard - Almatinskaya - landslide*. Available at: https://thinkhazard.org/en/report/1716-kazakhstan-almatinskaya/LS (Accessed: August 20, 2022).
Think Hazard, (2020) *Almatinskaya region, Alamty Kazakhstan- landsliding risks* , *Think Hazard - Almatinskaya - landslide*. Available at: https://thinkhazard.org/en/report/1716-kazakhstan-almatinskaya/LS (Accessed: August 20, 2022).
Vanapalli, S. K., & Oh, W. T. (2010, July). Mechanics of unsaturated soils for the design of Foundation Structures. Retrieved August 20, 2022, from https://www.researchgate.net/publication/262353348_Mechanics_of_unsaturated_soils_for_the_design_of_foundation_structures
Vanapalli, S. K., & Oh, W. T. (2010, July). Mechanics of unsaturated soils for the design of Foundation Structures. Retrieved August 20, 2022, from https://www.researchgate.net/publication/262353348_Mechanics_of_unsaturated_soils_for_the_design_of_foundation_structures

Weather and climate (2010). *Weather and Climate information for every country in the world.* [online] Weather-and-climate.com. Available at: https://weather-and-climate.com/.
Weather and climate (2010). *Weather and Climate information for every country in the world.* [online] Weather-and-climate.com. Available at: https://weather-and-climate.com/.

Wijaya, M., & Leong, E. C. (2016). Equation for unimodal and bimodal soil–water characteristic curves. *Soils and Foundations*, *56*(2), 291–300. https://doi.org/10.1016/j.sandf.2016.02.011
Wijaya, M., & Leong, E. C. (2016). Equation for unimodal and bimodal soil–water characteristic curves. *Soils and Foundations*, *56*(2), 291–300. https://doi.org/10.1016/j.sandf.2016.02.011

Yarifudin, A. and Satyanaga, A. (2021). Variability of Bimodal Soil-Water Characteristic Curves under Different Confining Pressures. *Applied and Environmental Soil Science*, 2021, pp.1–10. doi:10.1155/2021/5569491.
Yarifudin, A. and Satyanaga, A. (2021). Variability of Bimodal Soil-Water Characteristic Curves under Different Confining Pressures. *Applied and Environmental Soil Science*, 2021, pp.1–10. doi:10.1155/2021/5569491.

Zhai, Q., Rahardjo, H., Satyanaga, A. and Dai, G. (2020). Estimation of the soil-water characteristic curve from the grain size distribution of coarse-grained soils. *Engineering Geology*, 267, p.105502. doi: 10.1016/j.enggeo.2020.105502
Zhai, Q., Rahardjo, H., Satyanaga, A. and Dai, G. (2020). Estimation of the soil-water characteristic curve from the grain size distribution of coarse-grained soils. *Engineering Geology*, 267, p.105502. doi: 10.1016/j.enggeo.2020.105502
Zhai, Q., Rahardjo, H., Satyanaga, A. and Priono (2017). Effect of bimodal soil-water characteristic curve on the estimation of permeability function. *Engineering Geology*, 230, pp.142–151. doi: 10.1016/j.enggeo.2017.09.025.
Zhai, Q., Rahardjo, H., Satyanaga, A. and Priono (2017). Effect of bimodal soil-water characteristic curve on the estimation of permeability function. *Engineering Geology*, 230, pp.142–151. doi: 10.1016/j.enggeo.2017.09.025.
Zhao, Y. *et al.* (2008) "Maximum bulk density of British Columbia forest soils from the Proctor test: Relationships with selected physical and Chemical Properties," *Soil Science Society of America Journal*, 72(2), pp. 442–452. Available at: https://doi.org/10.2136/sssaj2007.0075.
Zhao, Y. *et al.* (2008) "Maximum bulk density of British Columbia forest soils from the Proctor test: Relationships with selected physical and Chemical Properties," *Soil Science Society of America Journal*, 72(2), pp. 442–452. Available at: https://doi.org/10.2136/sssaj2007.0075.

Chapter 8 - APPENDIX A

8.1 Seepage and slope stability analyses for silty sand soil with different slope geometries.

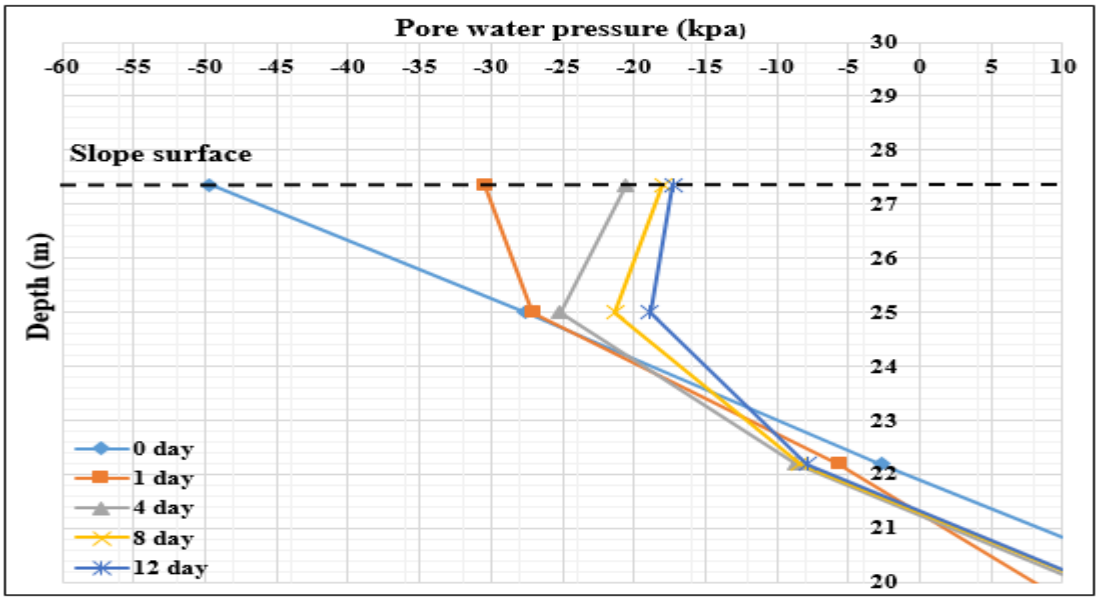

Figure A.1 Pore-water Pressure during rainfall (20m/day) for 12 days at mid slope (10 m, 27deg)

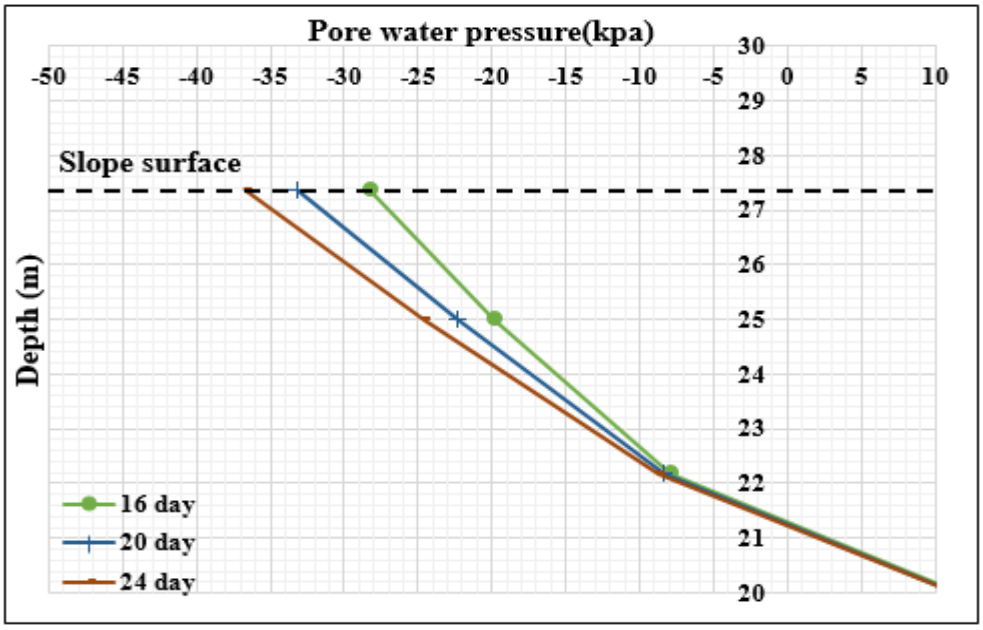

Figure A.2 Pore-water Pressure during dry periods at mid slope after 12 days' rainfall (10 m, 27 degree)

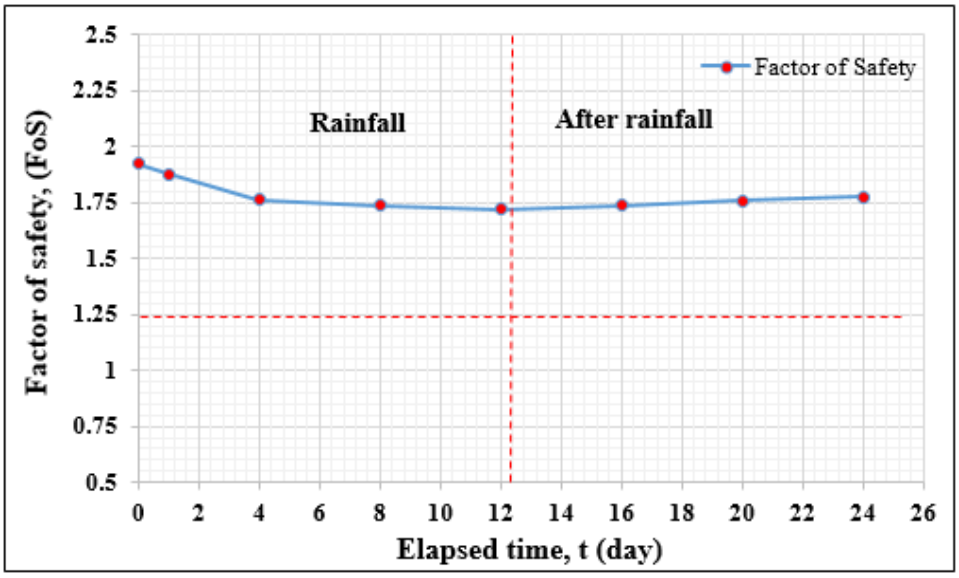

Figure A.3 Factor of safety (FoS) for silty sand soil (10m with 27 degree)

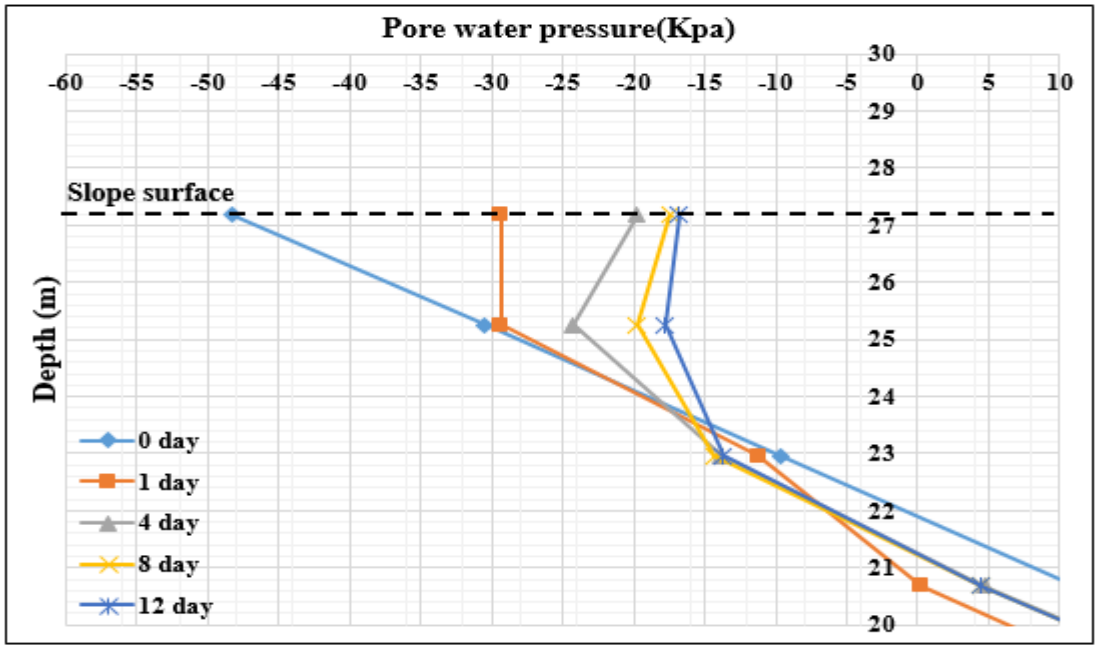

Figure A. 4 Pore-water Pressure during rainfall (20m/day) for 12 days at mid slope (10 m, 35deg)

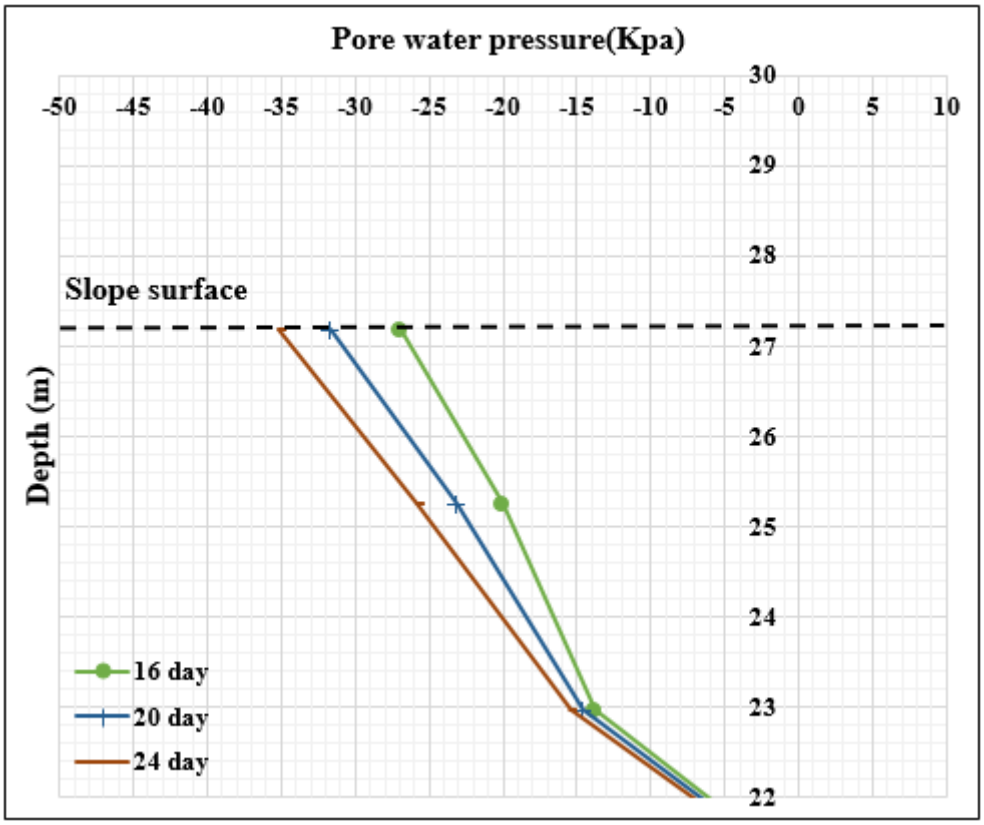

Figure A.5 Pore-water Pressure during dry periods at mid slope after 12 days' rainfall (10 m, 35 degree)

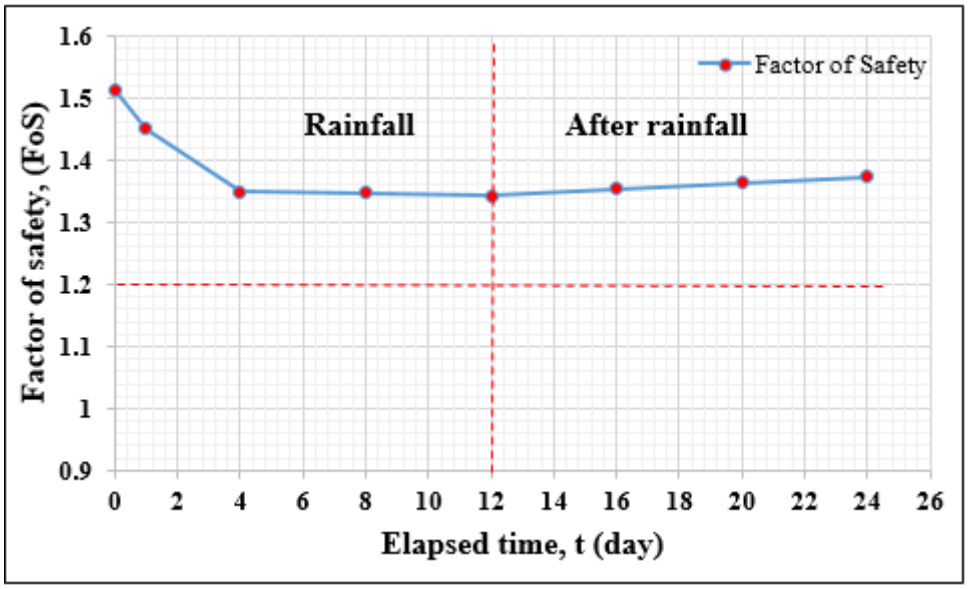

Figure A.6 Factor of safety (FoS) for silty sand soil (10m with 35⁰ degree)

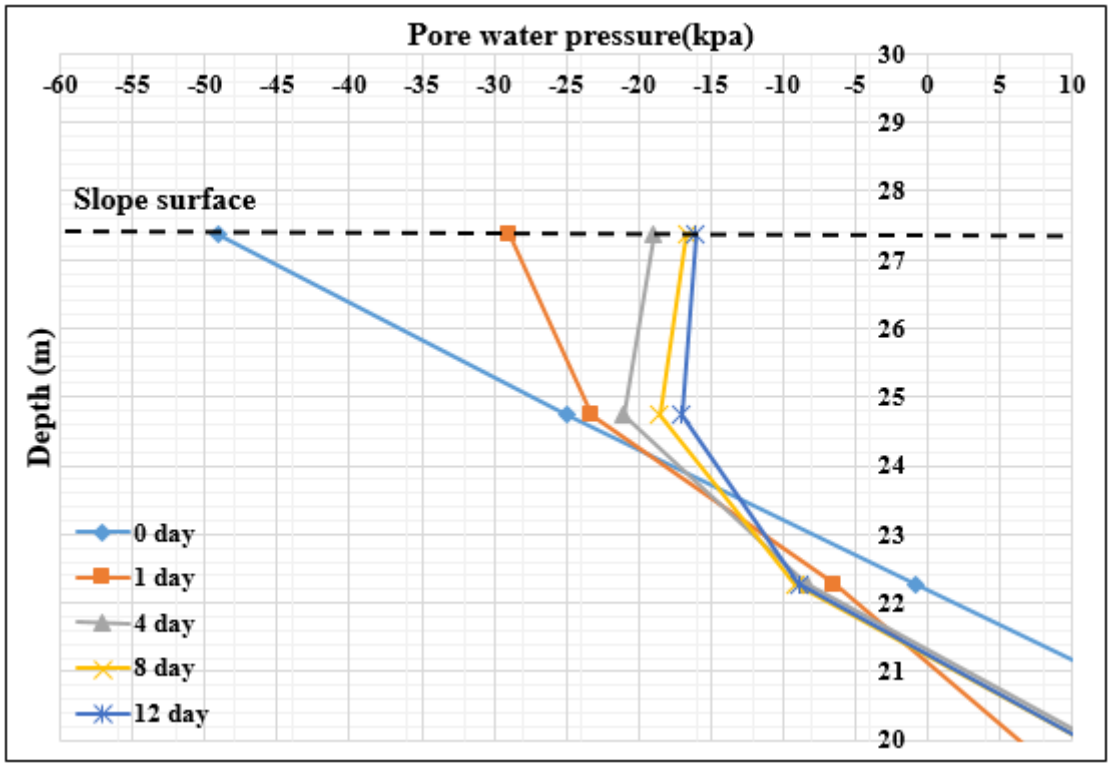

Figure A.7 Pore-water Pressure during rainfall (20m/day) for 12 days at mid slope (10 m, 45deg)

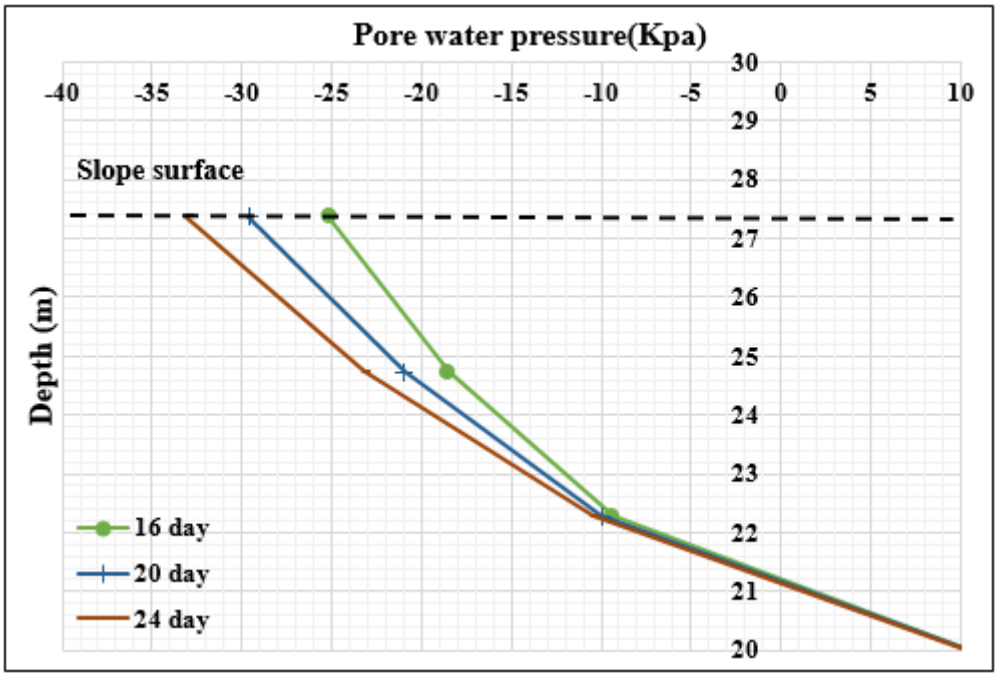

Figure A.8 Pore-water Pressure during dry periods at mid slope after 12 days' rainfall (10 m, 45 degree)

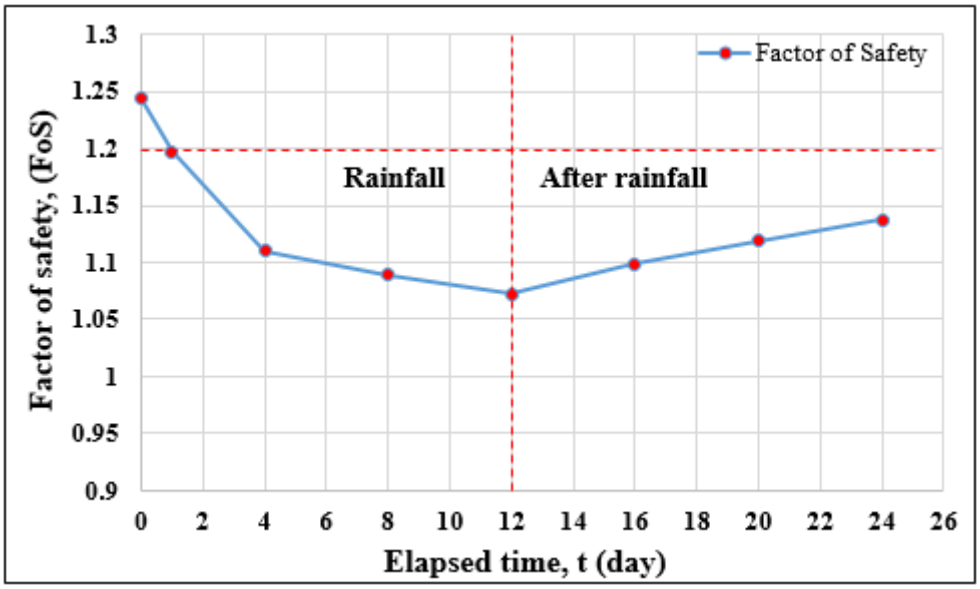

Figure A.9 Factor of safety (FoS) for silty sand soil (10m with 45^{0} degree)

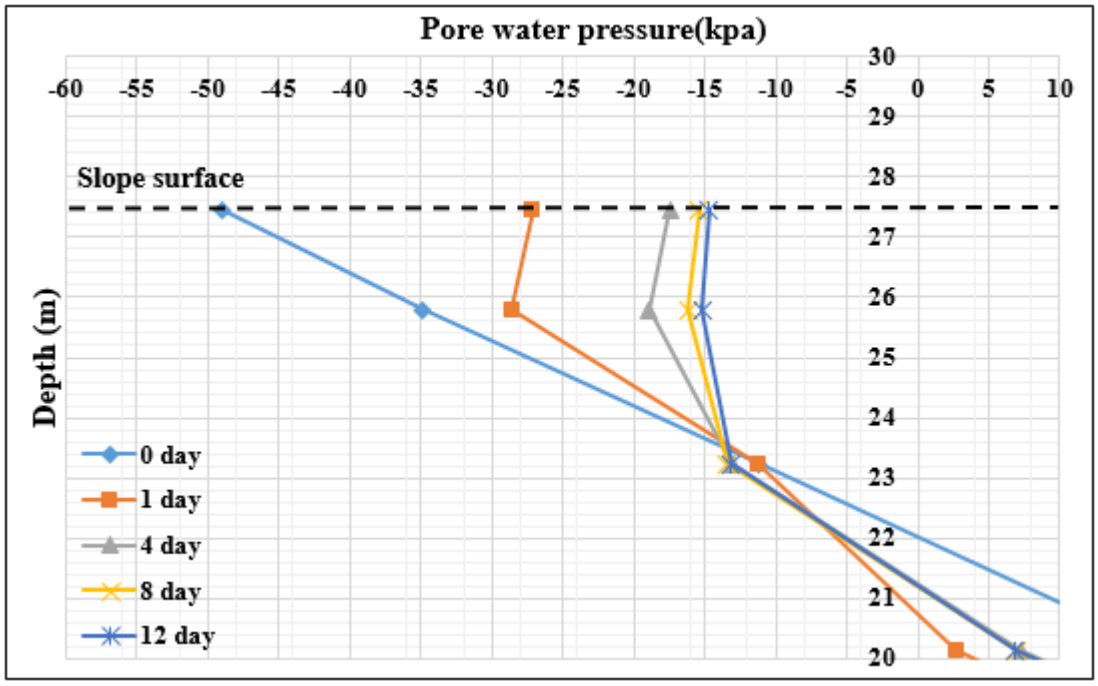

Figure A.10 Pore-water Pressure during rainfall (20m/day) for 12 days at mid slope (10 m, 60deg)

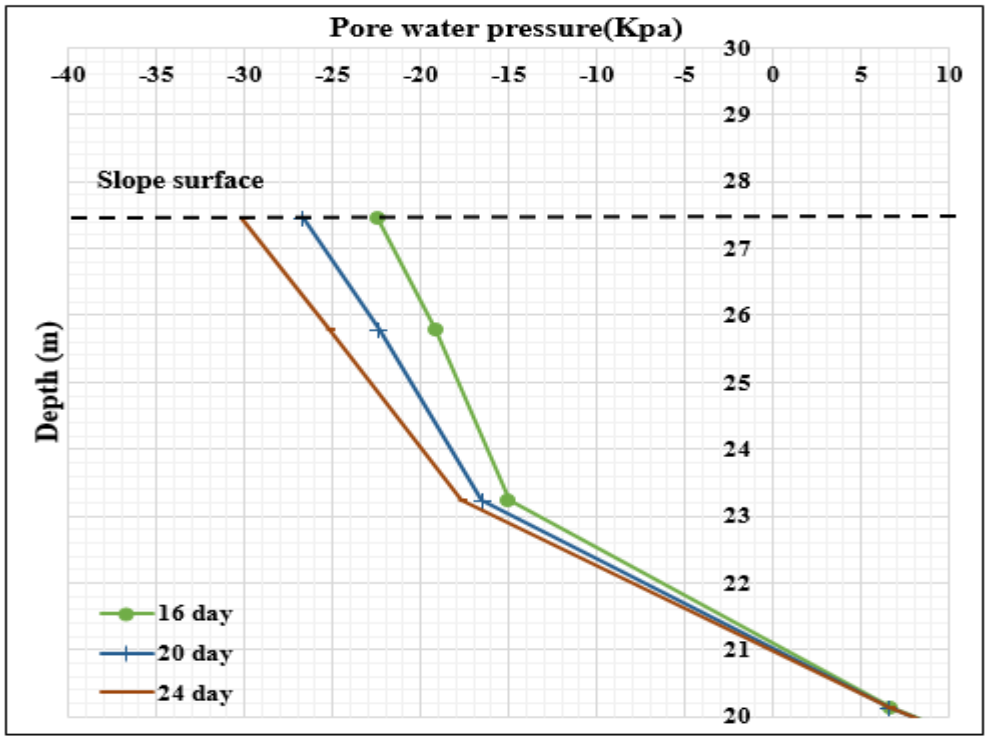

Figure A.11 Pore-water Pressure during dry periods at mid slope after 12 days' rainfall (10 m, 60 degree)

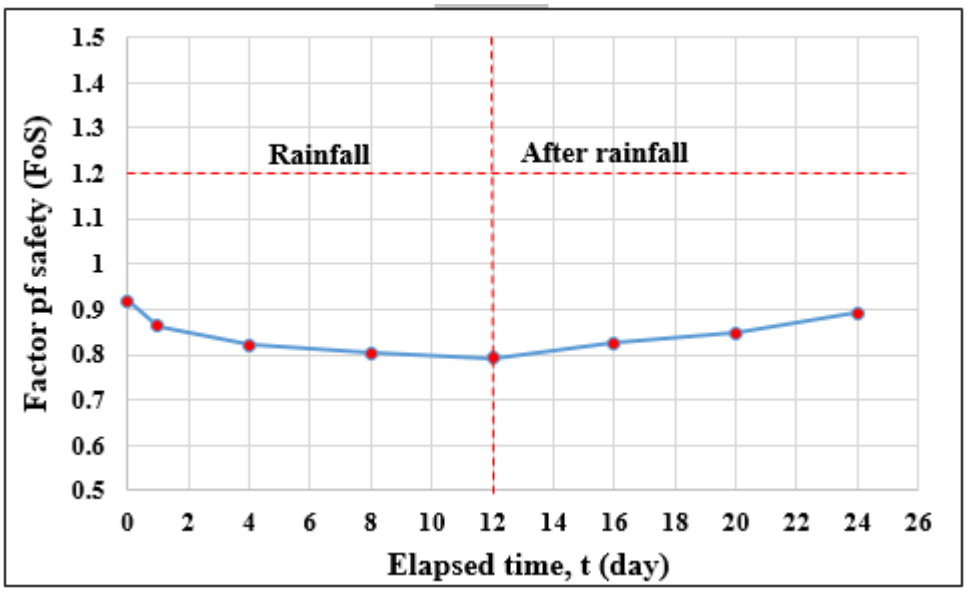

Figure A.12 Factor of safety (FoS) for silty sand soil, (10m with 60⁰ degree)

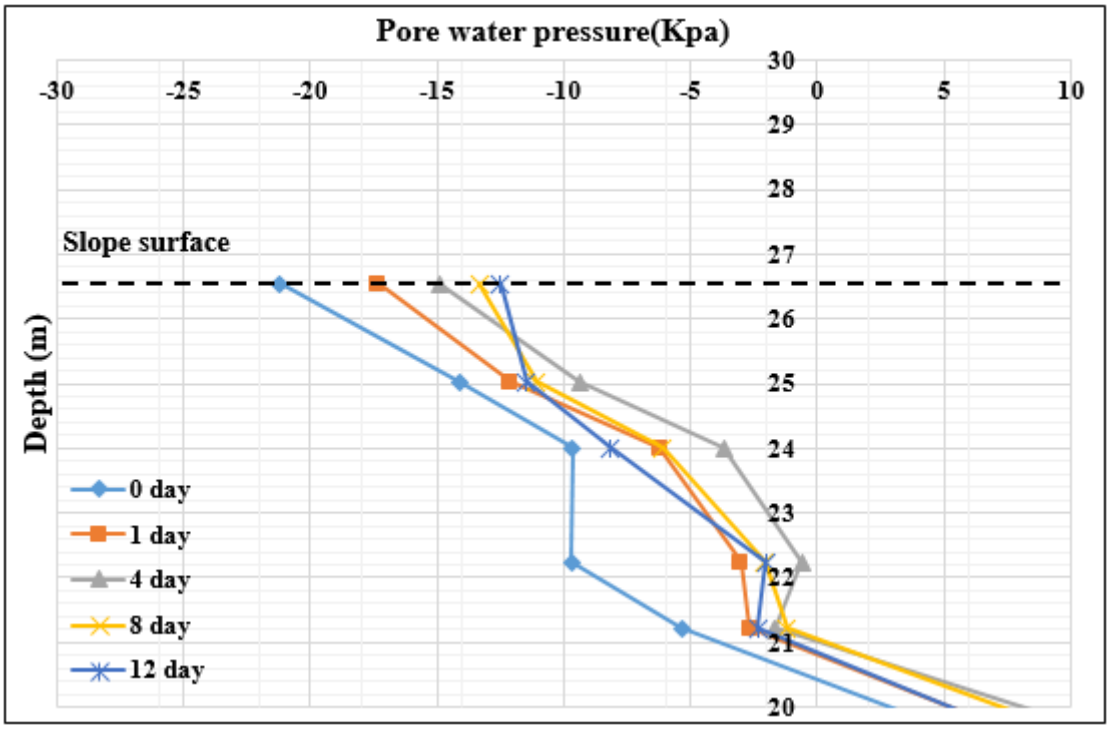

Figure A.13 Pore-water Pressure during rainfall (20m/day) for 12 days at mid slope (10 m, 80deg)

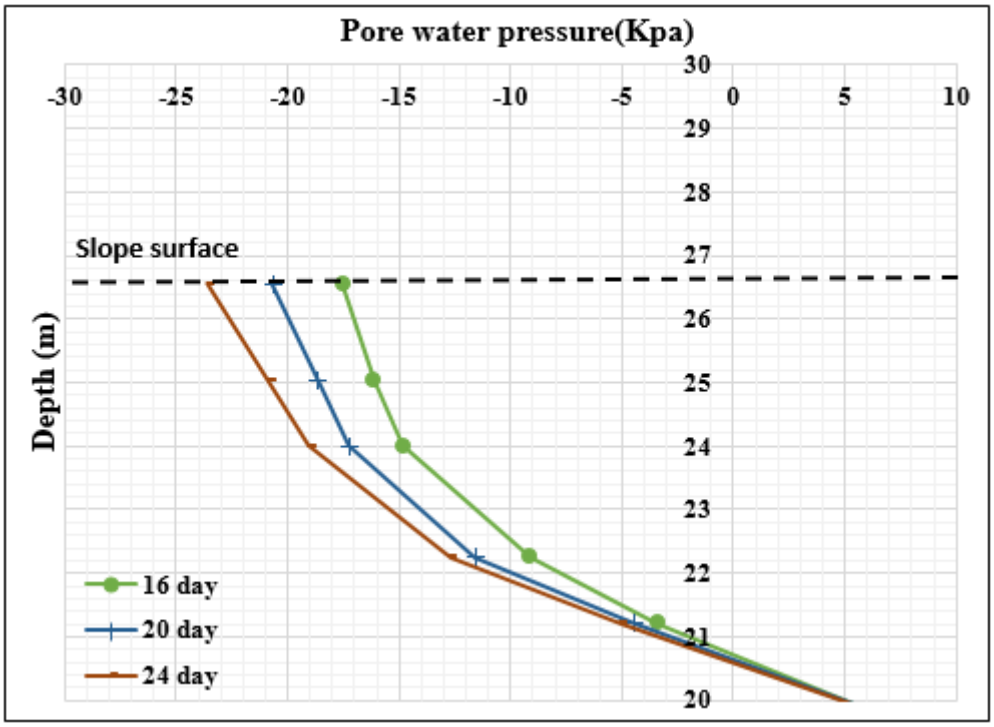

Figure A.14 Pore-water Pressure during dry periods at mid slope after 12 days' rainfall (10 m, 80 degree)

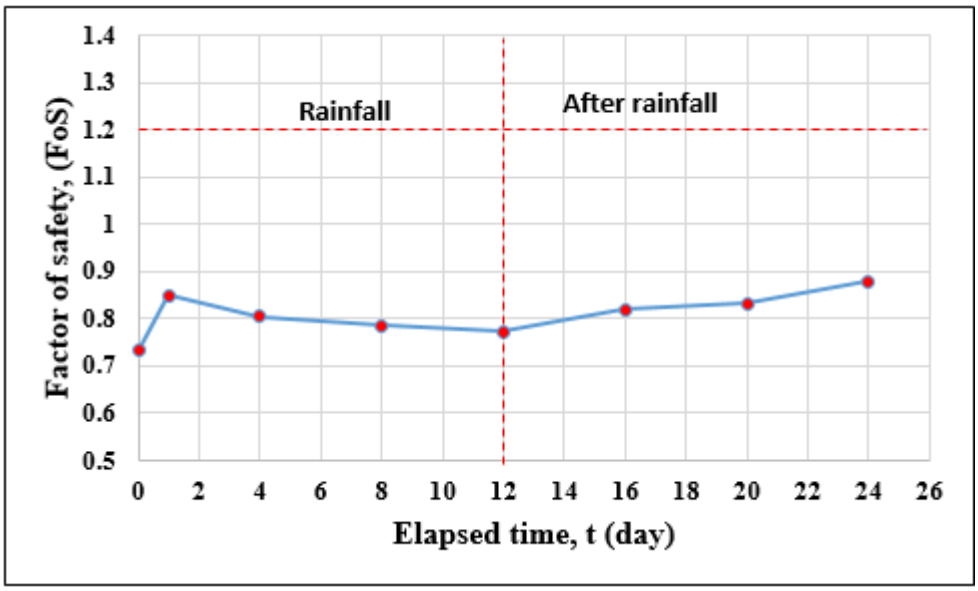

Figure A.15 Factor of safety (FoS) for silty sand soil (10m with 80⁰ degree)

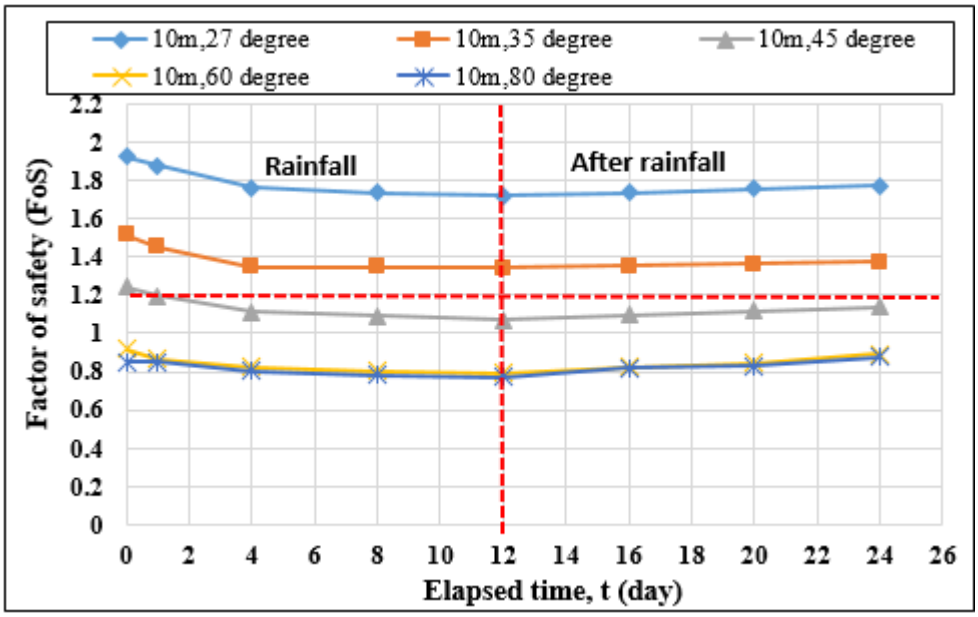

Figure A.16 Factor of safety (FoS) for silty sand, (10m with 27º,35º,45º,60º and 80º degrees)

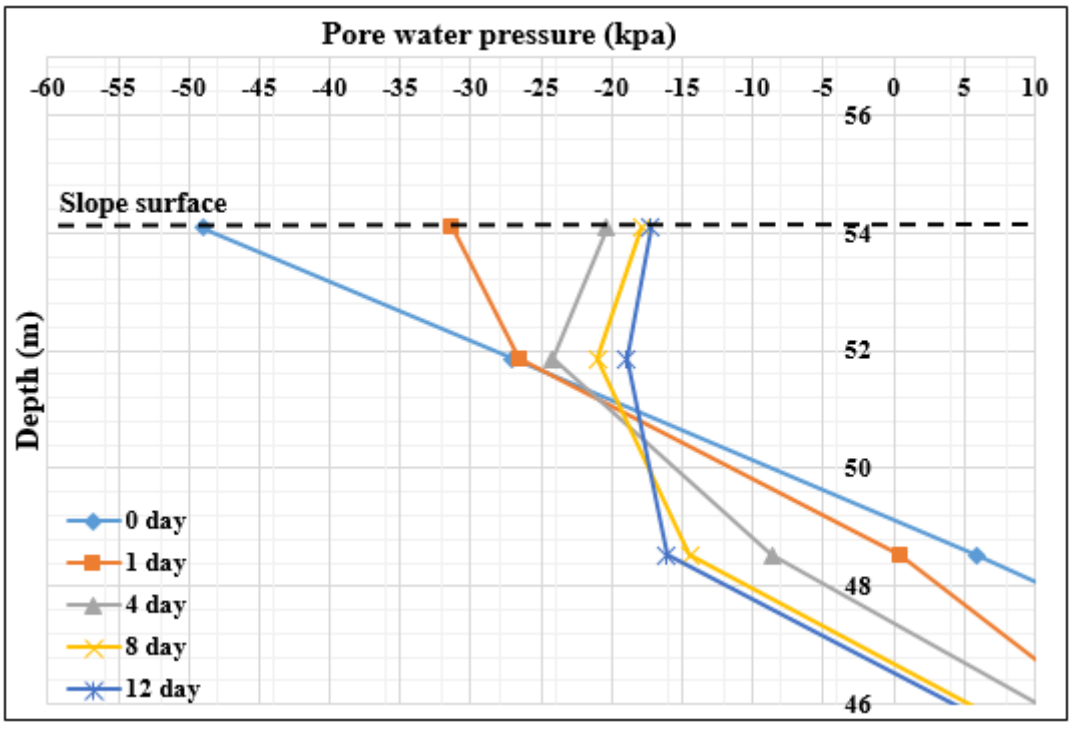

Figure A.17 Pore-water Pressure during rainfall (20m/day) for 12 days at mid slope (20m, 27degee)

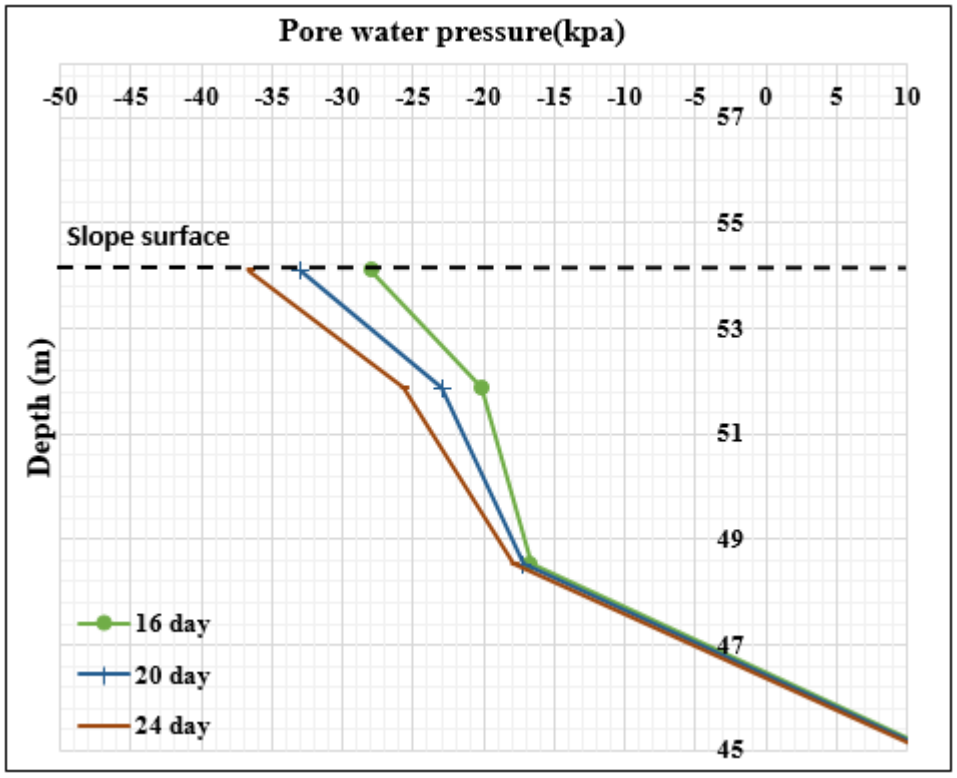

Figure A.18 Pore-water Pressure during dry periods at mid slope after 12 days' rainfall (20 m, 27 degree)

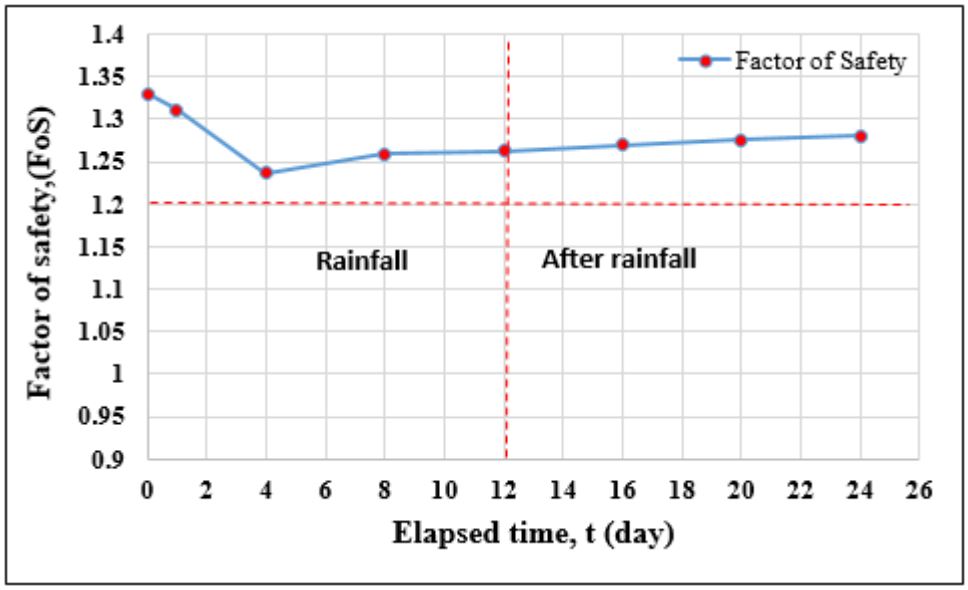

Figure A.19 Factor of safety (FoS) for silty sand soil, (20m with 27⁰ degree)

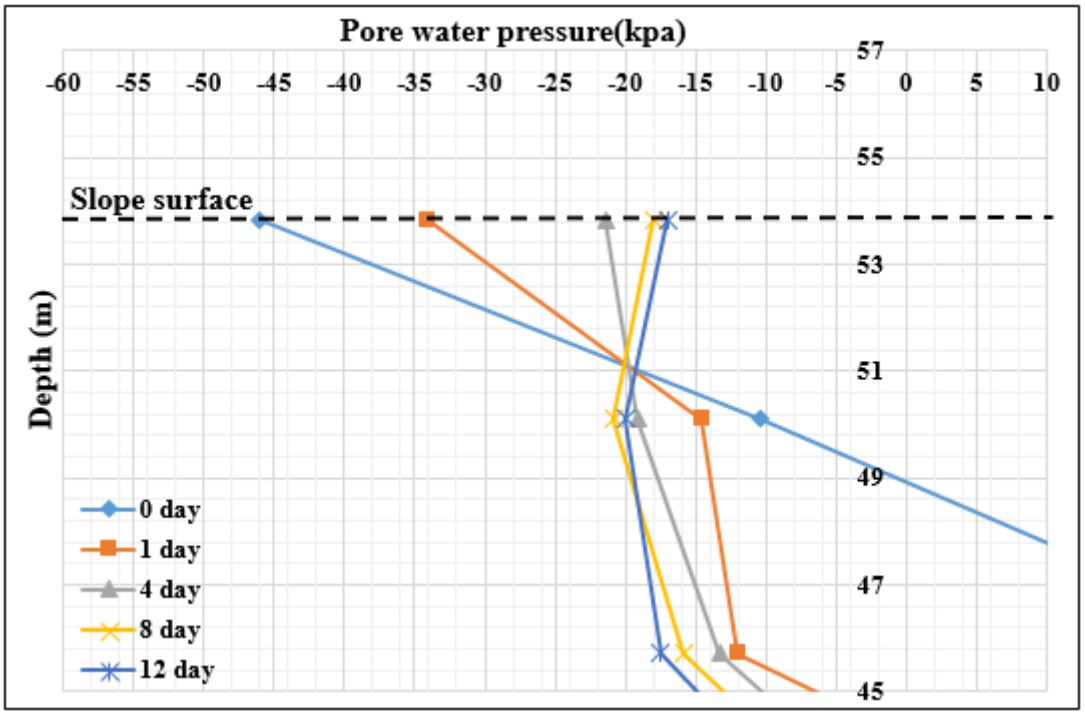

Figure A.20 Pore-water Pressure during rainfall (20m/day) for 12 days at mid slope (20m, 35degee)

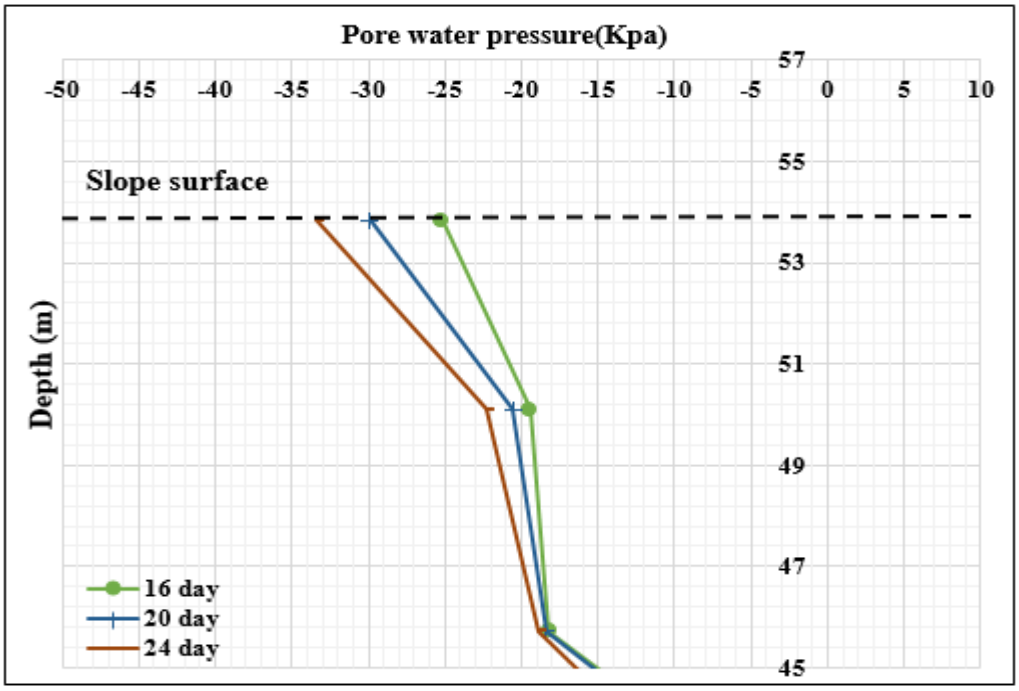

Figure A.21 Pore-water Pressure during dry periods at mid slope after 12 days' rainfall (20 m, 35 degree)

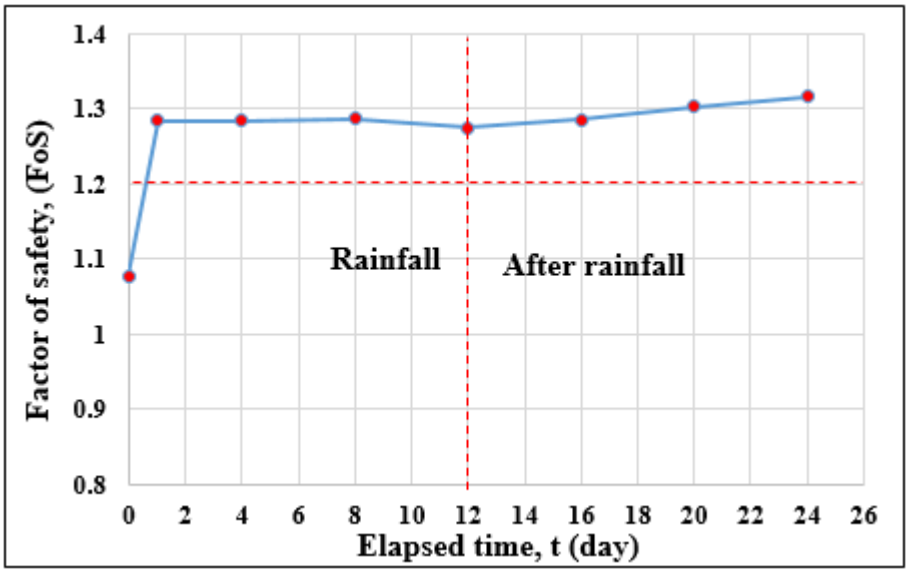

Figure A.22 Factor of safety (FoS) for silty sand soil, (20m with 35⁰ degree)

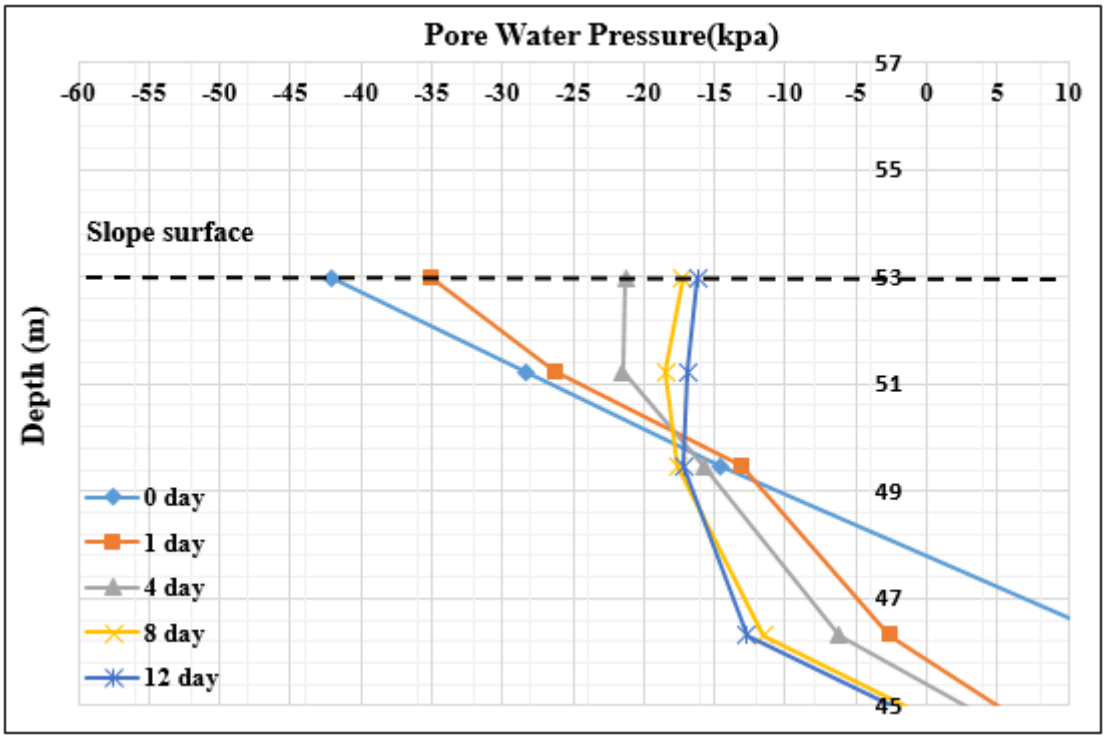

Figure A.23 Pore-water Pressure during rainfall (20m/day) for 12 days at mid slope (20 m, 45deg)

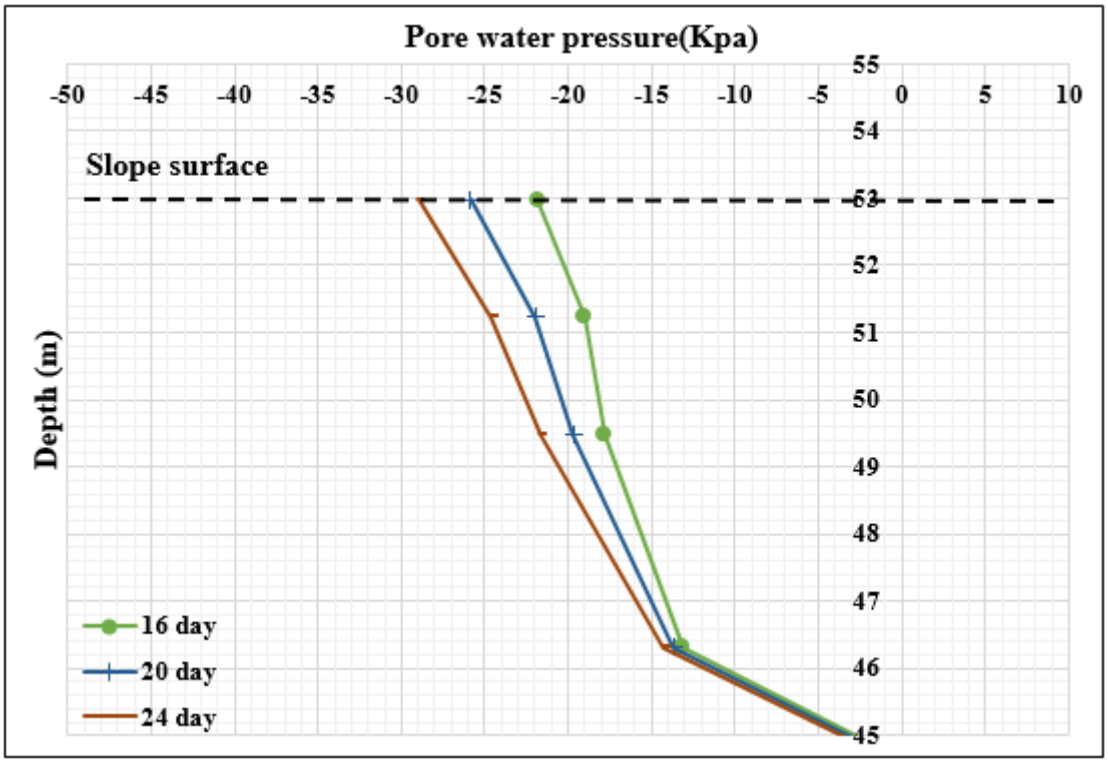

Figure A.24 Pore-water Pressure during dry periods at mid slope after 12 days' rainfall (20 m, 45 degree)

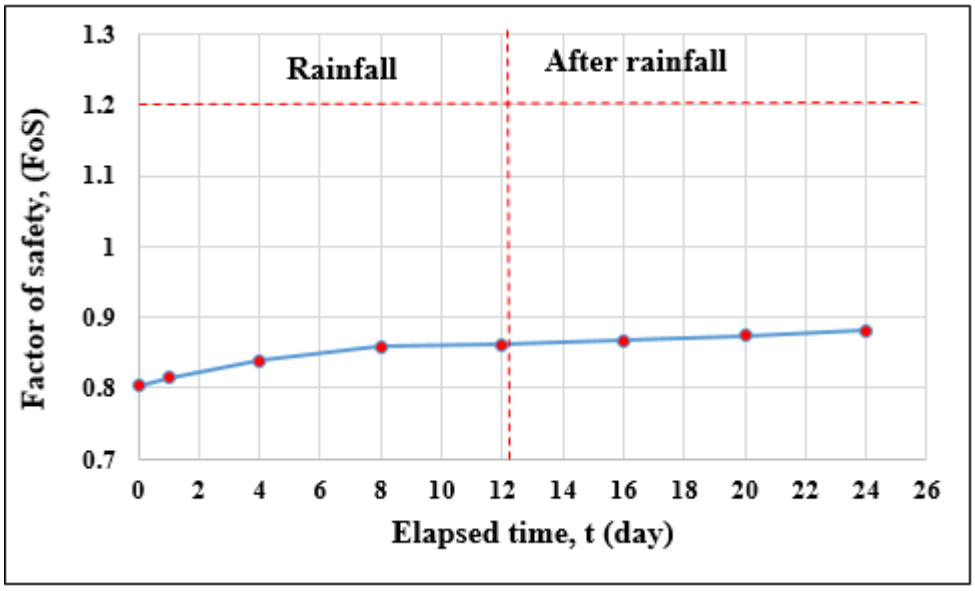

Figure A.25 Factor of safety (FoS) for silty sand soil, (20m with 45^{0} degree)

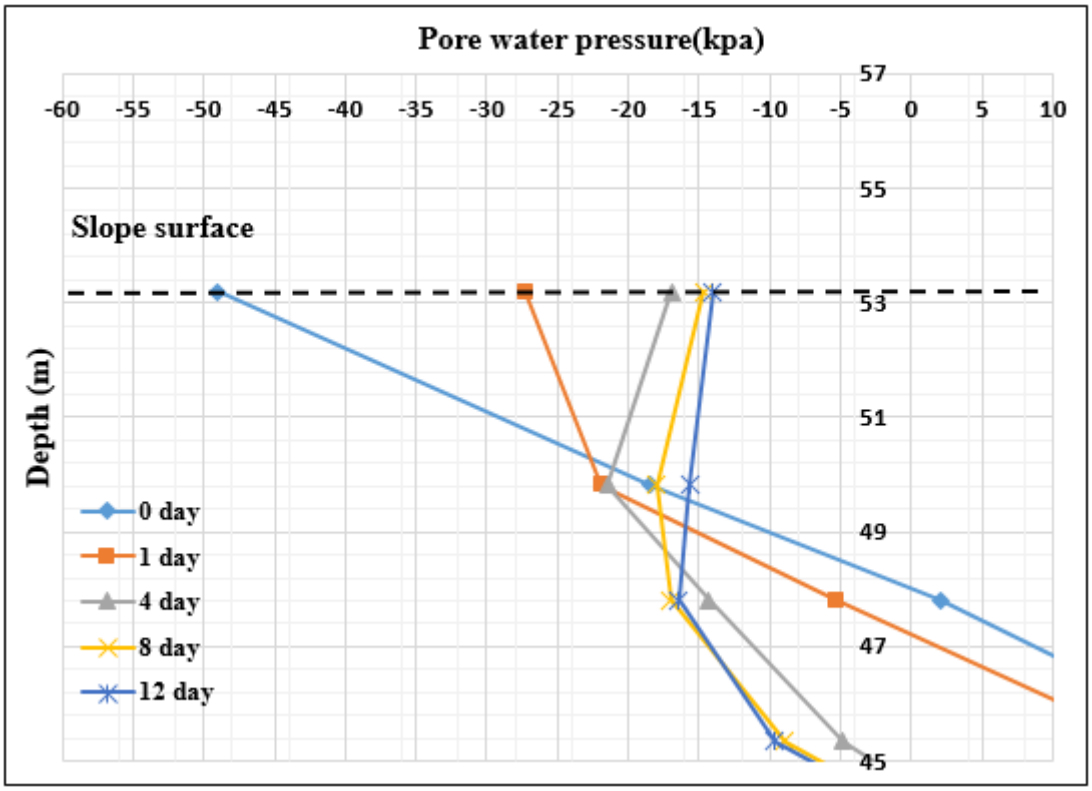

Figure A.26 Pore-water Pressure during rainfall (20m/day) for 12 days at mid slope (20 m, 60deg)

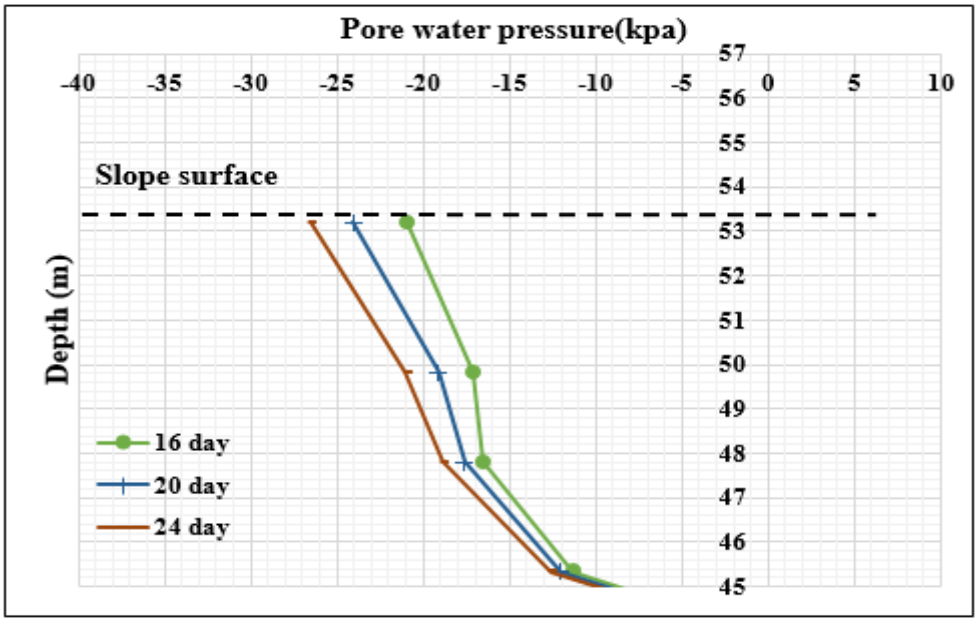

Figure 27 Pore-water Pressure during dry periods at mid slope after 12 days' rainfall (20 m, 60 degree)

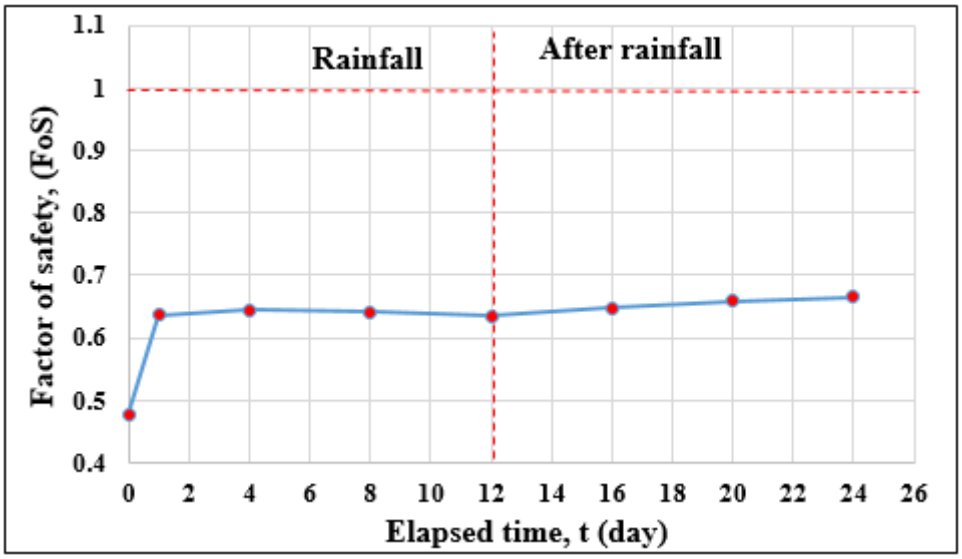

Figure A.28 Factor of safety (FoS) for silty sand soil, (20m with 60^{o} degree)

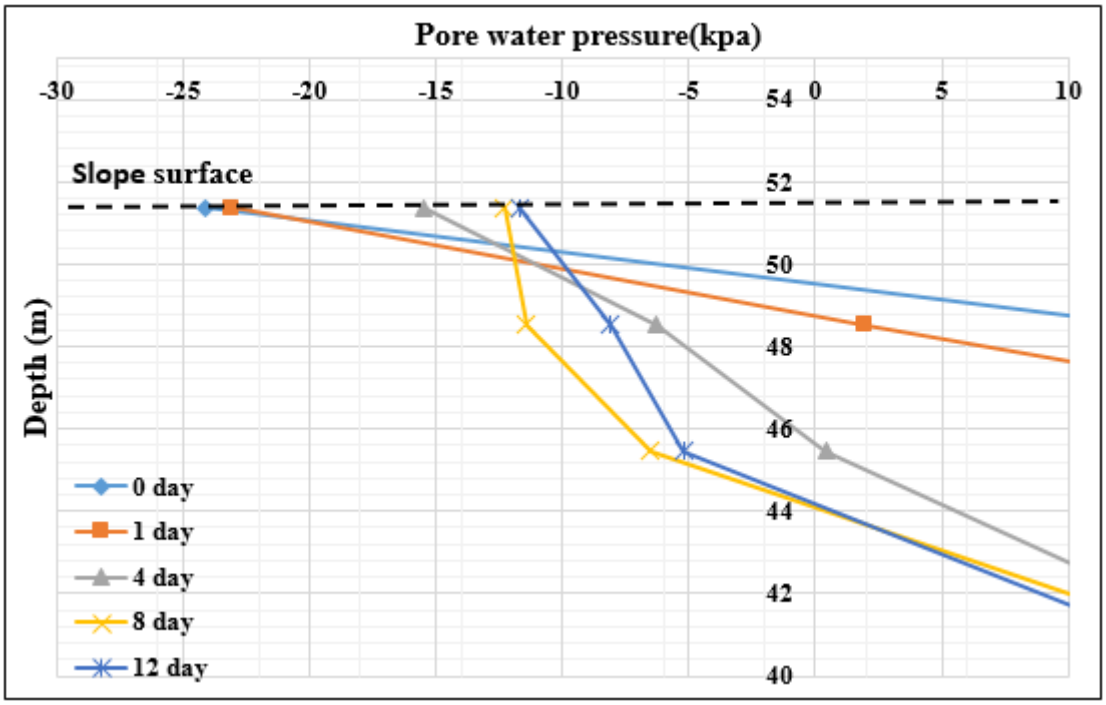

Figure A.29 Pore-water Pressure during rainfall (20m/day) for 12 days at mid slope (20 m, 80deg)

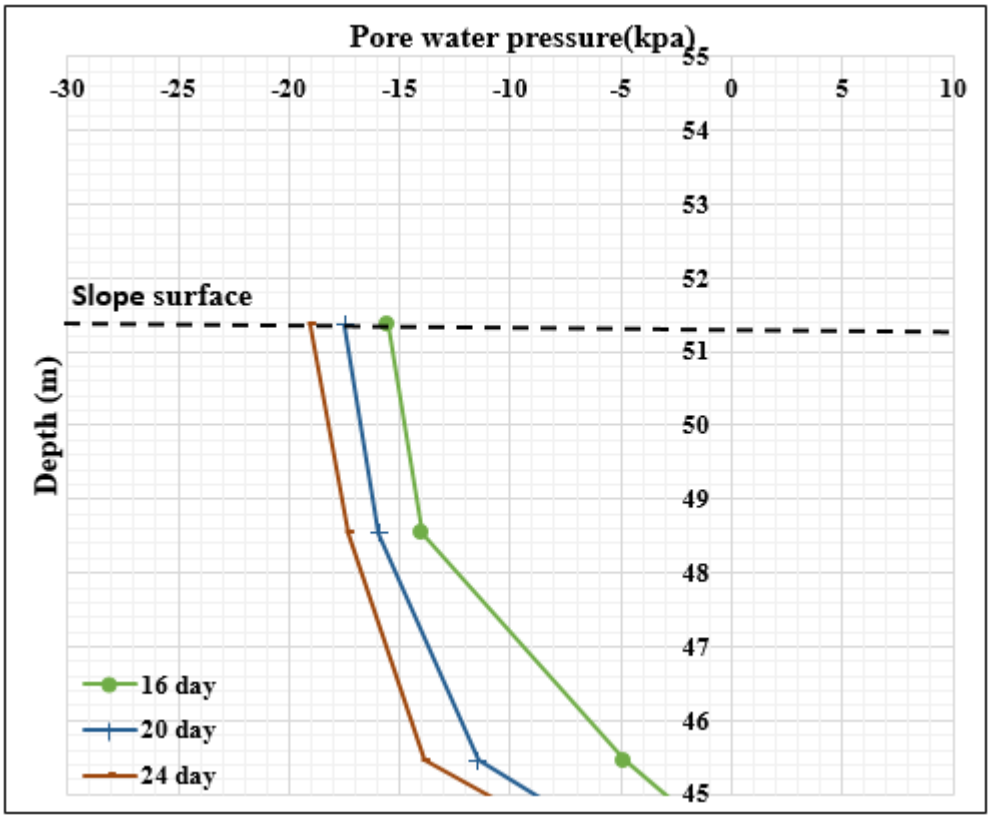

Figure A.30 Pore-water Pressure during dry periods at mid slope after 12 days' rainfall (20 m, 80 degree)

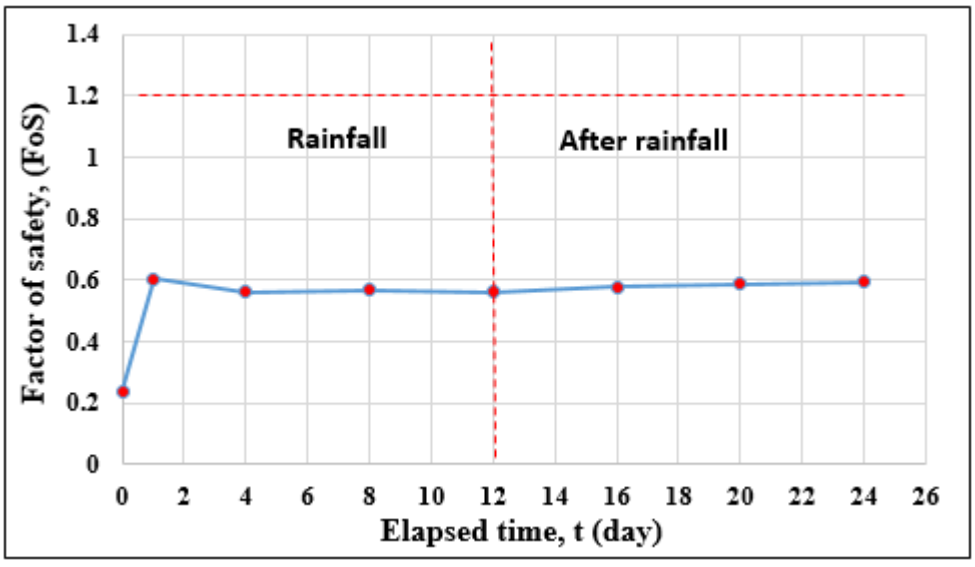

Figure A.31 Factor of safety (FoS) for silty sand soil, (20m with 80⁰ degree)

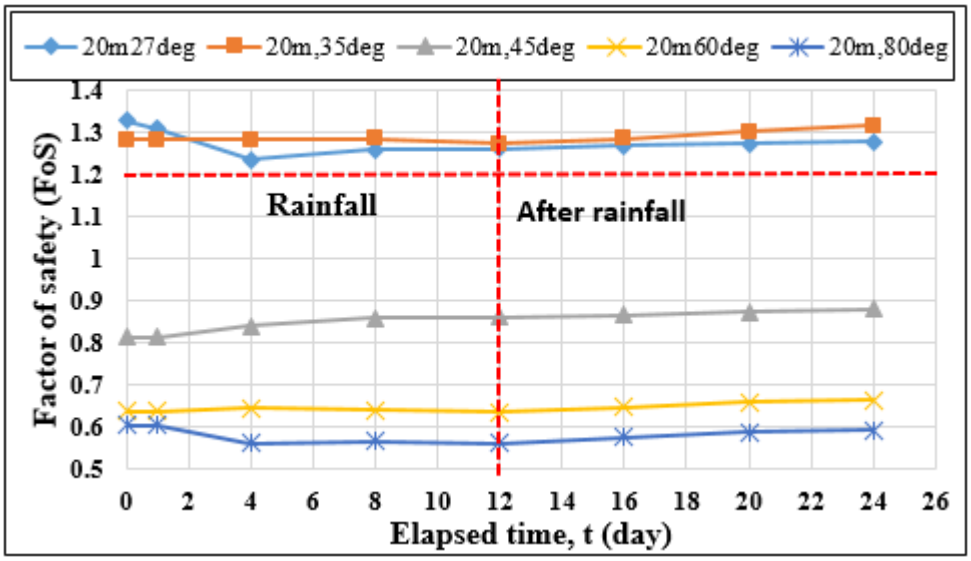

Figure A.32 Factor of safety (FoS) for fine grained soil, (20m with 27⁰,35⁰,45⁰,60⁰ and 80⁰ degrees)

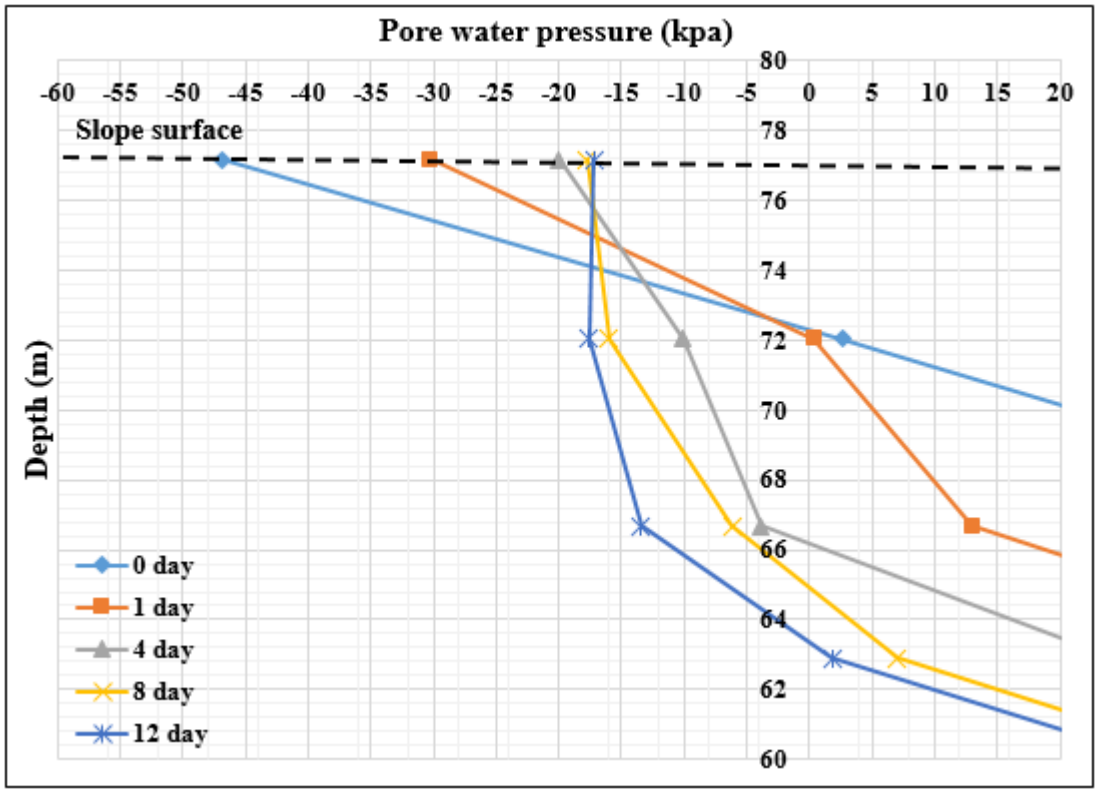

Figure A.33 Pore-water Pressure during rainfall (20m/day) for 12 days at mid slope (30 m, 27deg)

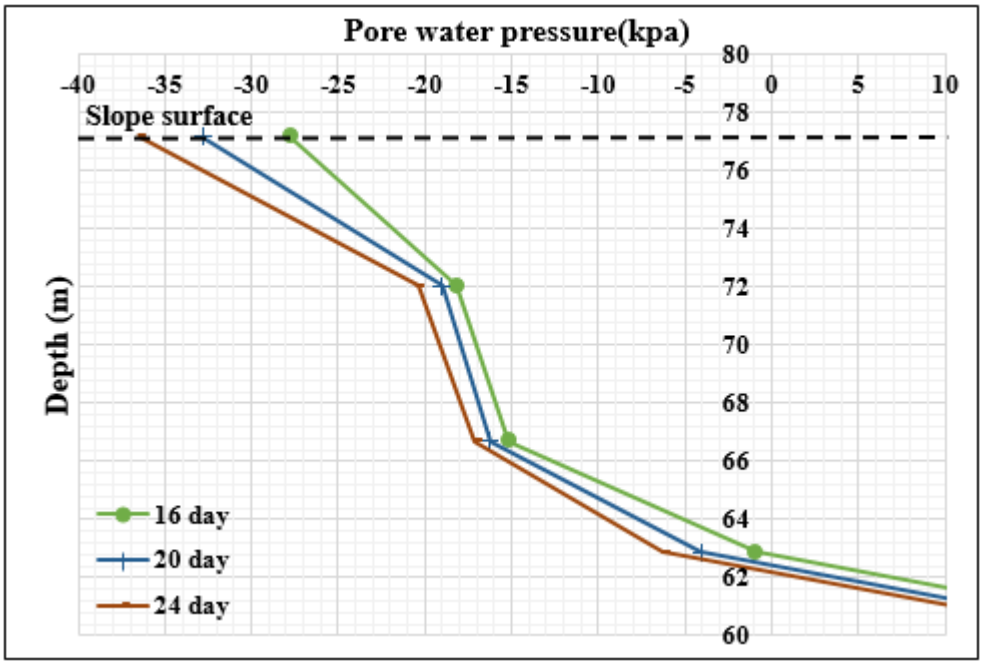

Figure A.34 Pore-water Pressure during dry periods at mid slope after 12 days' rainfall (30m, 27 degree)

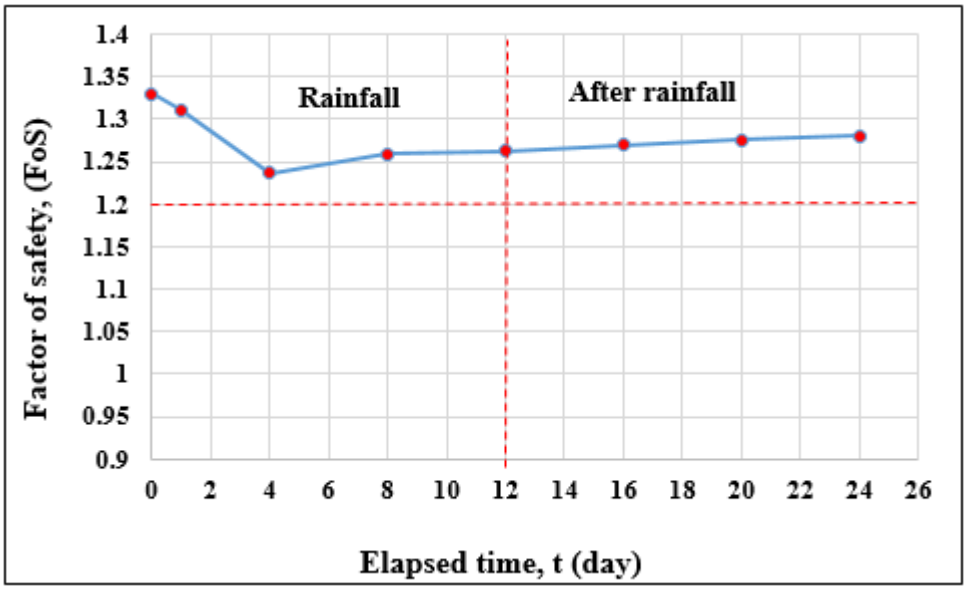

Figure A.35 Factor of safety (FoS) for silty sand soil, (30m with 27^{0} degree)

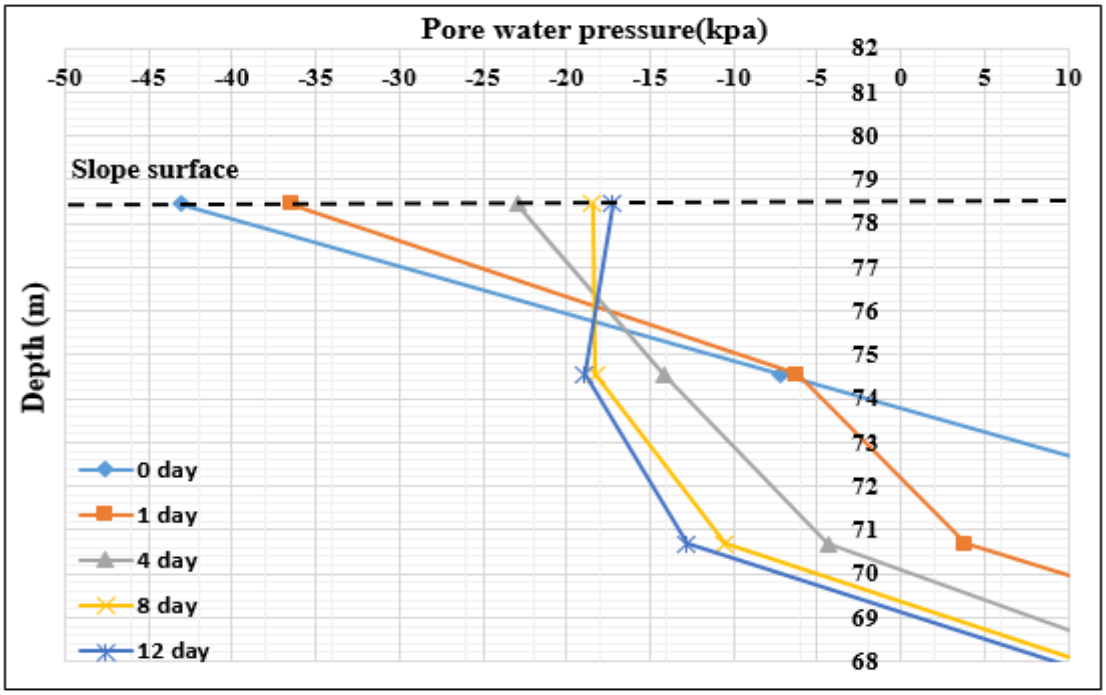

Figure A.36 Pore-water Pressure during rainfall (20m/day) for 12 days at mid slope (30m, 35deg)

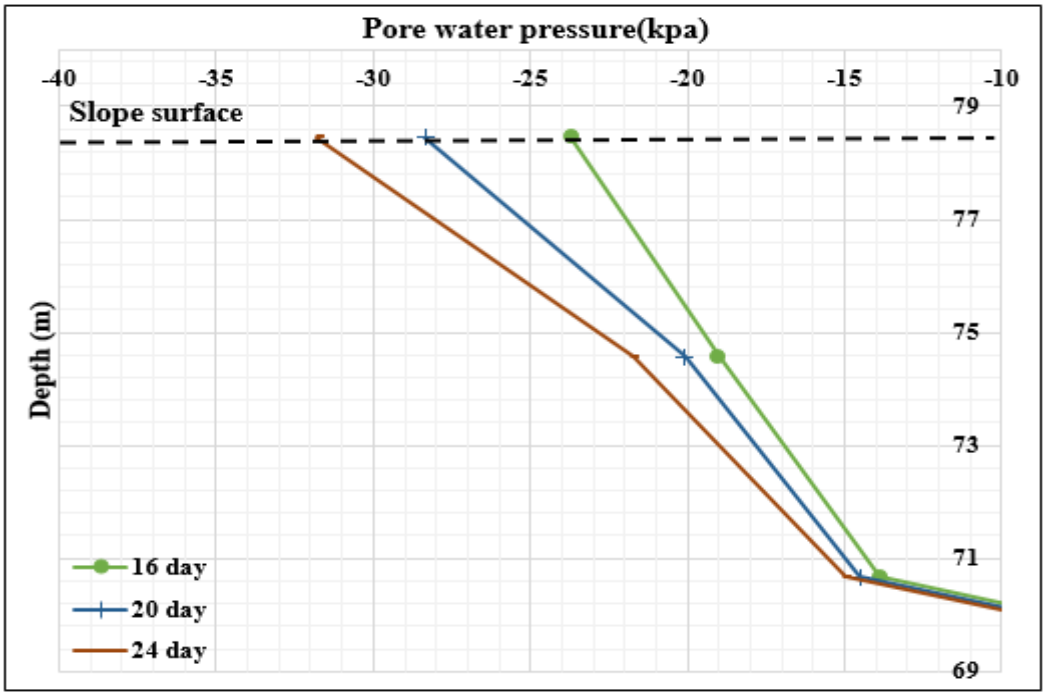

Figure A.37 Pore-water Pressure during dry periods at mid slope after 12 days' rainfall (30m,35 degree)

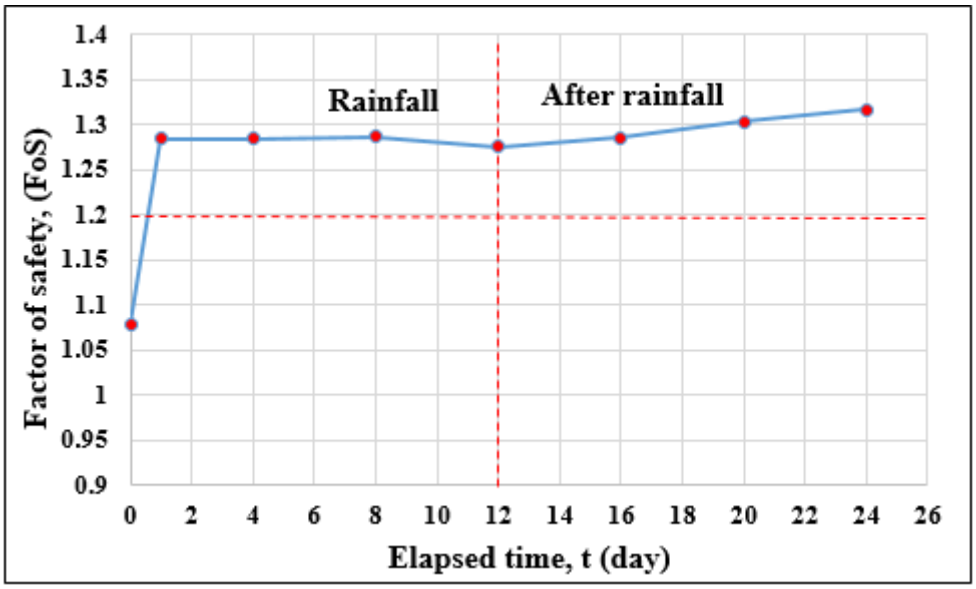

Figure A.38 Factor of safety (FoS) for silty sand soil, (30m with 35⁰ degree)

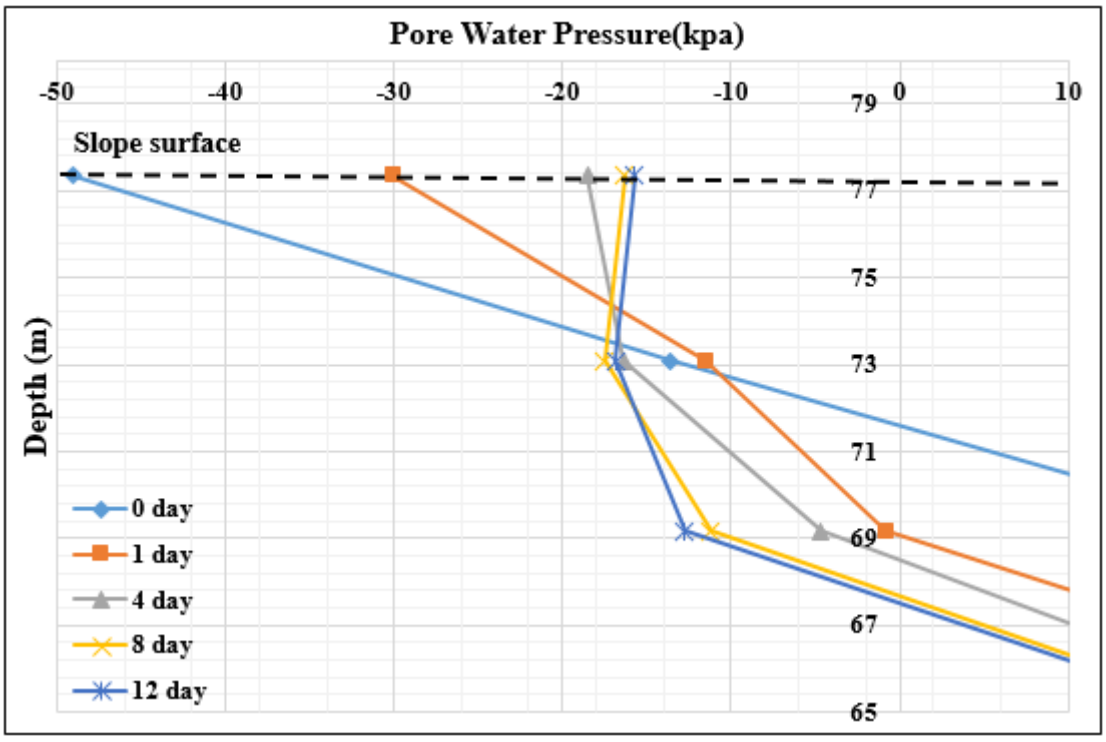

Figure A.39 Pore-water Pressure during rainfall (20m/day) for 12 days at mid slope (30m, 45deg)

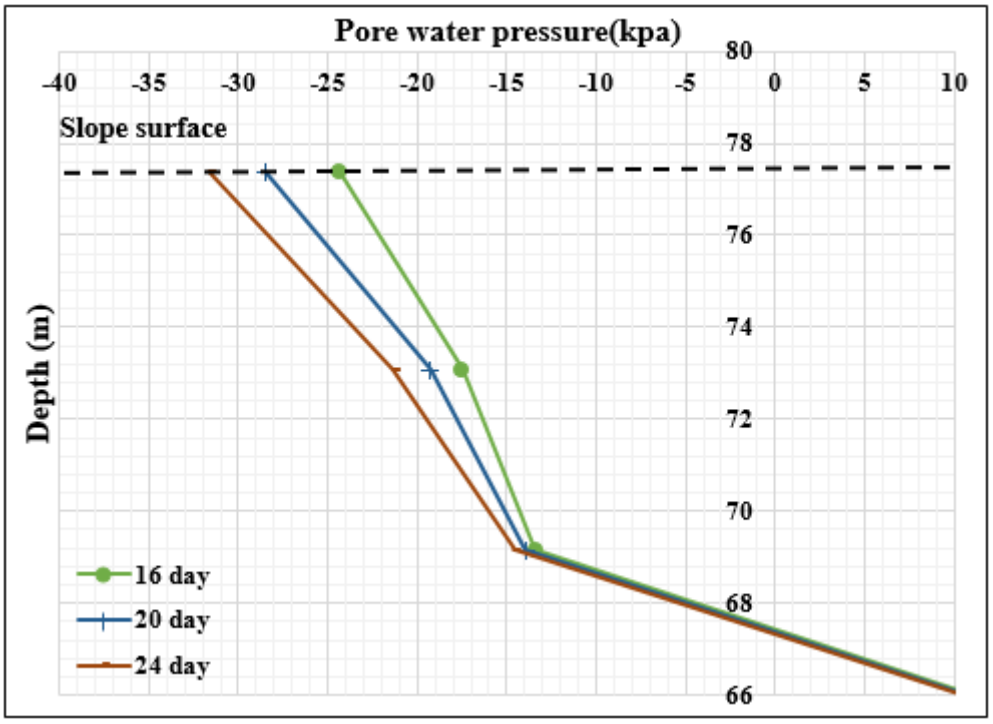

Figure A.40 Pore-water Pressure during dry periods at mid slope after 12 days' rainfall (30m, 45 degree)

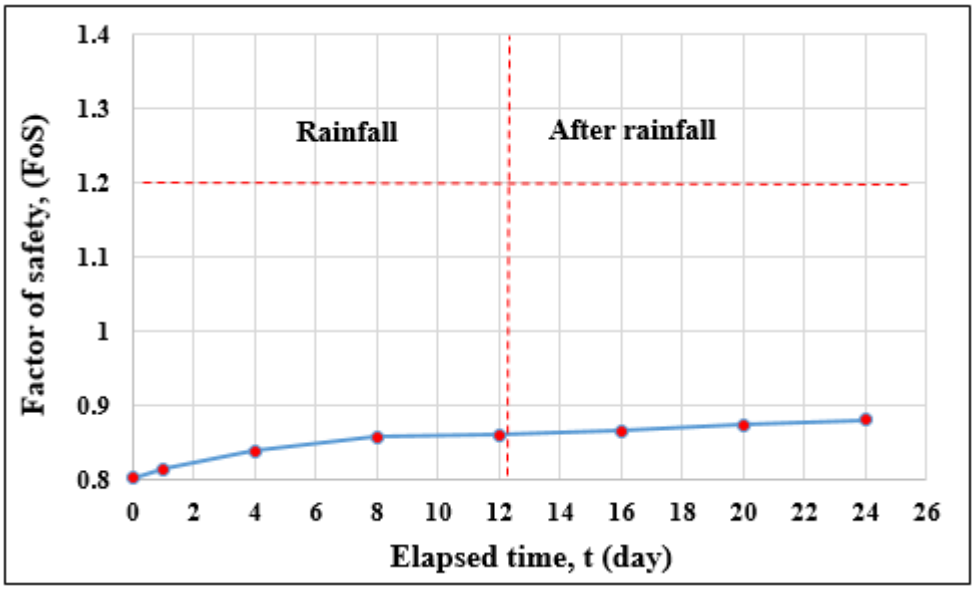

Figure A.41 Factor of safety (FoS) for silty sand soil, (20m with 45⁰ degree)

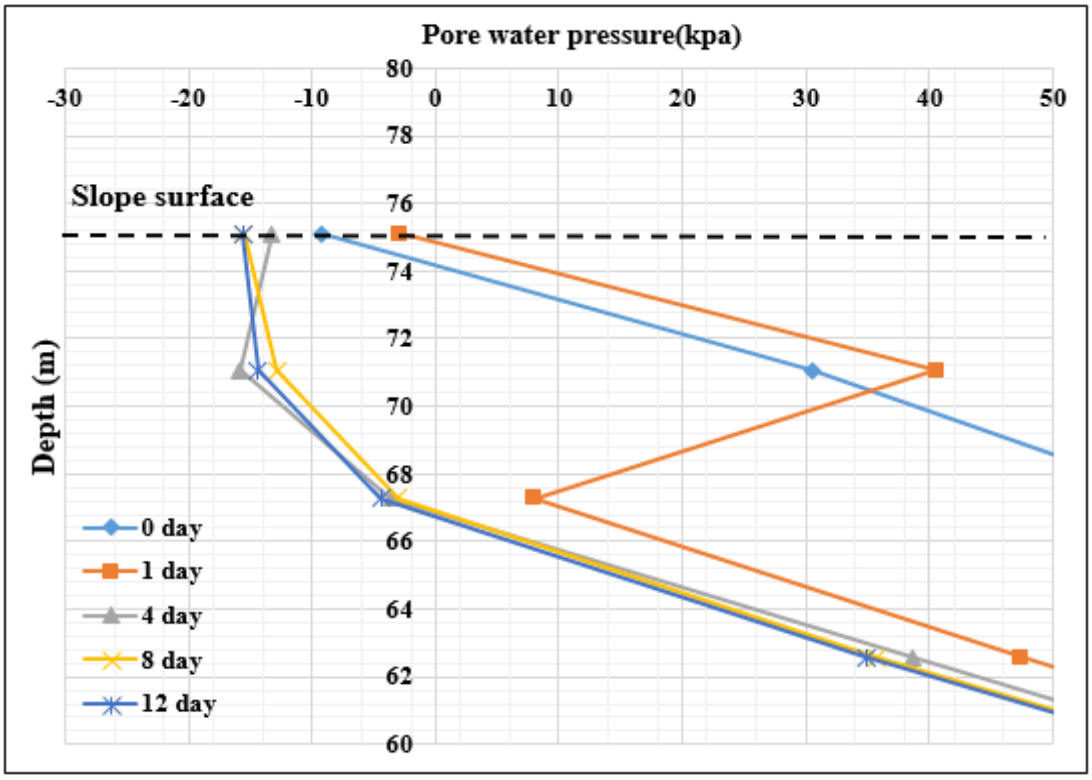

Figure A.42 Pore-water Pressure during rainfall (20m/day) for 12 days at mid slope (30 m, 60deg)

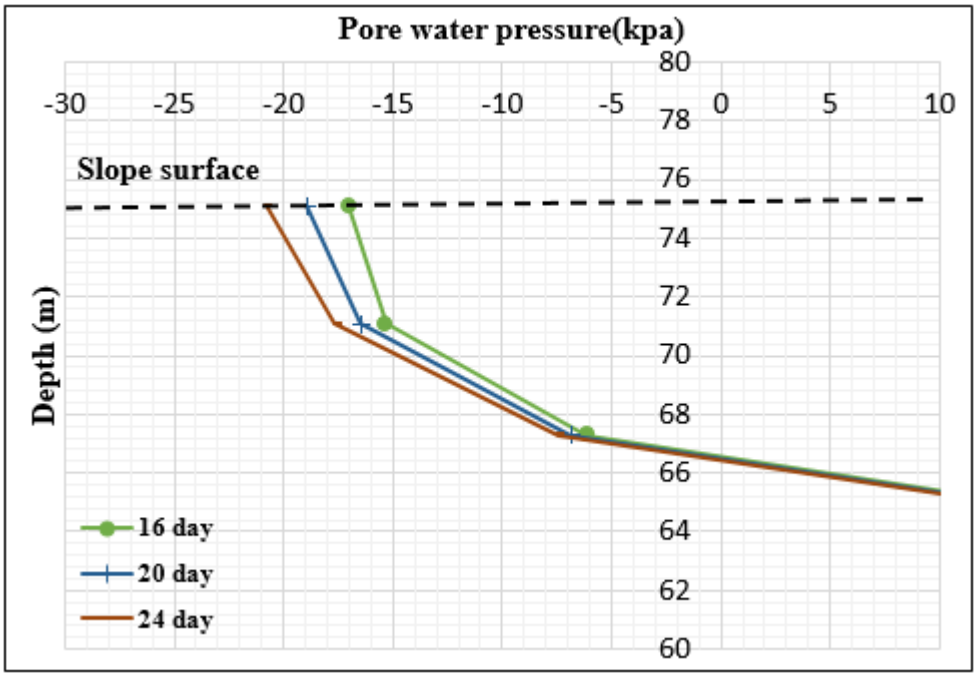

Figure A.43 Pore-water Pressure during dry periods at mid slope after 12 days' rainfall (30m,60 degree)

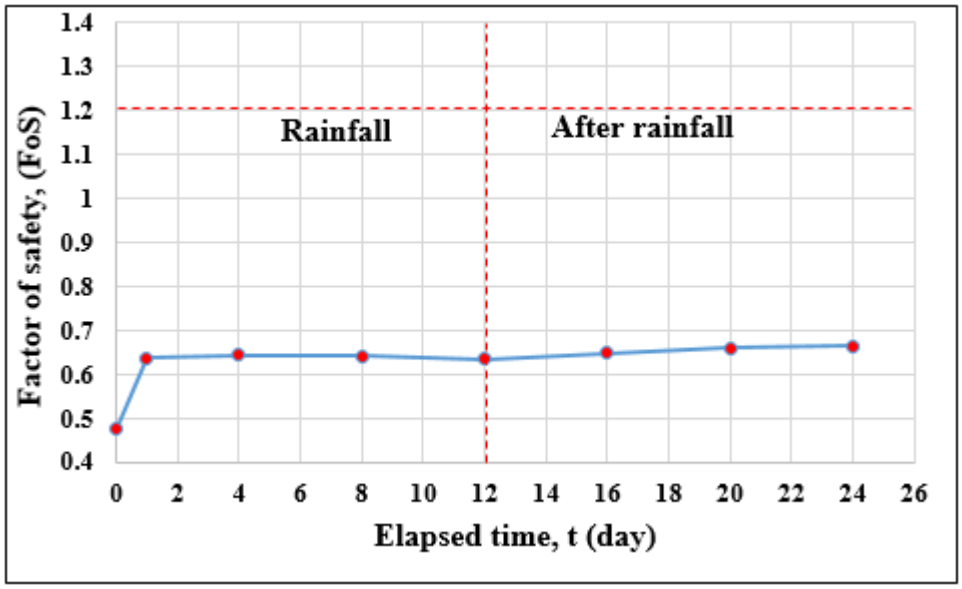

Figure A.44 Factor of safety (FoS) for silty sand soil, (30m with 60^{o} degree)

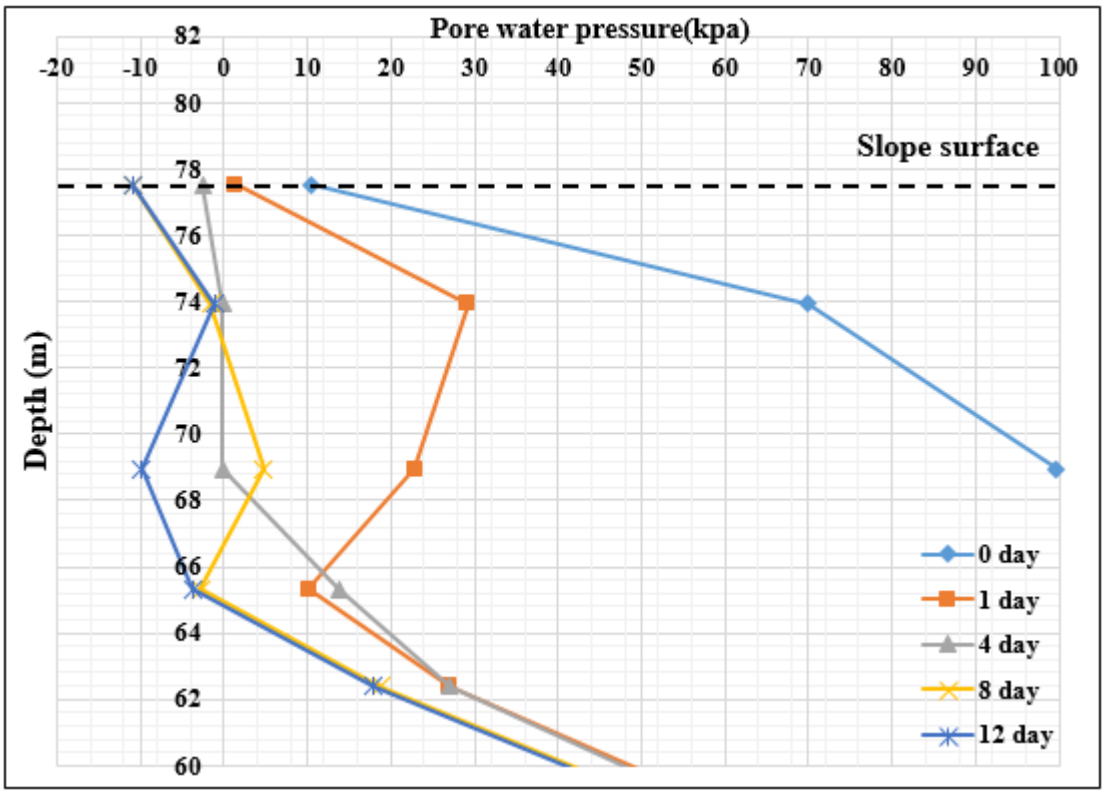

Figure A.45 Pore-water Pressure during rainfall (20m/day) for 12 days at mid slope (30m, 80deg)

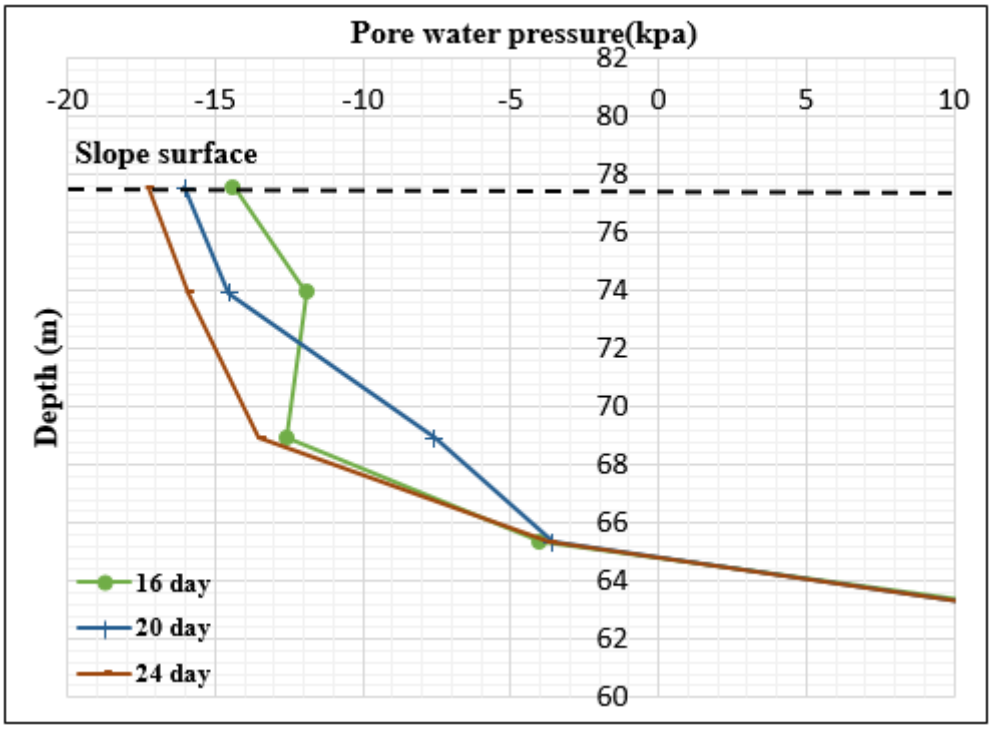

Figure A.46 Pore-water Pressure during dry periods at mid slope after 12 days' rainfall (30m,80 degree)

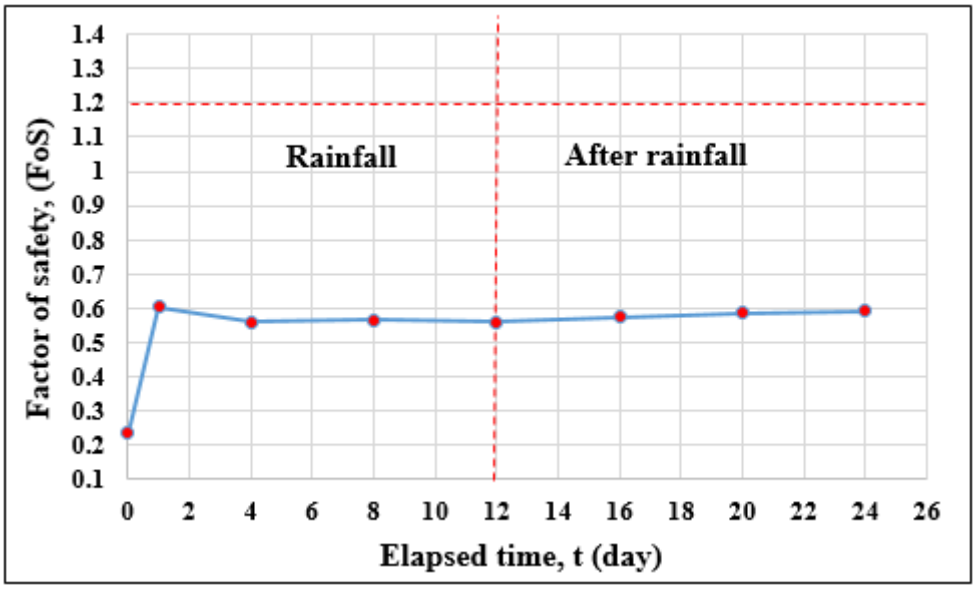

Figure A.47 Factor of safety (FoS) for silty sand soil, (30m with 80^{0} degree)

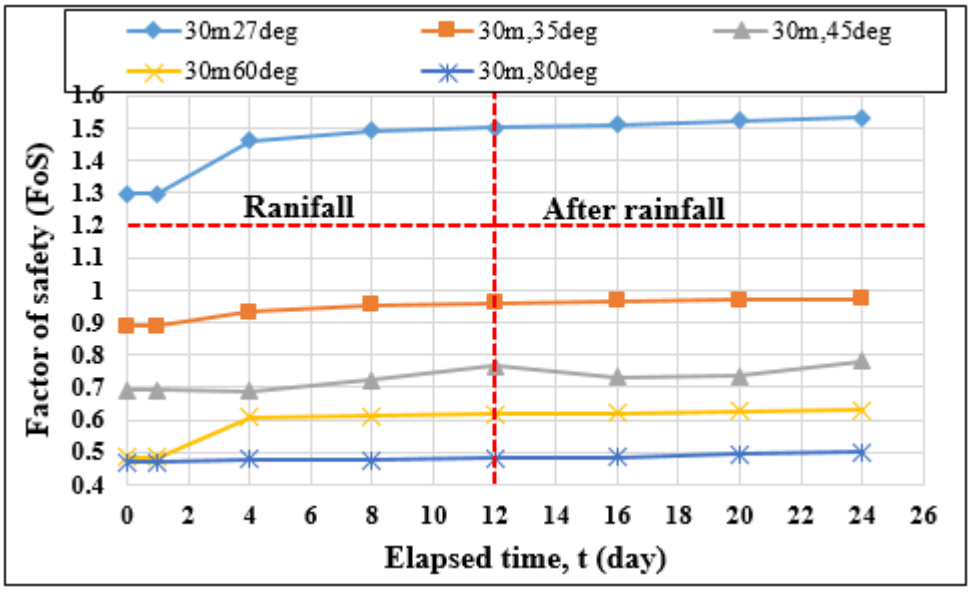

Figure A.48 Factor of safety (FoS) for silty sand soil, (30m with 27⁰,35⁰,45⁰,60⁰ and 80⁰ degrees)

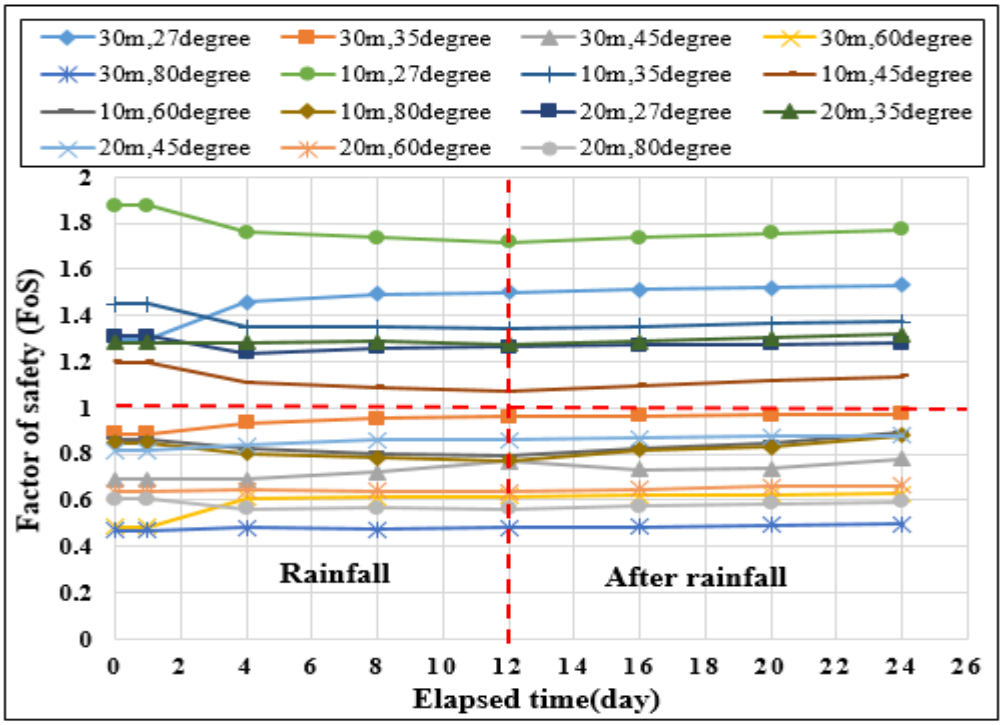

Figure A.49 Factor of safety (FoS) for silty sand soil (MH), (10m,20m and 30m height with 27⁰,35⁰,45⁰,60⁰ and 80⁰ degrees)

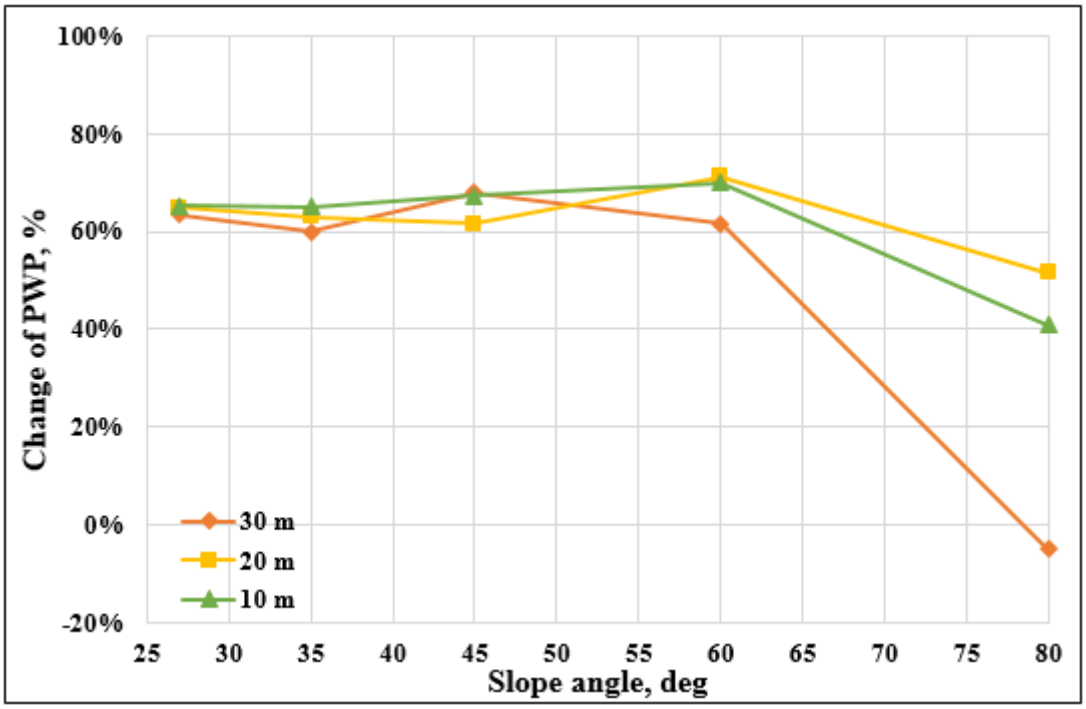

Figure A.51 Changes in pore water pressure during 20mm/day rainfall for 10m,20, and 30m height with 27⁰,35⁰,45⁰,60⁰ and 80⁰ degrees

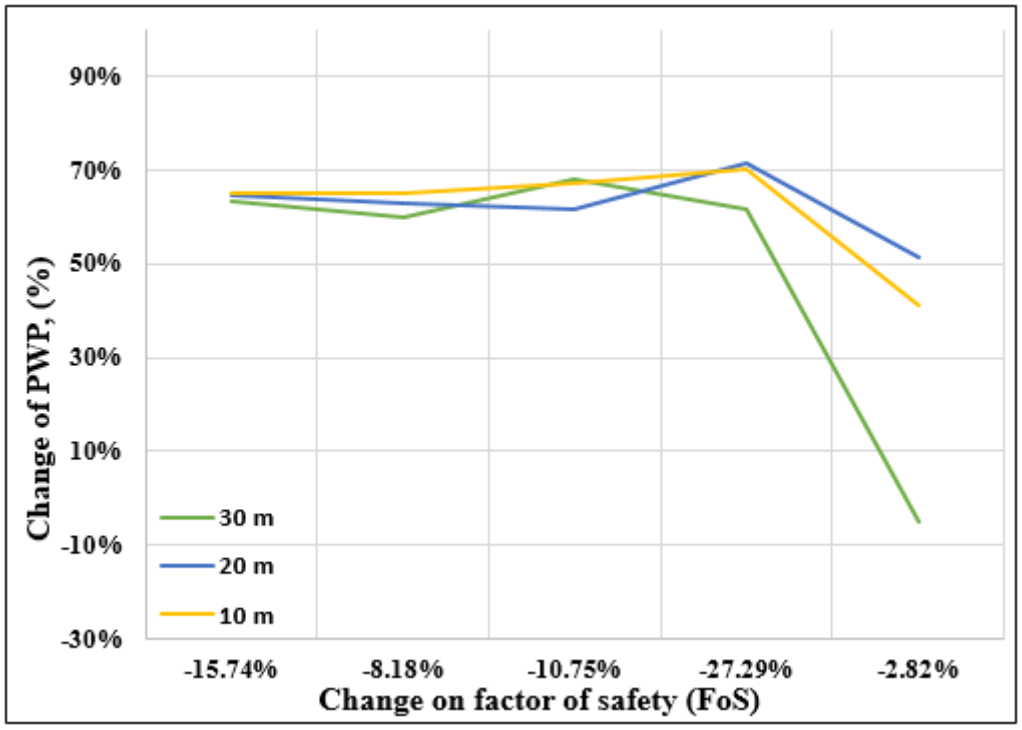

Figure A.52 Pore water pressure VS Factor of safety (FoS) during 20mm/day rainfall for 10m,20, and 30m height with 27⁰,35⁰,45⁰,60⁰ and 80⁰ degrees

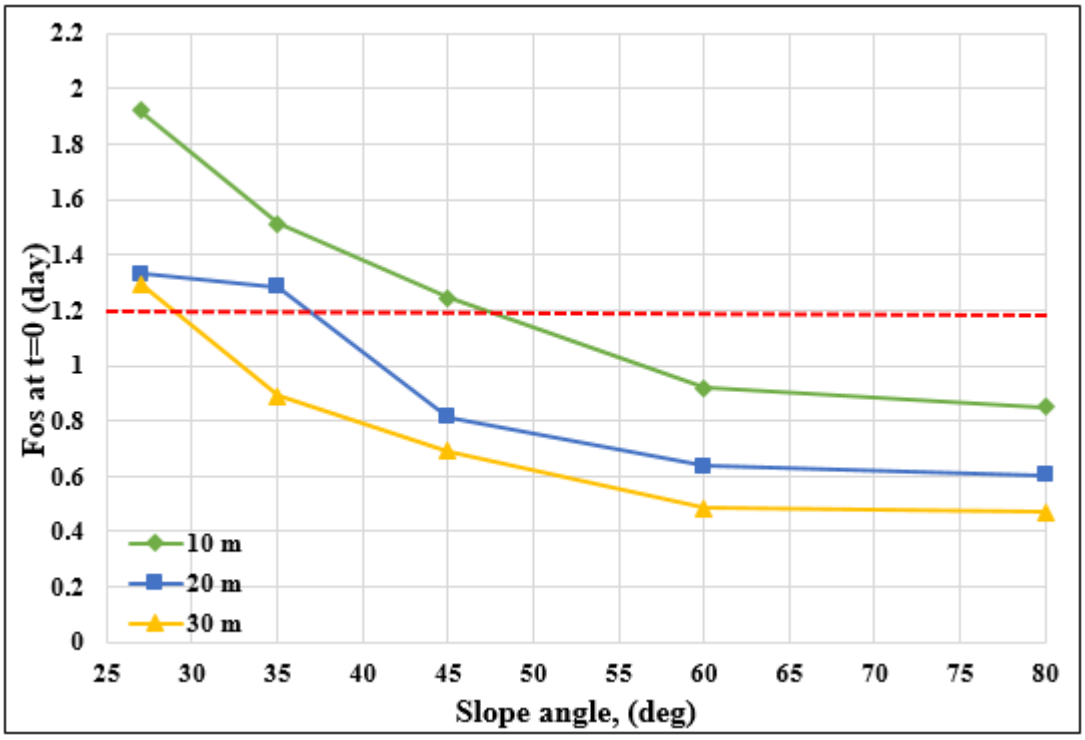

Figure A.54 Factor of safety (FoS) VS angles (27,35,45,60,80) degrees during initial time t=0

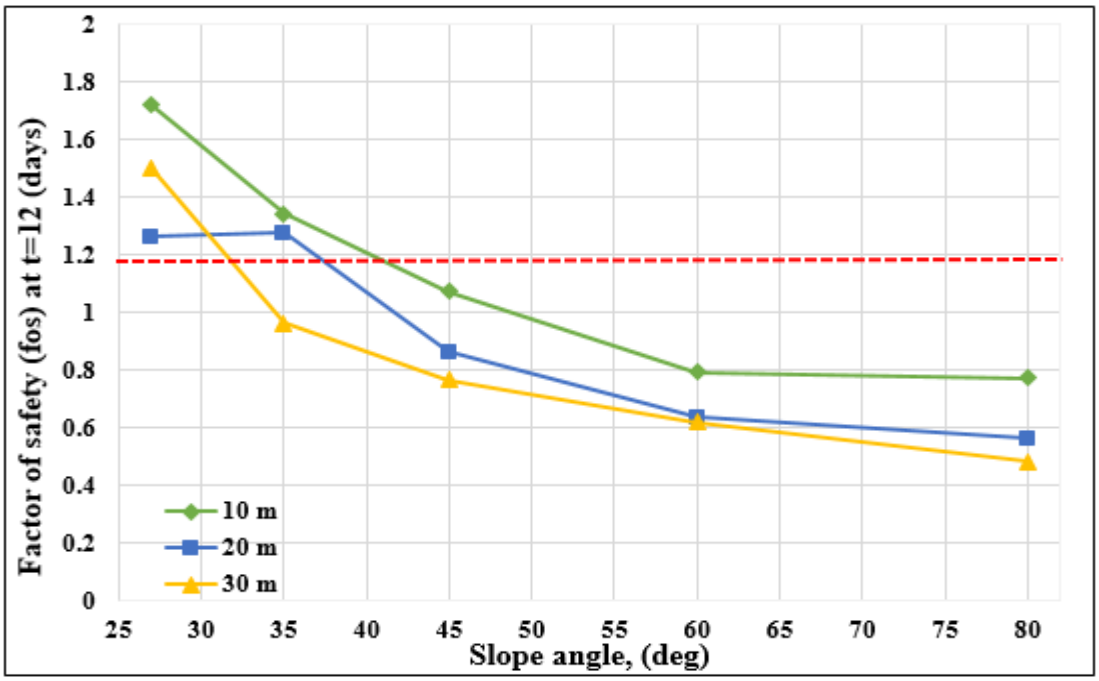

Figure A.55 Factor of safety (FoS) VS angles (27,35,45,60,80) degrees at t=12 days

8.2 Results from Seepage and slope stability analyses for Sandy silt soil with different slope geometries

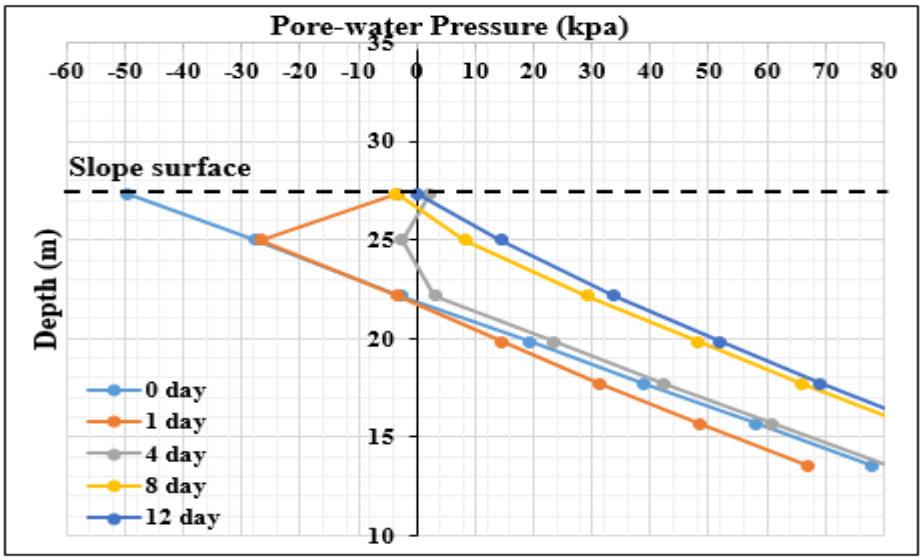

Figure A. 56 Pore-water Pressure during rainfall (20m/day) for 12 days at mid slope (10 m, 27deg)

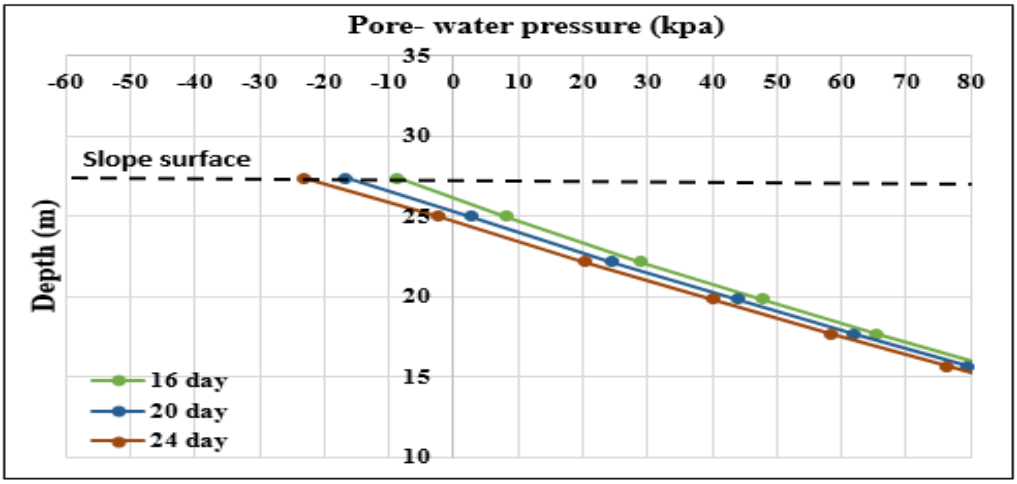

Figure A.57 Pore-water Pressure during dry periods at mid slope after 12 days (10 m, 27 degree)

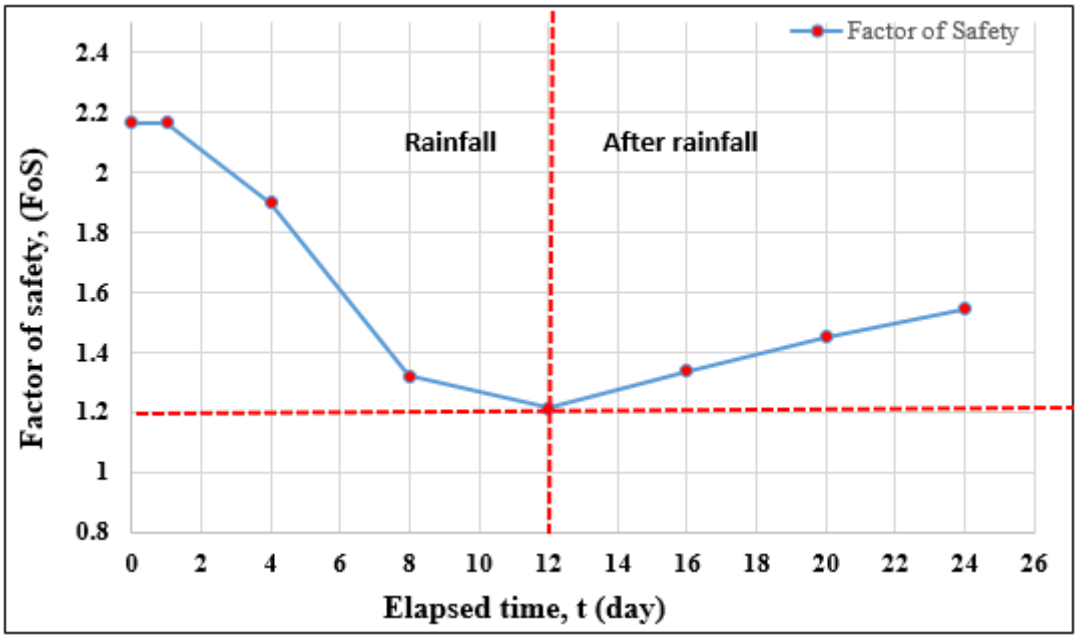

Figure A.58 Factor of safety (FoS) for 10 m, 27 degree

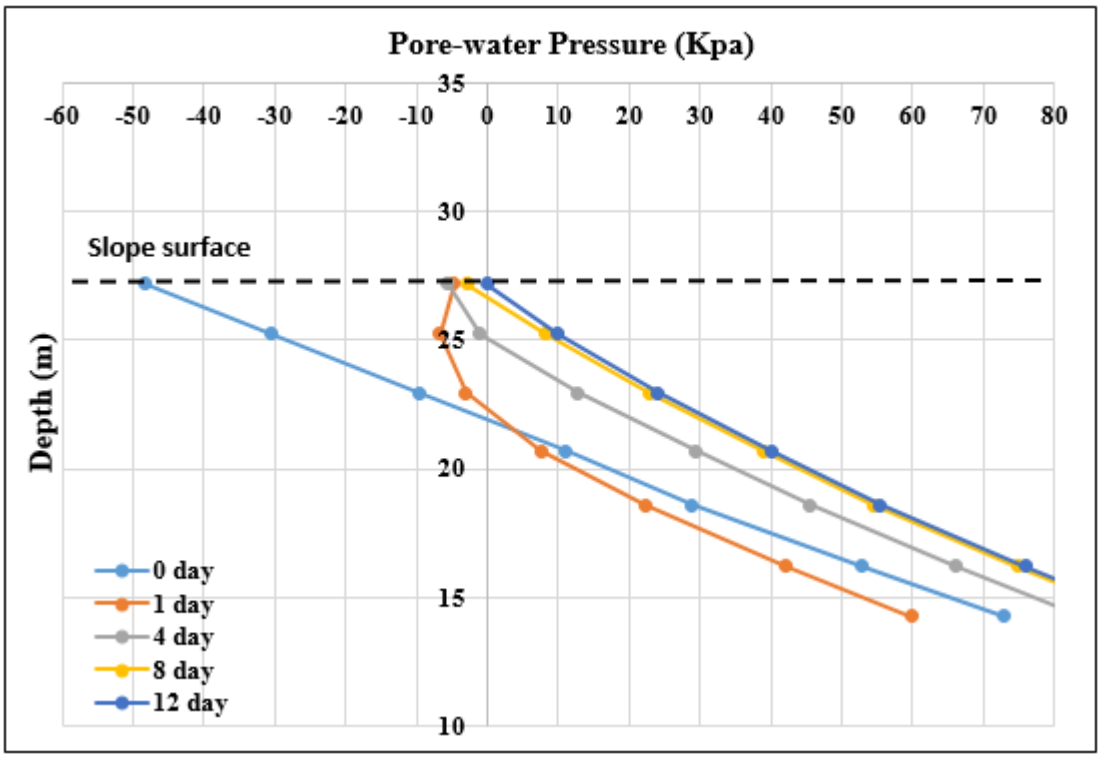

Figure A.58 Pore-water Pressure during rainfall (20m/day) for 12 days at mid slope (10 m, 35deg)

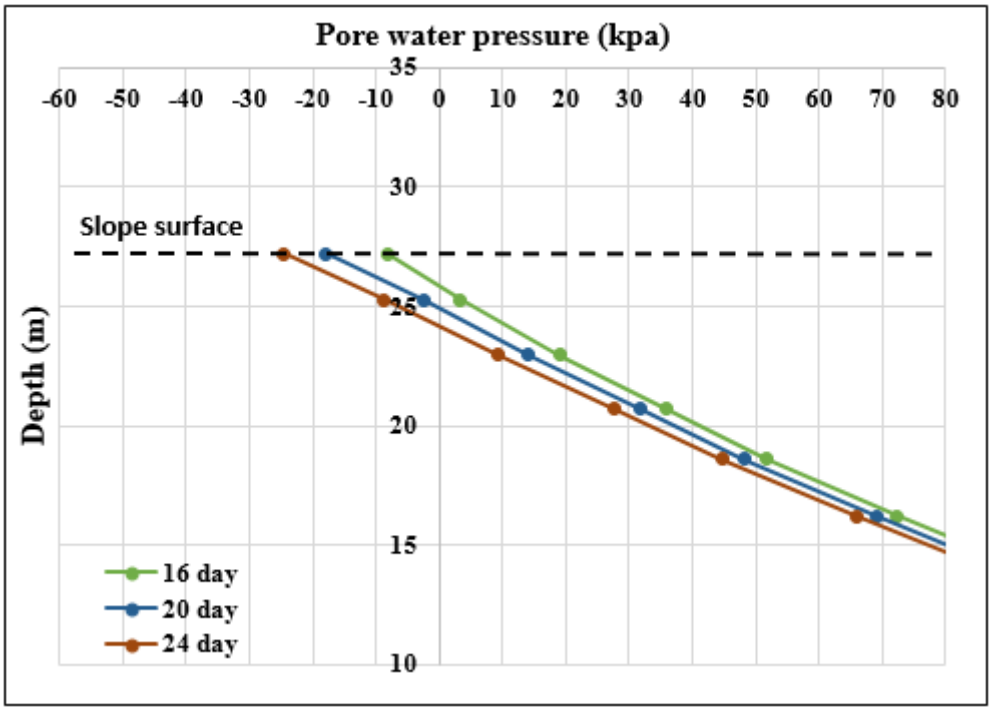

Figure A.59 Pore-water Pressure during dry periods at mid slope after 12 days (10 m, 35deg)

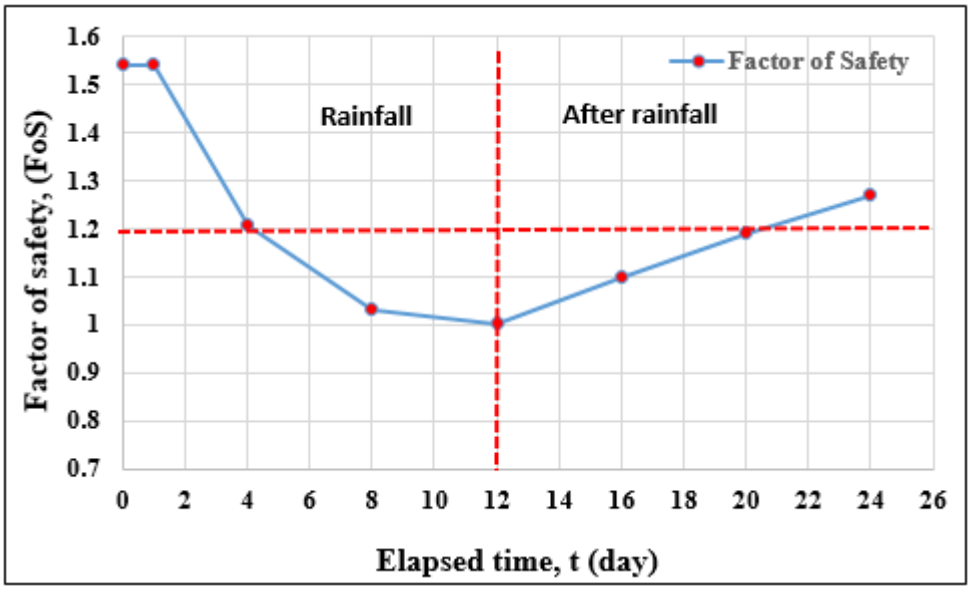

Figure A.60 Factor of safety (FoS) for 10m 35 degree

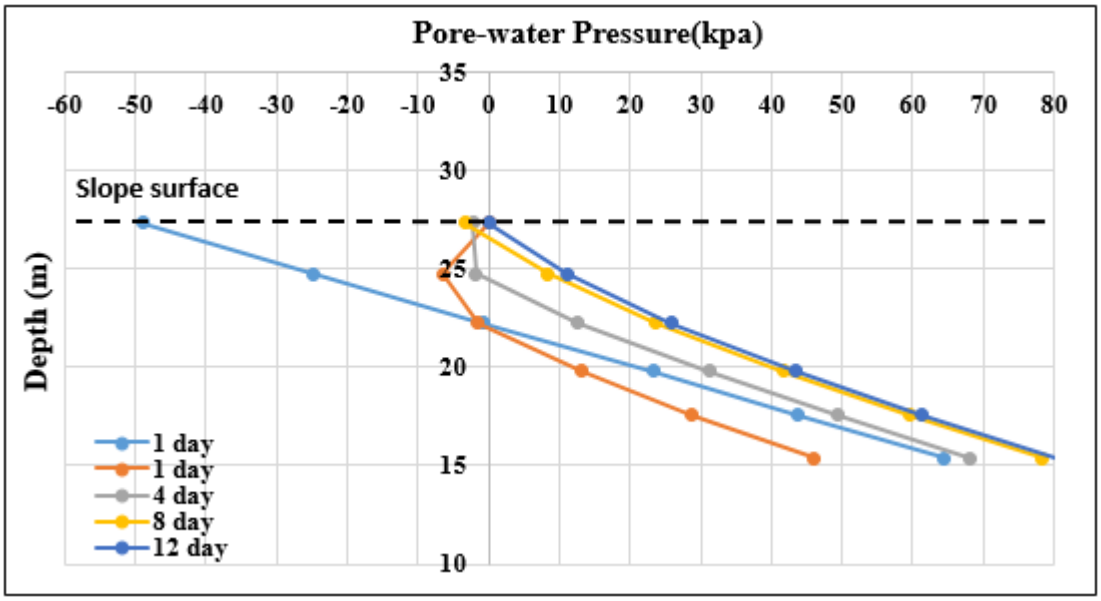

Figure A.61 Pore-water Pressure during rainfall (20m/day) for 12 days at mid slope (10 m, 45deg)

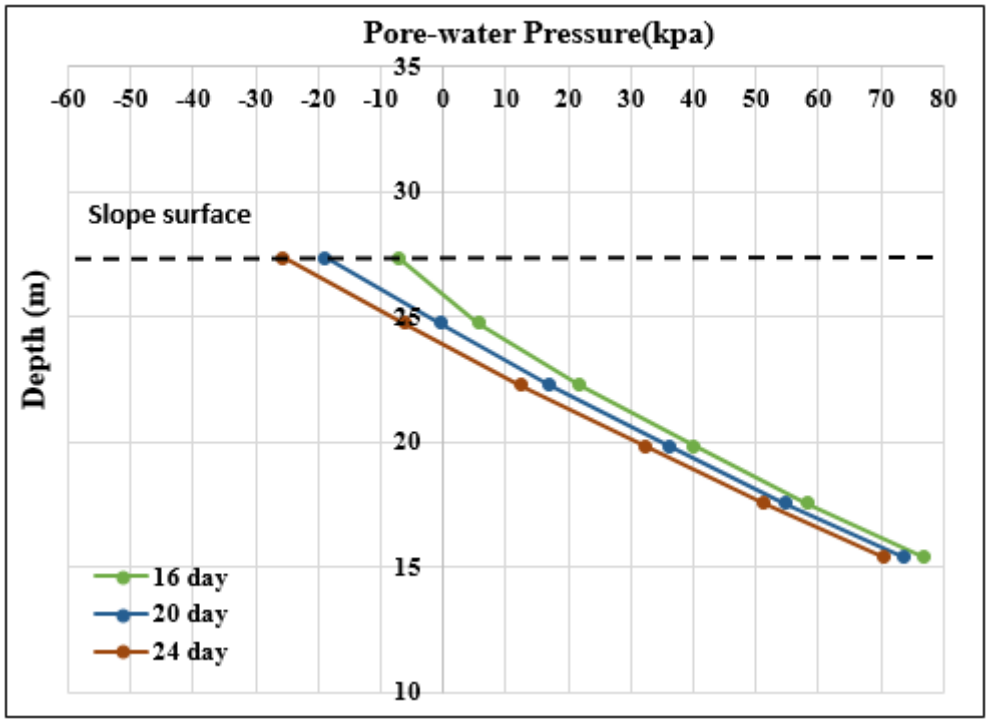

Figure A.62 Pore-water Pressure during dry periods at mid slope after 12 days (10 m, 45deg)

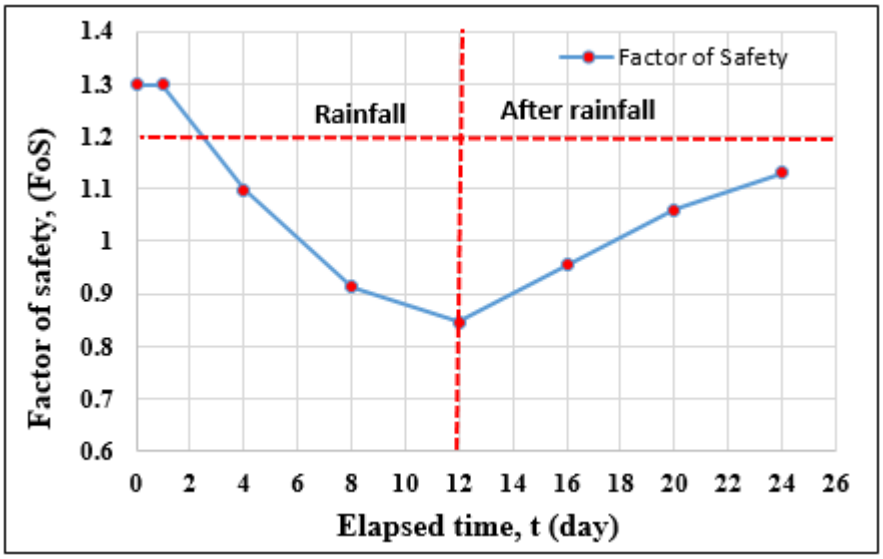

Figure A.63 Factor of safety (FoS) for 10m 45 degree

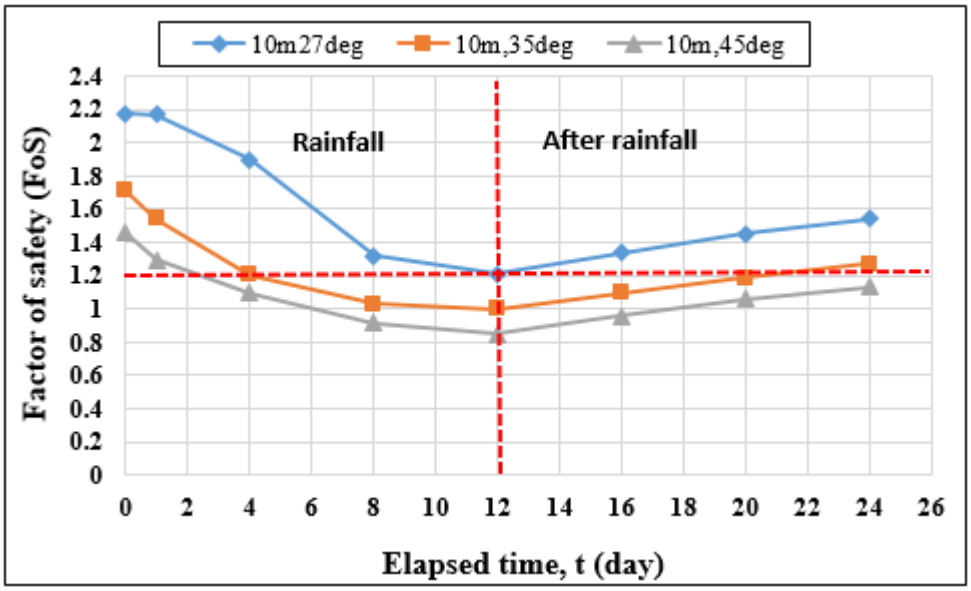

Figure A.64 Factor of safety (FoS) for 10m height with 27,35 and 45 degrees

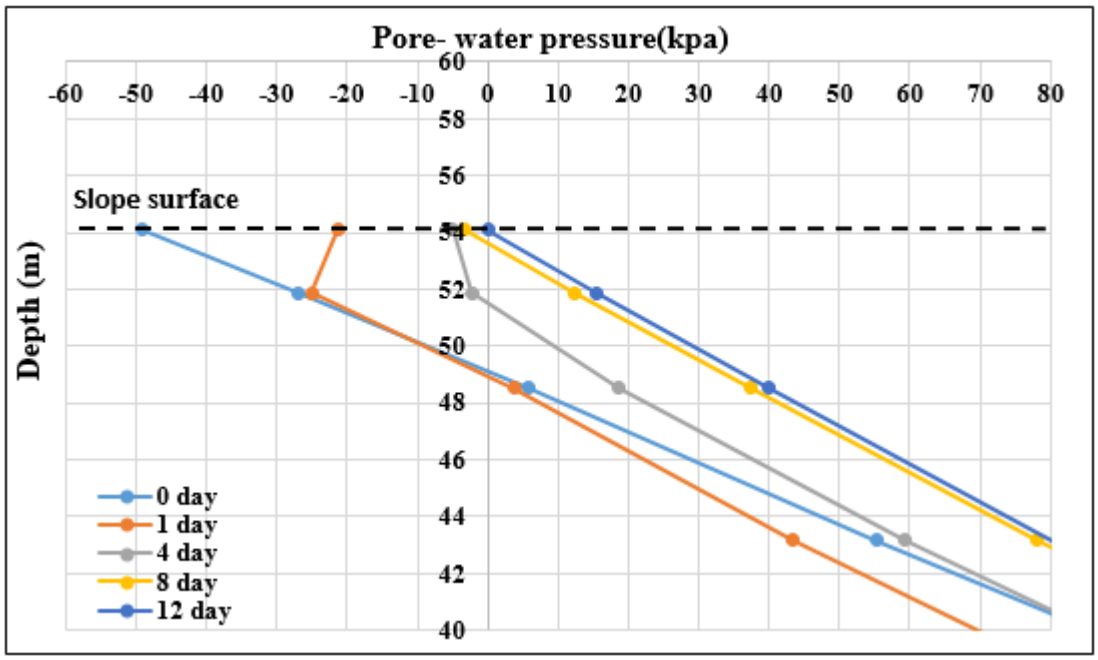

Figure A.65 Pore-water Pressure during rainfall (20mm/day) at mid slope for 12 days (20 m, 27deg)

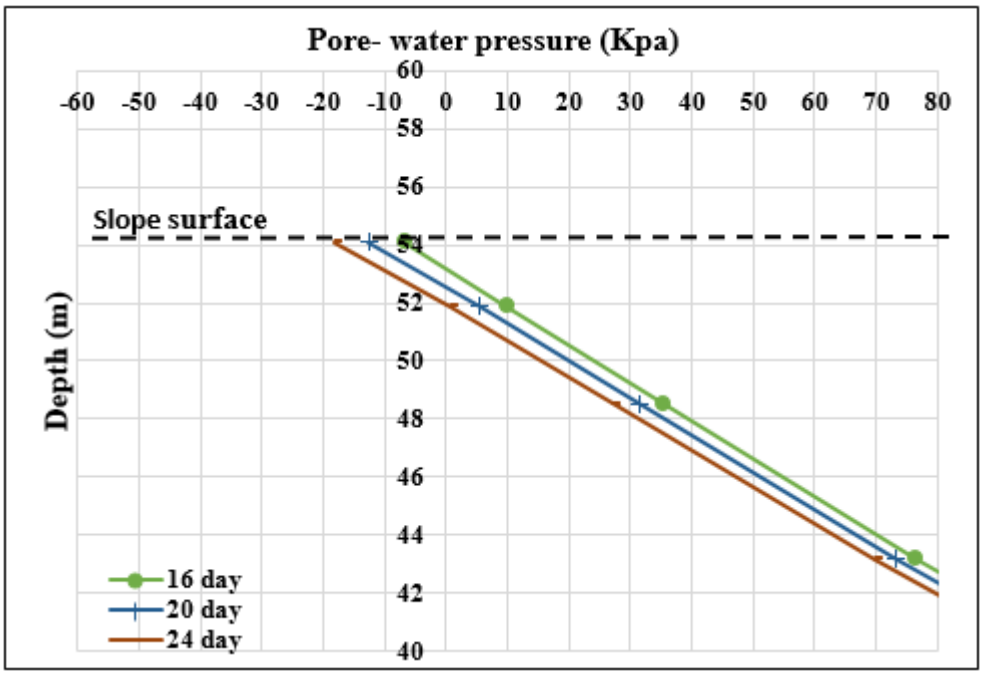

Figure A.66 Pore-water Pressure during dry periods at mid slope after 12 days (20 m, 27deg)

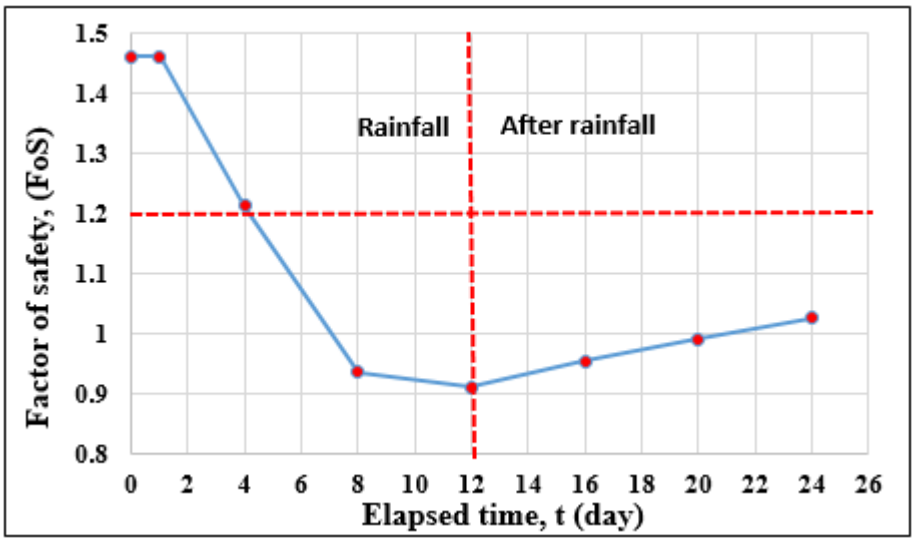

Figure A.67 Factor of safety (FoS) for 20m height and 27 degree

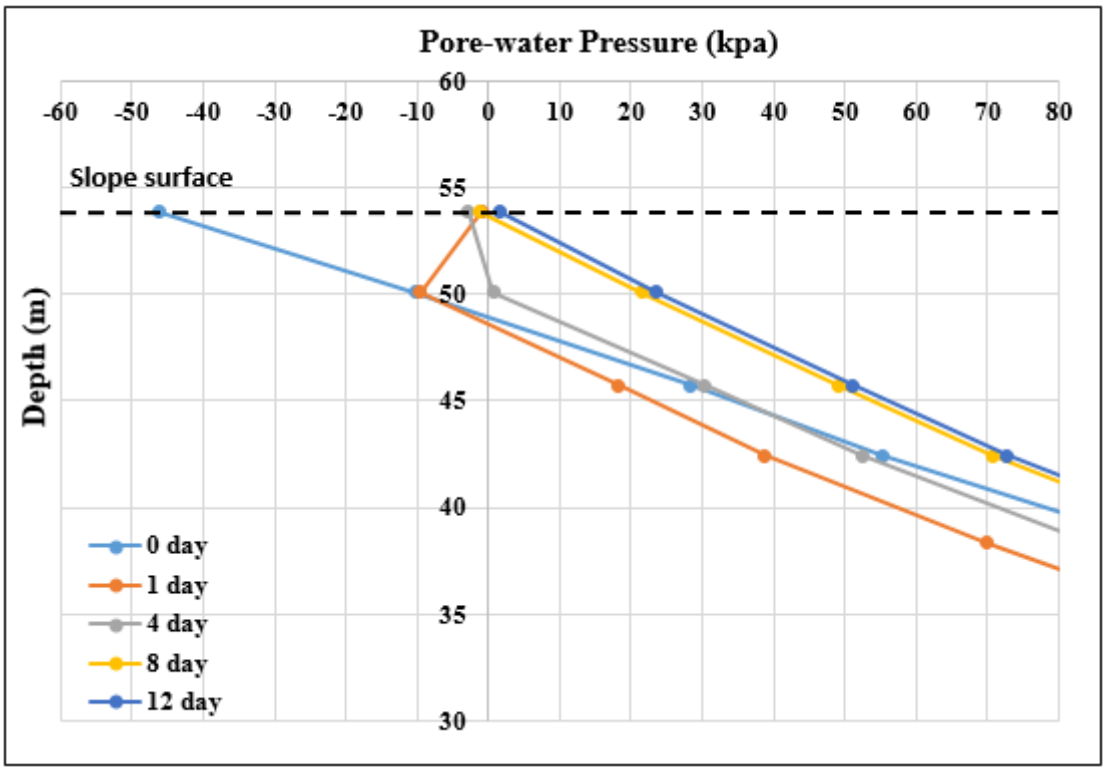

Figure A.68 Pore-water Pressure during rainfall (20mm/day) at mid slope for 12 days (20 m, 35deg)

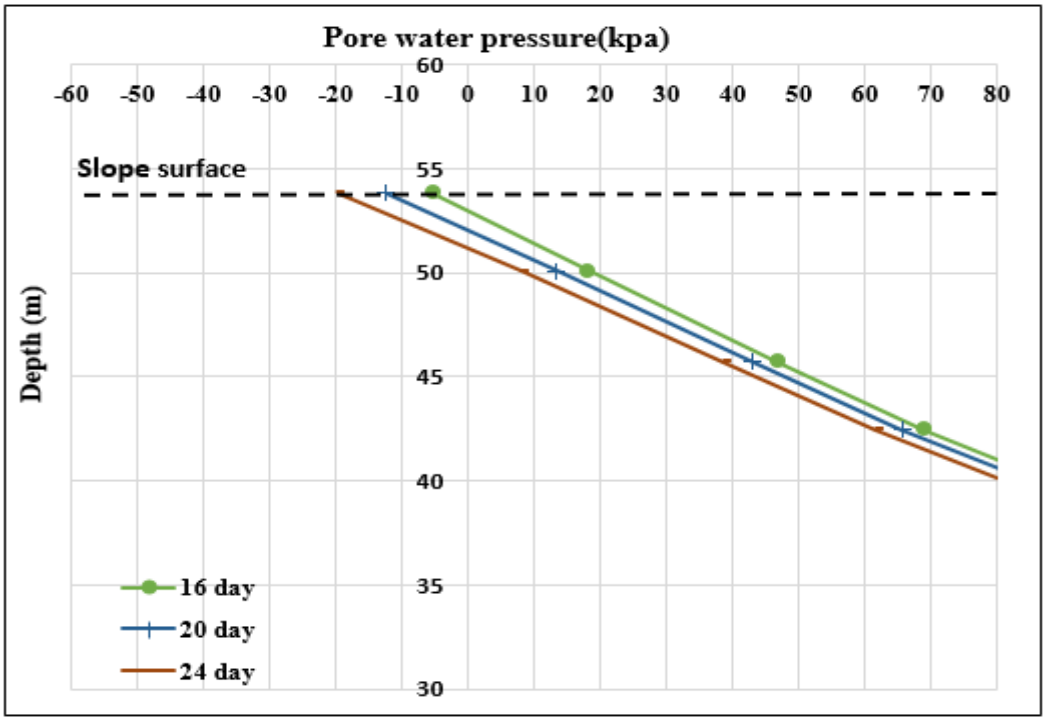

Figure A.69 Pore-water Pressure during dry periods at mid slope after 12 days (20 m, 35deg)

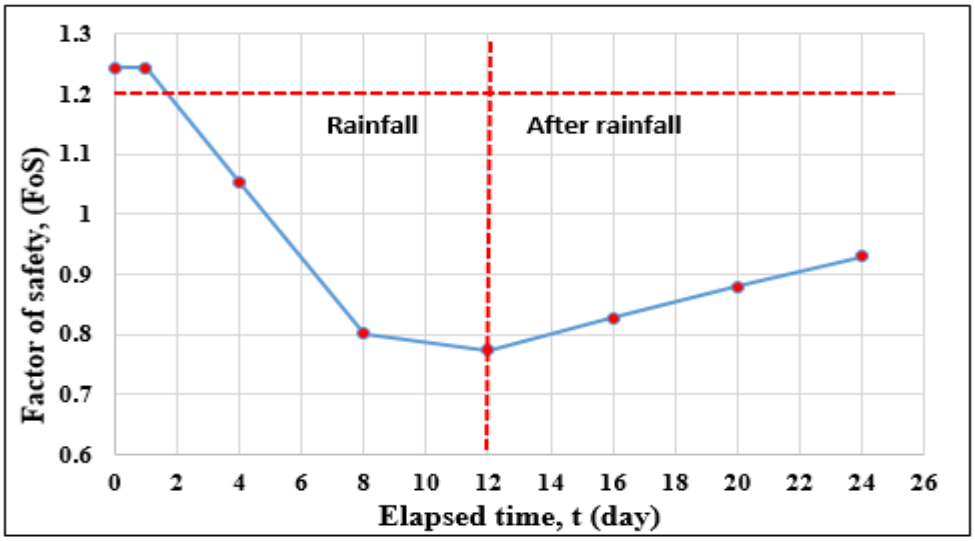

Figure A.70 Factor of safety (FoS) for 20m height and 35 degree

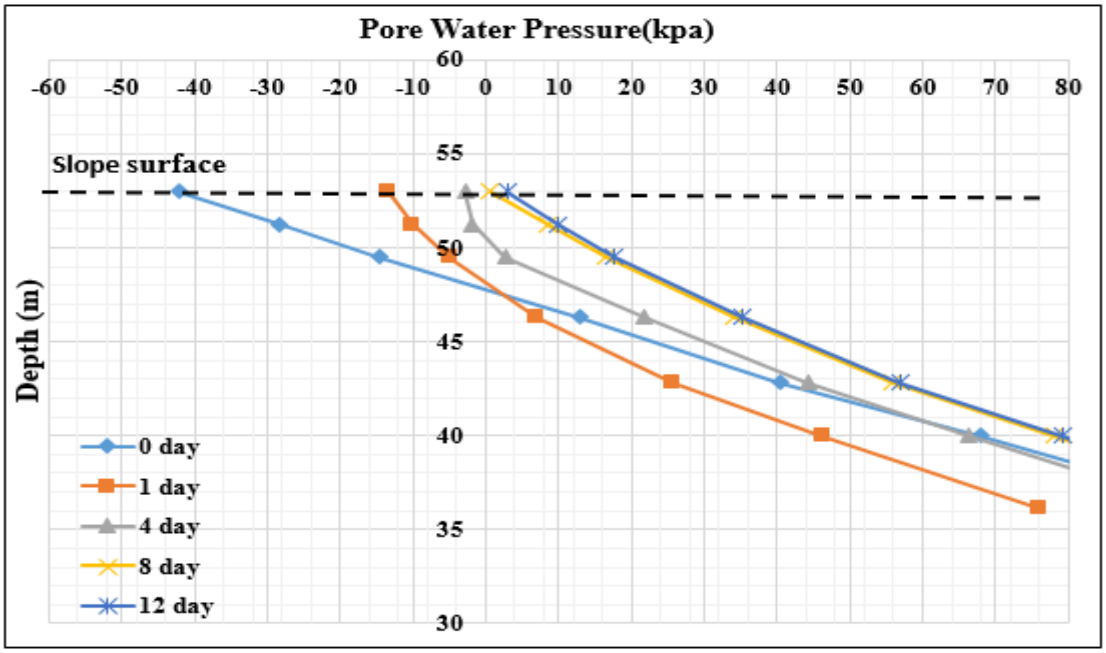

Figure A.71 Pore-water Pressure during rainfall (20mm/day) at mid slope for 12 days (20 m, 45deg)

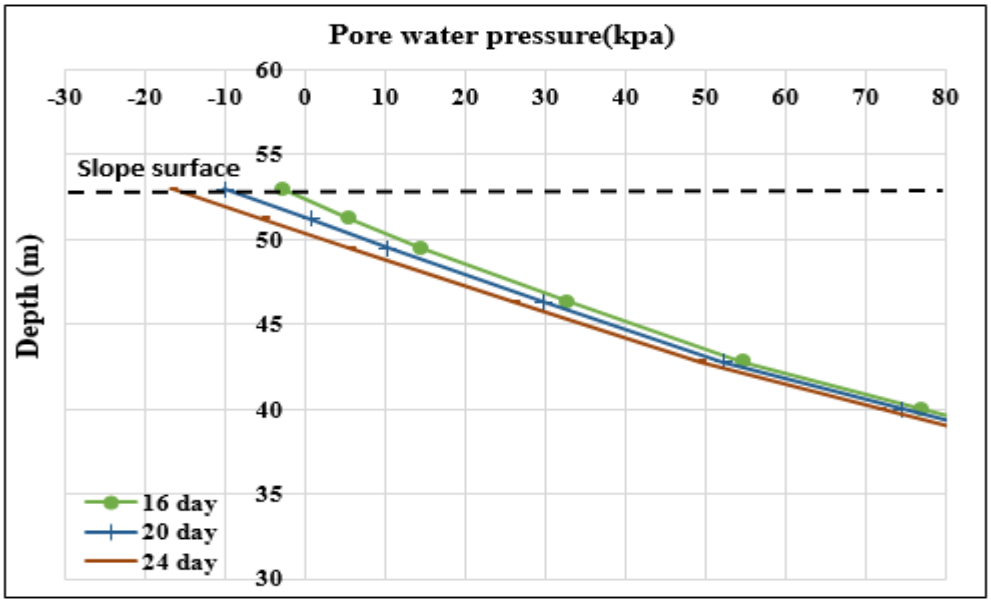

Figure A.72 Pore-water Pressure during dry periods at mid slope after 12 days (20 m, 45deg)

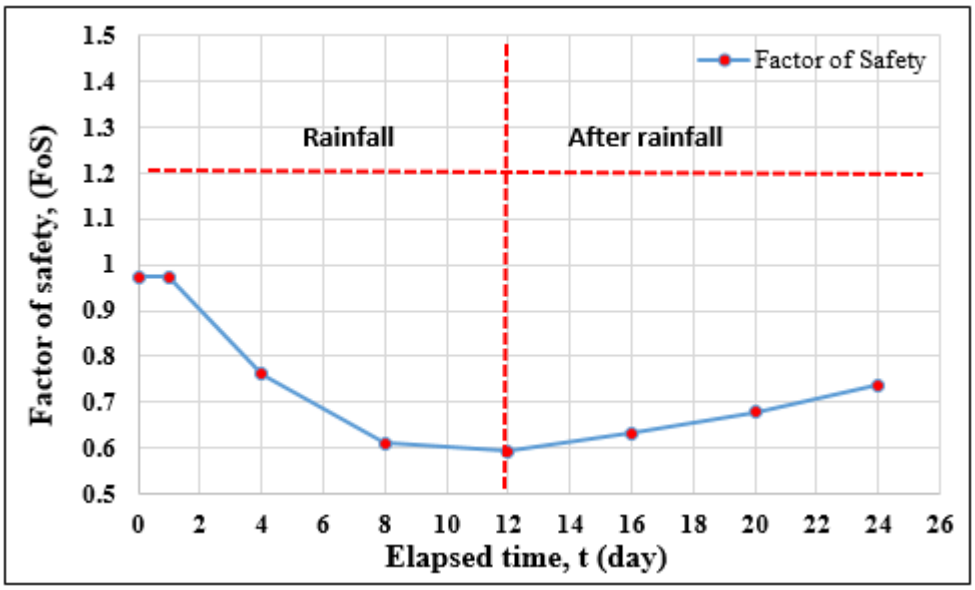

Figure A.73 Factor of safety (FoS) for 20m height and 45 degree

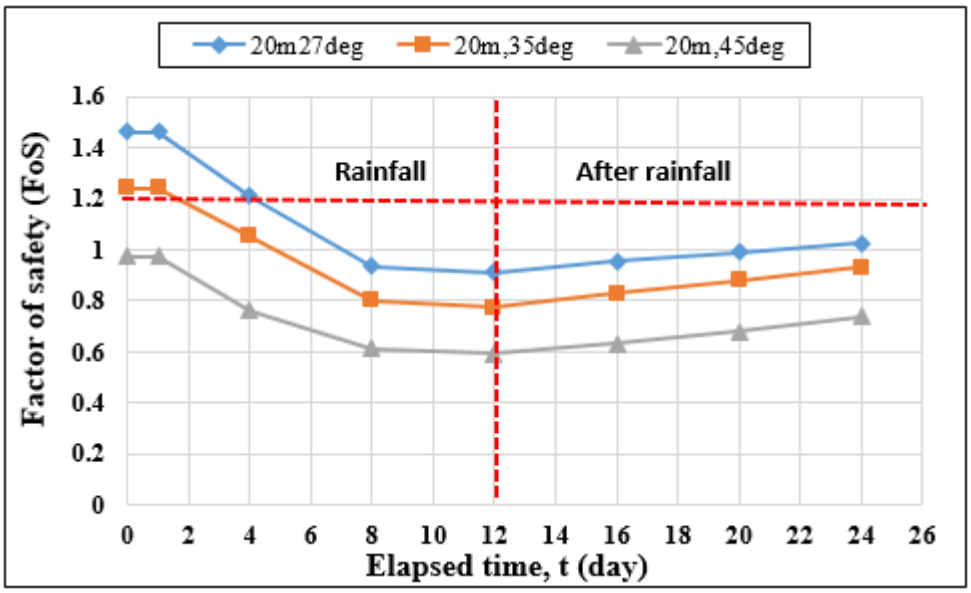

Figure A.74 Factor of safety (FoS) for 20m height with 27,35 and 45 degrees

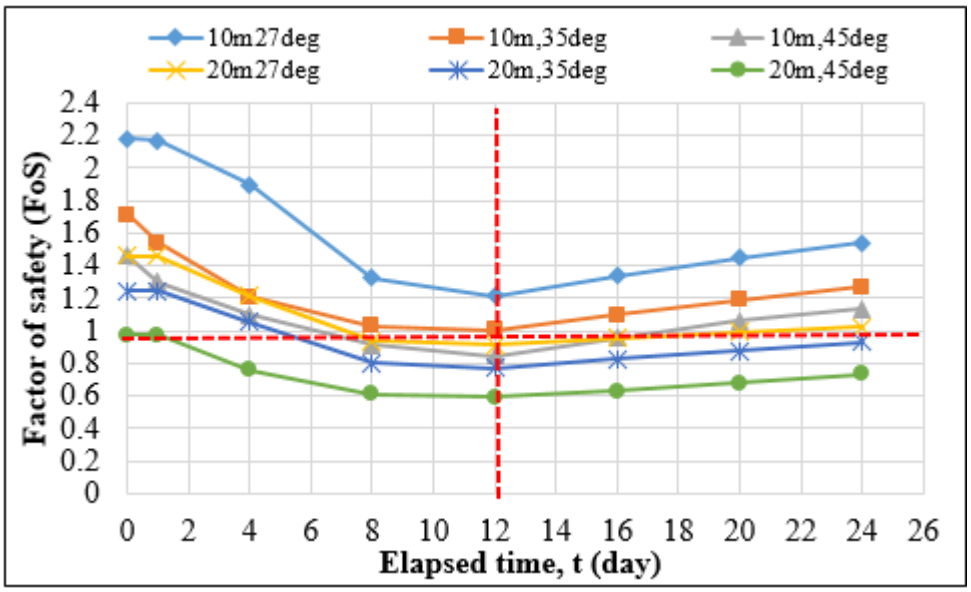

Figure A.75 Factor of safety (FoS) VS elapsed time (day) for all investigated slopes 10m and 20m height with 27,35, and 45 degrees

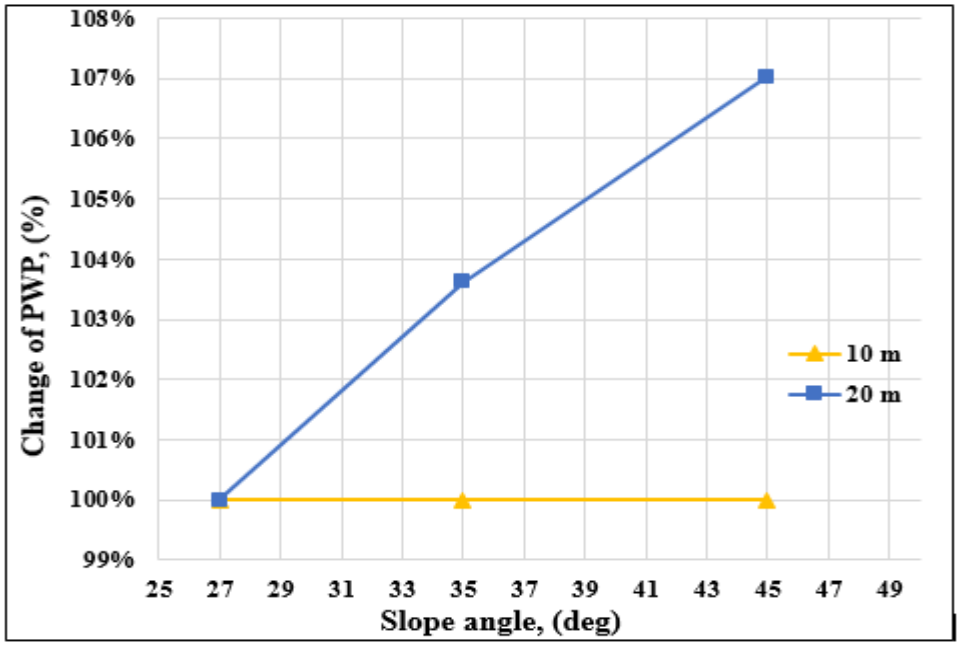

Figure A.76 Changes in Factor of safety (FoS) during 20mm/day rainfall for 10m and 20m height with 27º,35ºand 45ºdegrees

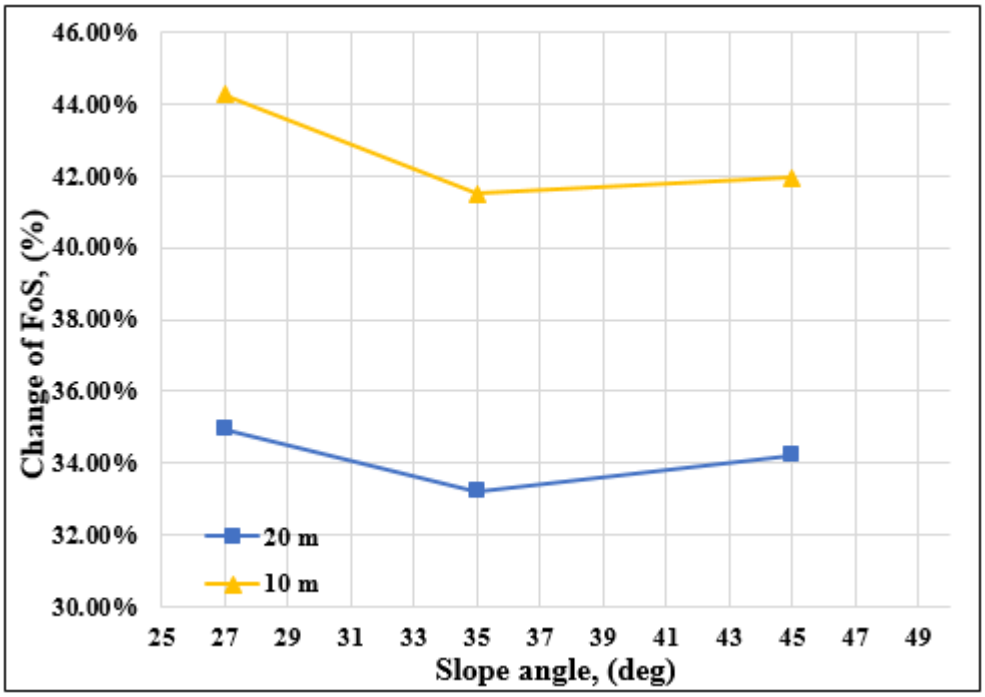

Figure A.77 Changes in Factor of safety(FoS) during 20mm/day rainfall for 10m and 20, height with 27º,35º and 45ºdegrees

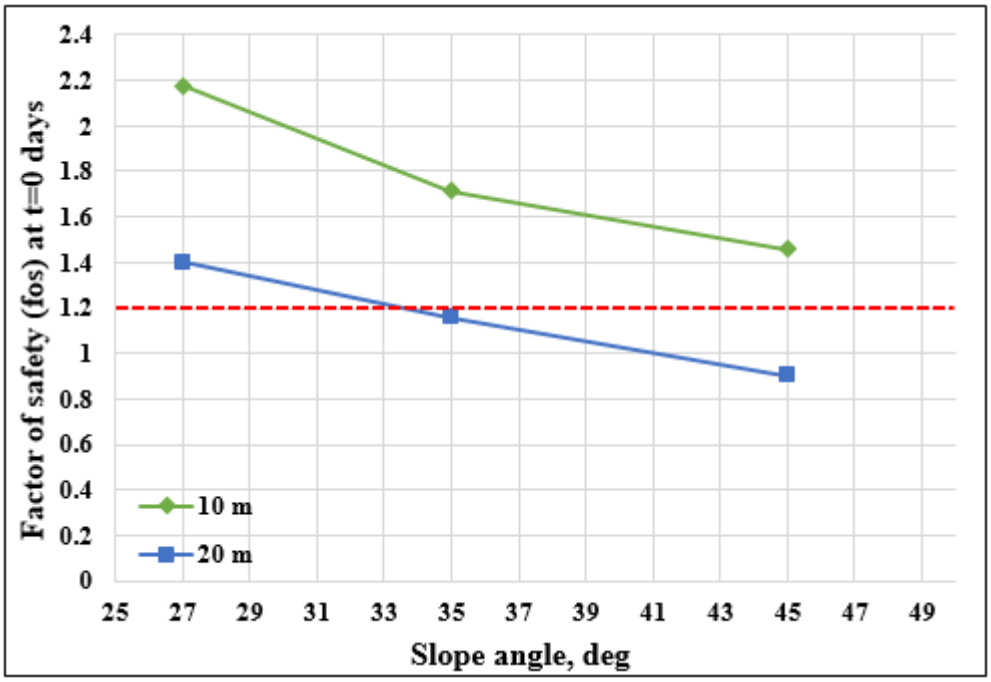

Figure A.78 Changes in Factor of safety(FoS) during 20mm/day rainfall for 10m and 20m height with 27º,35º and 45ºdegrees

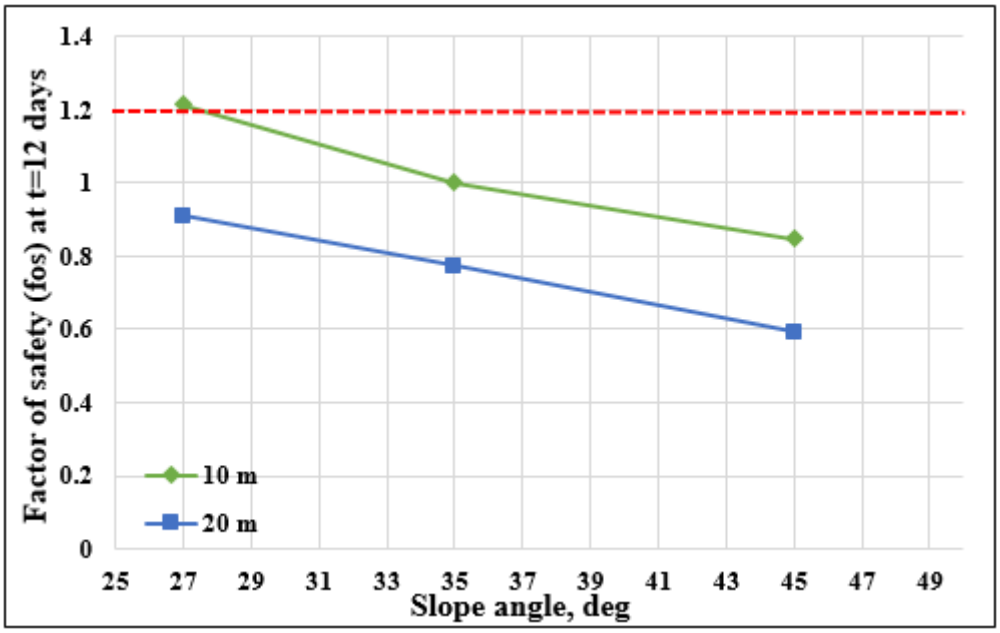

Figure A.79 Changes on factor of safety (FoS) 10m and 20m height with 27,35 and 45 degrees at t=12 days

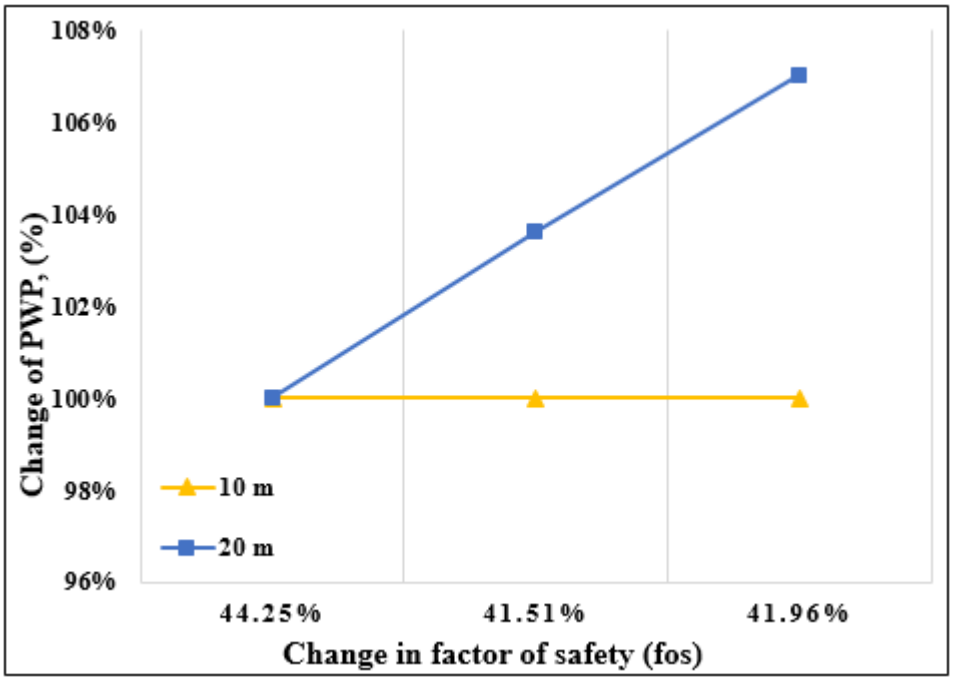

Figure A.80 Pore water pressure VS Factor of safety (FoS) during 20mm/day rainfall for 10m,20, and 30m height with 27⁰,35⁰ and 45⁰,degrees

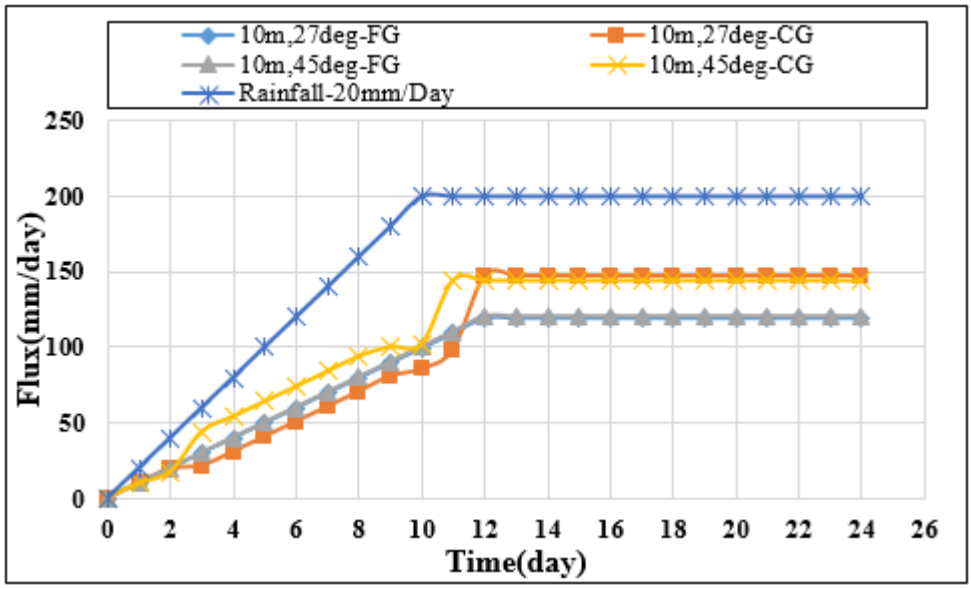

Figure A.81 Rainfall infiltration for sandy silt sand silty sand soils (10m, with 27 and 45 degrees)

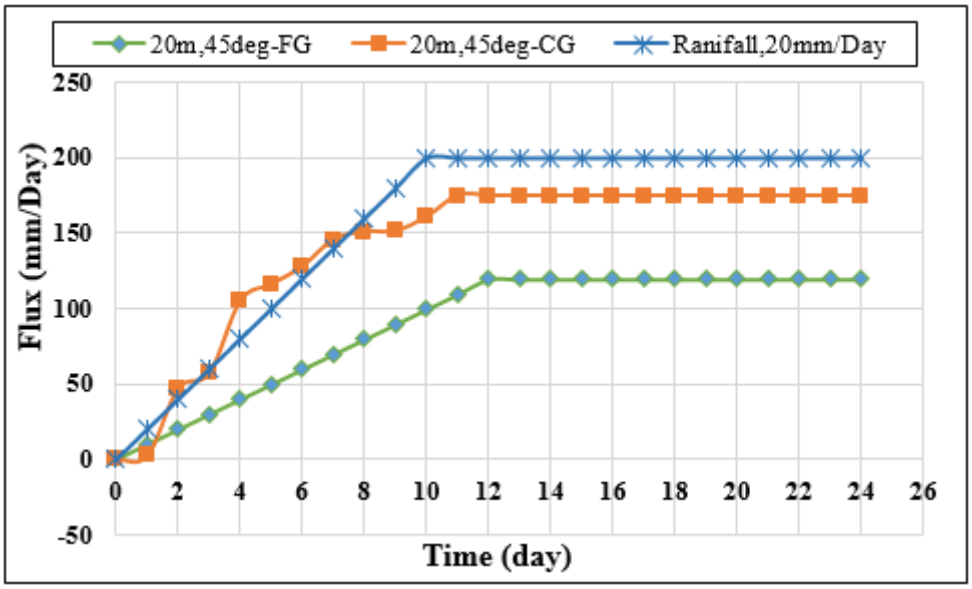

Figure A.82 Rainfall infiltration for sandy silt sand silty sand soils (20m, with 45 degrees)

Table A. 1 Factor of safety (FoS) for 10m height and 27 degree

Time(day)	height(m)	Degree	Factor of safety(FoS)
0	10	27	1.9215137
1	10	27	1.8763149
4	10	27	1.7620937
8	10	27	1.7376307
12	10	27	1.7177367
16	10	27	1.7375455
20	10	27	1.7556975
24	10	27	1.7725635

Table A. 2 Factor of safety (FoS) for 10m height and 35 degree

Time(day)	height(m)	Degree	Factor of safety(FoS)
0	10	35	1.5130283
1	10	35	1.4504537
4	10	35	1.3498354
8	10	35	1.347982
12	10	35	1.3430975
16	10	35	1.3538165
20	10	35	1.3634947
24	10	35	1.3725175

Table 3 Factor of safety (FoS) for 10m height and 45 degree

Time(day)	height(m)	Degree	Factor of safety(FoS)
0	10	45	1.2440727
1	10	45	1.196777
4	10	45	1.1096797
8	10	45	1.088612
12	10	45	1.0718704
16	10	45	1.0981841
20	10	45	1.1185992
24	10	45	1.1371697

Table A. 4 Factor of safety (FoS) for 10m height and 60 degree

Time(day)	height(m)	Degree	Factor of safety(FoS)
0	10	60	0.91769761
1	10	60	0.86398211
4	10	60	0.8221009
8	10	60	0.80335913
12	10	60	0.792983
16	10	60	0.82448854
20	10	60	0.84736147
24	10	60	0.89218946

Table A. 5 Factor of safety (FoS) for 10m height and 80 degree

Time(day)	height(m)	Degree	Factor of safety(FoS)
0	10	80	0.84918606
1	10	80	0.84918606
4	10	80	0.80391625
8	10	80	0.78442982
12	10	80	0.77286858
16	10	80	0.81800966
20	10	80	0.83168856
24	10	80	0.87908276

Table A. 6 Factor of safety(FoS) for 20m height and 27 degree

Time(day)	Height(m)	Degree	Factor of safety(FoS)
0	20	27	1.3304095
1	20	27	1.3113452
4	20	27	1.23694
8	20	27	1.2592685
12	20	27	1.2624517
16	20	27	1.2698458
20	20	27	1.2755981
24	20	27	1.2803917

Table A. 7 Factor of safety(FoS) for 20m height and 35degree

Time(day)	Height(m)	Degree	Factor of safety(FoS)
0	20	35	1.2845463
1	20	35	1.2845463
4	20	35	1.284536
8	20	35	1.2866502
12	20	35	1.2755116
16	20	35	1.2857806
20	20	35	1.303377
24	20	35	1.3168371

Table A. 8 Factor of safety(FoS) for 20m height and 45 degree

Time(day)	Height(m)	Degree	Factor of safety(FoS)
0	20	45	0.81525857
1	20	45	0.81525857
4	20	45	0.8394022
8	20	45	0.85897723
12	20	45	0.86160679
16	20	45	0.86723353
20	20	45	0.87451834
24	20	45	0.88166335

Table A. 9 Factor of safety(FoS) for 20m height and 60 degree

Time(day)	Height(m)	Degree	Factor of safety(FoS)
0	20	60	0.63695108
1	20	60	0.63695108
4	20	60	0.64410981
8	20	60	0.64112728
12	20	60	0.63523439
16	20	60	0.64808229
20	20	60	0.65884179
24	20	60	0.66459898

Table A. 10 Factor of safety(FoS) for 20m height and 80 degree

Time(day)	Height(m)	Degree	Factor of safety(FoS)
0	20	80	0.60443628
1	20	80	0.60443628
4	20	80	0.56129929
8	20	80	0.5670753
12	20	80	0.56090569
16	20	80	0.57563122
20	20	80	0.58743306
24	20	80	0.59361688

Table A. 11 Factor of safety(FoS) for 30m height and 27 degree

Time(day)	Height(m)	Degree	Factor of safety(fos)
0	30	27	1.295594
1	30	27	1.295594
4	30	27	1.4591394
8	30	27	1.4927941
12	30	27	1.4995382
16	30	27	1.5106218
20	30	27	1.5213925
24	30	27	1.5319971

Table A. 12 Factor of safety(FoS) for 30m height and 35 degree

Time(day)	Height(m)	Degree	Factor of safety(fos)
0	30	35	0.88795125
1	30	35	0.88795125
4	30	35	0.93364779
8	30	35	0.95430478
12	30	35	0.96058946
16	30	35	0.96514787
20	30	35	0.96853492
24	30	35	0.9715814

Table A. 13 Factor of safety(FoS) for 30m height and 45degree

Time(day)	Height(m)	Degree	Factor of safety(fos)
0	30	45	0.69194918
1	30	45	0.69194918
4	30	45	0.6894371
8	30	45	0.72089119
12	30	45	0.76630354
16	30	45	0.73220233
20	30	45	0.73605804
24	30	45	0.77997638

Table A. 14 Factor of safety(FoS) for 30m height and 60 degree

Time(day)	Height(m)	Degree	Factor of safety(fos)
0	30	60	0.48529221
1	30	60	0.48529221
4	30	60	0.60799574
8	30	60	0.61227146
12	30	60	0.61771433
16	30	60	0.62172658
20	30	60	0.62524892
24	30	60	0.62887516

Table A. 15 Factor of safety(FoS) for 30m height and 80 degree

Time(day)	Height(m)	Degree	Factor of safety(fos)
0	30	80	0.4691602
1	30	80	0.4691602
4	30	80	0.47940431
8	30	80	0.4741492
12	30	80	0.48238961
16	30	80	0.48361108
20	30	80	0.49341715
24	30	80	0.49841574

Table A. 16 Changes in Factor of safety(FoS) for 10m height with 27⁰,35⁰,45⁰,60⁰ and 80⁰ degrees

T(day)	27	35	45	60	80
1day	1.92151	1.513028	1.244073	0.917698	0.849186
12 days	1.71774	1.343098	1.07187	0.792983	0.772869
T0-T12	0.20	0.17	0.17	0.12	0.08
% drop	10.61%	11.23%	13.84%	13.59%	8.99%

Table A. 17 changes in Factor of safety(FoS) for 20m height with 27⁰,35⁰,45⁰,60⁰ and 80⁰ degrees

T(day)	27	35	45	60	80
1day	1.33041	1.284546	0.815259	0.636951	0.60444
12 days	1.26245	1.275512	0.861607	0.635234	0.56091
T0-T12	0.07	0.01	-0.05	0.00	0.04
% drop	5.11%	0.70%	-5.69%	0.27%	7.20%

Table A. 18 changes in Factor of safety(FoS) for 30m height with 27⁰,35⁰,45⁰,60⁰ and 80⁰ degrees

T(day)	27	35	45	60	80
1day	1.295594	0.887951	0.691949	0.485292	0.46916
12 days	1.499538	0.960589	0.766304	0.617714	0.48239
T0-T12	-0.20	-0.07	-0.07	-0.13	-0.01
% drop	-15.74%	-8.18%	-10.75%	-27.29%	-2.82%

Table A. 19 Changes in pore water pressure during 20mm/day rainfall for 10m height with 27⁰,35⁰,45⁰,60⁰ and 80⁰ degrees

	Height	0 day	12 day	t0-t12	
deg	Y (m)	PWP (kPa)	PWP (kPa)	PWP (kPa)	%change
27	27.3618	-49.698	-17.295	-32.40	65%
35	27.182	-48.2673	-16.809	-31.46	65%
45	27.36842	-49.035	-16.0196	-33.02	67%
60	27.44681	-49.035	-14.7019	-34.33	70%
80	26.5366	-21.1975	-12.5154	-8.68	41%

Table A. 20 Changes in pore water pressure during 20mm/day rainfall for 20m height with 27⁰,35⁰,45⁰,60⁰ and 80⁰ degrees

	Height	0 day	12 day	t0-t12	
deg	Y (m)	PWP (kPa)	PWP (kPa)	PWP (kPa)	%change
27	54.09091	-49.035	-17.2427	-31.79	65%
35	53.83688	-46.0586	-17.0087	-29.05	63%
45	52.98246	-42.1529	-16.2141	-25.94	62%
60	53.18681	-49.035	-14.0723	-34.96	71%
80	51.36585	-24.1584	-11.7026	-12.46	52%

Table A. 21 Changes in pore water pressure during 20mm/day rainfall for 30m height with 27⁰,35⁰,45⁰,60⁰ and 80⁰ degrees

		0 day	12 day	t0-t12	
deg	Y (m)	PWP (kPa)	PWP (kPa)	PWP (kPa)	%change
27	77.17557	-46.9033	-17.1669	-29.74	63%
35	78.44762	-43.0639	-17.2215	-25.84	60%
45	77.3494	-49.035	-15.7484	-33.29	68%
60	78.44928	-39.0942	-15.0453	-24.05	62%
80	77.54098	10.45084	-10.9632	-0.51	-5%

Table A. 22 changes in Factor of safety(FoS) for 10m height with 27⁰,35⁰ and 45⁰ degrees

T(day)	27	35	45
1day	2.17774	1.712912	1.459376
12 days	1.214031	1.001895	0.847024
T0-T12	0.96	0.71	0.61
% drop	44.25%	41.51%	41.96%

Table A.23 changes in Factor of safety(FoS) for 20m height with 27⁰,35⁰ and 45⁰ degrees

T(day)	27	35	45
1day	1.399759	1.15742	0.902305
12 days	0.910394	0.772932	0.593579
T0-T12	0.49	0.38	0.31
% drop	34.96%	33.22%	34.22%

Table A.24 Changes in pore water pressure during 20mm/day rainfall for 10m height with 27⁰,35⁰ and 45⁰ degrees

	Height	**0 day**	**12 day**	**t0-t12**	
deg	**Y (m)**	**PWP (kPa)**	**PWP (kPa)**	**PWP (kPa)**	**%change**
27	27.3618	-49.698	0	-49.70	100%
35	27.182	-48.2673	0	-48.27	100%
45	27.36842	-49.035	0	-49.04	100%

Table A. 25 Changes in pore water pressure during 20mm/day rainfall for 20m height with 27^0,35^0 and 45^0degrees

	Height	0 day	12 day	t0-t12	
deg	Y (m)	PWP (kPa)	PWP (kPa)	PWP (kPa)	%change
27	54.09091	-49.035	0	-49.04	100%
35	53.83688	-46.0586	1.664269	-47.72	104%
45	52.98246	-42.1529	2.960136	-45.11	107%